CONTRIBUTION TO THE ADVANCED ANALYSIS AND PREVENTION OF THE MECHANISMS OF NATURAL FIRE INDUCED STRUCTURAL COLLAPSE IN HIGH-RISE BUILDINGS

APORTACIÓN AL ANÁLISIS AVANZADO Y PREVENCIÓN DE LOS MECANISMOS DE COLAPSO ESTRUCTURAL DE EDIFICIOS DE GRAN ALTURA ANTE UNA SOLICITACIÓN DE INCENDIO REAL

Doctoral Thesis presented by / *Tesis Doctoral presentada por*

Angel Guerrero Castells *Ingeniero Industrial con Suficiencia Investigadora*

in February 2009 to obtain the degree of Doctor in Industrial Engineering

en Febrero de 2009 para obtener el grado de Doctor Ingeniero Industrial.

Thesis Directors / *Directores de la Tesis:*

Dr Frederic Marimon Carvajal from the / *de la Universidad Politécnica de Cataluña*

Dr Francesco Pesavento from the / *de la Università degli Studi di Padova*

PROGRAMA DE DOCTORADO DE ANÁLISIS ESTRUCTURAL

Departamento de Resistencia de Materiales y Estructuras en la Ingeniería

Escuela Técnica Superior de Ingenieros Industriales de Barcelona

Appendix 4B

Appendix 4B.1 INPUT FILES FOR THE HYGRO-THERMO-CHEMO-MECHANICAL CALCULATIONS

In this Appendix are shown the Input files developed for the calculations done by means of the software Hitecosp [B.1]. These Input files are composed by four sections [B.2]:

Block 1: Contains the name of used files and the title of the problem,

Block 2: Contains the general data of the problem,

Block 3: Contains the data for the mesh generation and the numbering of the nodes,

Block 4: Contains the data for the initial and the boundary conditions.

In order to understand the Input files included herein, a general description of the contents of each block – excerpted from the User Guide [B.2] – is attached next:

FIRST BLOCK. NAME OF THE USED FILES AND TITLE OF THE PROBLEM.

The first block is that of the general data or control data of the execution. Its structure is described in the following:

Title (c72)
Restart_code (i) , Problem_type (i)
File_name_BIN_preceding (c20) [only if Restart_code = 2]
File_name_BIN_succeding (c20)
File_name_PRN (c20)
Time_step (r) , Steps_number (i) , Print_steps_number (i)
Convergence_criterion (r) , Max_number_iterations (i)
Grav_acc (r) , Grav_angle (r)
Code_pre (i) , x_scale_factor (r) , y_scale_factor (r)
Nodes_number (i) , Elements_number (i) , Element_nodes_num (i) , Gauss_points_num(i)
Conditioned_nodes_num (i)

The meaning of the above shown data is summarised in *table 4B.1*:

DATA	*MEANING*	*VALUE*
Title	Title of the job in execution	
Restart_code	Code which indicates if it is a first execution or a restart	= -1 if first execution with constant initial conditions; = 1 if first execution with initial conditions varying for each node; = 2 if restart
Problem type	Problem type Indicates the type of the problem	= 0 if 2D Plain; = 1 if 2D Axial-symmetric
File_name_BIN_preceding	Name of the binary file produced in the previous execution	It has to be indicated only if it is a restart
File_name_BIN_succeding	Name of the binary file to be produced at the end of the execution	---
File_name_PRN	Name of the output file	---
Time step	Advised time step	---
Steps_number	Number of time steps	---
Print_steps_number	Number of time steps after which the results are saved	---
Convergence_criterion	Value of the convergence criterion	Of the order of magnitude of 1.E-5
Max_number_iterations	Maximum number of iterations inside a	E.g. 30

	time step	
Grav_acc	Value of the gravity acceleration	---
Grav_angle	Angle between the gravity and the mesh	---
Code_pre	Code for the mesh generation	= 0 if Castem2000 or GID are used; = 1 if with auto-generation
x_scale_factor	Scale factor of the mesh for the x axis	---
y_scale_factor	Scale factor of the mesh for the y axis	---
Nodes_number	Number of nodes of the mesh	---
Elements_number	Number of elements of the mesh	---
Element_nodes_num	Number of nodes for an element	= 8 if quad with 8 nodes
Gauss_points_num	Number of integration points	= 3 if 3x3
Conditioned_node_num	Number of nodes on which one or more boundary conditions are imposed	---

Table 4B-1. *Meaning of the parameters of Block 1.*

Important: At the beginning of a transitory (first run), with the absolute time equal to zero, it is necessary to proceed with an execution of 10 time steps equal to 1.-06 seconds. In fact at the initial instant the system is not in a state of equilibrium because the initial conditions for the thermo hygral D.O.F. (e.g. gas pressure, capillary pressure and temperature), do not correspond to the initial conditions for the mechanical D.O.F. (e.g. X and Y displacements).

BLOCK 2: GENERAL DATA FOR THE MESH GENERATION

The second block includes the data which describe the mesh.

When the input file has been produced with the codes Castem2000 or GID (Code_pre =0) it is necessary to give:

Node_num (i) , X_coor (r) , Y_coor (r) for every node
……..
Element_num (i) , (num_node_k (i) , per k=1,Element_nodes_num), Material_id for every element
……..

When the auto-generation of a simple mesh (rectangular and subdivided in rows and columns) is desired (Code_pre = 1):

Num_rows (i) , Num_columns (i) , Nodes_numeration_code (i)
(Column_k_coor_x (r), k=1,Num_columns + 1)
(Row_k_coor_y (r) , k=1,Num_rows + 1)
Num_mat
Element_from, Element_to, Element_step, Material_id for Num_mat rows
……..

The meaning of the mentioned data is summarised in *table 4B.2*:

DATA	***MEANING***	***VALUE***
Node_num	Identifier number of the node	---
X_coor	X co-ordinate of the node	---
Y_coor	Y co-ordinate of the node	---
Element_num	Identifier number of the element	---
Num_node_k	Id. number of the k-th node	---
Material_id	Identifier of the material	---
Num_rows	Number of rows of elements	---
Num_columns	Number of columns of elements	---
Nodes_numeration_code	Code for the automatic numeration of the nodes	= 0 if it numbers according to the rows; = 1 if it numbers according to the columns

Column_k_coor_x	X co-ordinate of the k-th column of nodes	---
Row_k_coor_y	Y co-ordinate of the k-th row of nodes	---
Num_mat	Total number of materials to assign to elements	---
Element_from	First element to assign this material	---
Element_to	Last element to assign this material	---
Element_step	Number of elements after which to assign this material	---
Material_id	Identifier of the material	---

Table 4B-2. *Meaning of the parameters of Block 2.*

BLOCK 3: DATA FOR THE INITIAL CONDITIONS

The third block is that of the data which define the initial conditions of the system. These are the following:

In case of first run with constant conditions on all the mesh (Restart_code = -1) :

Pg (r) , Pc (r) , T (r) , Ux (r) , Uy (r)

In case of first run where the initial conditions vary for each node (Restart_code = 1):

ID (i) , Pg (r) , Pc (r) , T (r) , Ux (r) , Uy (r) for every node

In the following table the meaning of the data is shown:

DATA	*MEANING*	*VALUE*
ID	Identifier of the node useful for the user	integer
Pg	Initial gas pressure	E.g.: 0.0 Pa
Pc	Initial capillary pressure	E.g.: 0.0 Pa
T	Initial temperature	E.g.: 298.15 K
Ux	Initial x displacement	E.g.: 0.0
Uy	Initial y displacement	E.g.: 0.0

Table 4B-3. *Meaning of the parameters of Block 3.*

BLOCK 4: DATA FOR THE BOUNDARY CONDITIONS

The last but also the larger block is the one which contains the data of the boundary conditions (constraints and loads) of the system. For every conditioned node the following data must be given:

Conditions_num (i) , Conditioned_node_num (i)

Dof_id (i) , Condition_id (i) , Value (r) , Coefficient (i) | for every condition

The meaning of the data to give is summarised in tables 4B-4 and 4B-5:

DATA	*MEANING*	*VALUE*
Conditions_num	Number of the imposed conditions	Not greater than 5
Conditioned_node_num	Number of the conditioned node	---
Dof_id	Identifier of the conditioned d.o.f	See next table
Condition_id	Identifier of the imposed condition	See next table
Value	Assigned value	See next table
Coefficient	Assigned coefficient	See next table

Table 4B-4. *Meaning of the parameters of Block 4.*

Dof_id	*DOF*	*Cond_id*	*Condition*	*Value*	*Coefficient*
1	PG	1 2	Imposed value Imposed flux of dry air	Fixed PG Pa Fixed air flux Kg $m^{-2}s^{-1}$	0.0 = 0.0 =
2	PC	1 2 3 4	Imposed value Imposed flux of dry air Imposed value of water vapour Imposed value of vapour pressure	Fixed PC Pa Fixed vapour flux Kg $m^{-2}s^{-1}$ Fixed room RH = Fixed vapour pressure Pa	0.0 = 0.0 = e.g. 0.05 m/s e.g. 0.05
3	T	1 2 3 4	Imposed value Imposed heat flux Var. heat flux (convection) Var. heat flux (radiation+convection)	Fixed T K Fixed heat flux W m^{-2} Fixed room T K (convect.) Fixed room T K (radiation)	0.0 = 298.15 K e.g. 20W$m^{-2}K^{-1}$ e.g. 20
4	UX	1 2	Imposed value Distributed load	Fixed Ux m Fixed stress Pa	0.0 = 0.0 =
5	UY	1 2	Imposed value Distributed load	Fixed Uy m Fixed stress Pa	0.0 = 0.0 =

Table 4B-5. *Types of values of the parameters of Block 4.*

Since it is not worthy to include herein the ten Input files corresponding to each of the ninety one cases calculated, only that corresponding to one of the three values of thicknesses considered will follow (it corresponds to the first stage of the calculations among the series of ten calculations stages developed for each combination).

The rest of them are exactly the same but for the number of nodes and elements, the values of the initial conditions – determining the value of the Initial Saturation Degree –, the calls to each heating profile and the call to the featuring material. In the following table is collected the combination whose Input file has been enclosed next:

		PC1 (RH) [%]			PC2 (K) [m^2]			PC3 (TH) [cm]			PC4 (Heating curve)			PC5 (Mat)	
#	Combination	40	50	60	10^{-19}	10^{-18}	10^{-17}	12	24	50	PAR1	PAR2	PAR3	C60	C90
5	TH12K018RH50PAR1C60		X			X		X			X			X	

Table 4B-6. *Set of combinations whose Input files are enclosed next.*

#5-TH12K018RH50PAR1C60, THICKNESS 12 CM

```
$ Description of the simulation
12 centimetres structural element*
$ Restart code , Problem type code
-1,0
$ Names of the output file and the binary file to be produced
'Wall_01.BIN'
'Wall_01.PRN'
$ Time and number step, number of time steps after which the results are saved
1e-6,10,10
$ Value of the convergence criterion, maximum number of iterations
1e-5,30
$ Gravity acceleration, angle between the gravity acceleration and the mesh
0,0
$ Code for the mesh generation, scale factors of the mesh for the x and y axis
0,0.01,0.01
$ Nodes, elements, nodes for an element, number of integration points
    603,    120,      8,3
$ Number of nodes on which one or more boundary conditions are imposed
    484
$ x and y coordinates of the nodes
        1         0.000000         0.000000 |      13         0.100000         0.500000
        2         0.050000         0.000000 |      14         0.200000         0.500000
        3         0.100000         0.000000 |      15         0.550000         0.000000
        4         0.150000         0.000000 |      16         0.300000         0.500000
        5         0.200000         0.000000 |      17         0.600000         0.000000
        6         0.250000         0.000000 |      18         0.400000         0.500000
        7         0.300000         0.000000 |      19         0.650000         0.000000
        8         0.350000         0.000000 |      20         0.700000         0.000000
        9         0.400000         0.000000 |      21         0.500000         0.500000
       10         0.450000         0.000000 |      22         0.750000         0.000000
       11         0.000000         0.500000 |      23         0.600000         0.500000
       12         0.500000         0.000000 |      24         0.800000         0.000000
```

25	0.850000	0.000000	102	1.850000	1.000000
26	0.700000	0.500000	103	1.900000	1.000000
27	0.900000	0.000000	104	2.150000	0.000000
28	0.800000	0.500000	105	2.100000	0.500000
29	0.950000	0.000000	106	1.950000	1.000000
30	1.000000	0.000000	107	2.200000	0.000000
31	0.000000	1.000000	108	2.000000	1.000000
32	0.050000	1.000000	109	2.250000	0.000000
33	0.100000	1.000000	110	2.200000	0.500000
34	0.150000	1.000000	111	2.050000	1.000000
35	0.200000	1.000000	112	2.300000	0.000000
36	0.900000	0.500000	113	2.100000	1.000000
37	0.250000	1.000000	114	2.350000	0.000000
38	0.300000	1.000000	115	2.300000	0.500000
39	1.050000	0.000000	116	2.150000	1.000000
40	0.350000	1.000000	117	2.400000	0.000000
41	0.400000	1.000000	118	2.200000	1.000000
42	0.450000	1.000000	119	2.450000	0.000000
43	1.100000	0.000000	120	2.400000	0.500000
44	0.500000	1.000000	121	2.250000	1.000000
45	1.000000	0.500000	122	2.500000	0.000000
46	0.550000	1.000000	123	2.300000	1.000000
47	1.150000	0.000000	124	2.500000	0.500000
48	0.600000	1.000000	125	2.550000	0.000000
49	0.650000	1.000000	126	2.350000	1.000000
50	1.200000	0.000000	127	2.400000	1.000000
51	1.100000	0.500000	128	2.600000	0.000000
52	0.700000	1.000000	129	2.450000	1.000000
53	1.250000	0.000000	130	2.600000	0.500000
54	0.750000	1.000000	131	2.650000	0.000000
55	0.800000	1.000000	132	2.500000	1.000000
56	1.200000	0.500000	133	2.700000	0.000000
57	1.300000	0.000000	134	2.550000	1.000000
58	0.850000	1.000000	135	2.700000	0.500000
59	0.900000	1.000000	136	2.750000	0.000000
60	1.350000	0.000000	137	2.600000	1.000000
61	0.950000	1.000000	138	2.800000	0.000000
62	1.300000	0.500000	139	2.650000	1.000000
63	1.400000	0.000000	140	2.800000	0.500000
64	1.000000	1.000000	141	2.850000	0.000000
65	1.450000	0.000000	142	2.700000	1.000000
66	1.050000	1.000000	143	2.900000	0.000000
67	1.100000	1.000000	144	2.750000	1.000000
68	1.400000	0.500000	145	2.900000	0.500000
69	1.500000	0.000000	146	2.950000	0.000000
70	1.150000	1.000000	147	2.800000	1.000000
71	1.550000	0.000000	148	3.000000	0.000000
72	1.200000	1.000000	149	2.850000	1.000000
73	1.500000	0.500000	150	3.000000	0.500000
74	1.600000	0.000000	151	3.050000	0.000000
75	1.250000	1.000000	152	2.900000	1.000000
76	1.300000	1.000000	153	3.100000	0.000000
77	1.650000	0.000000	154	2.950000	1.000000
78	1.600000	0.500000	155	3.100000	0.500000
79	1.350000	1.000000	156	3.150000	0.000000
80	1.700000	0.000000	157	3.000000	1.000000
81	1.400000	1.000000	158	3.200000	0.000000
82	1.750000	0.000000	159	3.050000	1.000000
83	1.450000	1.000000	160	3.200000	0.500000
84	1.700000	0.500000	161	3.250000	0.000000
85	1.800000	0.000000	162	3.100000	1.000000
86	1.500000	1.000000	163	3.300000	0.000000
87	1.550000	1.000000	164	3.150000	1.000000
88	1.850000	0.000000	165	3.300000	0.500000
89	1.800000	0.500000	166	3.350000	0.000000
90	1.600000	1.000000	167	3.200000	1.000000
91	1.900000	0.000000	168	3.400000	0.000000
92	1.650000	1.000000	169	3.250000	1.000000
93	1.950000	0.000000	170	3.400000	0.500000
94	1.900000	0.500000	171	3.300000	1.000000
95	1.700000	1.000000	172	3.450000	0.000000
96	2.000000	0.000000	173	3.350000	1.000000
97	1.750000	1.000000	174	3.500000	0.000000
98	2.050000	0.000000	175	3.500000	0.500000
99	1.800000	1.000000	176	3.400000	1.000000
100	2.000000	0.500000	177	3.550000	0.000000
101	2.100000	0.000000	178	3.450000	1.000000

179	3.600000	0.000000
180	3.600000	0.500000
181	3.500000	1.000000
182	3.650000	0.000000
183	3.550000	1.000000
184	3.700000	0.000000
185	3.700000	0.500000
186	3.600000	1.000000
187	3.750000	0.000000
188	3.650000	1.000000
189	3.800000	0.000000
190	3.700000	1.000000
191	3.800000	0.500000
192	3.850000	0.000000
193	3.750000	1.000000
194	3.900000	0.000000
195	3.800000	1.000000
196	3.900000	0.500000
197	3.950000	0.000000
198	3.850000	1.000000
199	4.000000	0.000000
200	3.900000	1.000000
201	4.000000	0.500000
202	4.050000	0.000000
203	3.950000	1.000000
204	4.100000	0.000000
205	4.000000	1.000000
206	4.100000	0.500000
207	4.150000	0.000000
208	4.050000	1.000000
209	4.200000	0.000000
210	4.100000	1.000000
211	4.200000	0.500000
212	4.250000	0.000000
213	4.150000	1.000000
214	4.300000	0.000000
215	4.200000	1.000000
216	4.300000	0.500000
217	4.350000	0.000000
218	4.250000	1.000000
219	4.400000	0.000000
220	4.300000	1.000000
221	4.400000	0.500000
222	4.450000	0.000000
223	4.350000	1.000000
224	4.500000	0.000000
225	4.400000	1.000000
226	4.500000	0.500000
227	4.550000	0.000000
228	4.450000	1.000000
229	4.600000	0.000000
230	4.500000	1.000000
231	4.600000	0.500000
232	4.650000	0.000000
233	4.550000	1.000000
234	4.700000	0.000000
235	4.600000	1.000000
236	4.700000	0.500000
237	4.750000	0.000000
238	4.650000	1.000000
239	4.800000	0.000000
240	4.700000	1.000000
241	4.800000	0.500000
242	4.850000	0.000000
243	4.750000	1.000000
244	4.900000	0.000000
245	4.800000	1.000000
246	4.900000	0.500000
247	4.950000	0.000000
248	4.850000	1.000000
249	5.000000	0.000000
250	4.900000	1.000000
251	5.000000	0.500000
252	4.950000	1.000000
253	5.050000	0.000000
254	5.000000	1.000000
255	5.100000	0.000000
256	5.100000	0.500000
257	5.050000	1.000000
258	5.150000	0.000000
259	5.100000	1.000000
260	5.200000	0.000000
261	5.200000	0.500000
262	5.150000	1.000000
263	5.250000	0.000000
264	5.200000	1.000000
265	5.300000	0.000000
266	5.300000	0.500000
267	5.250000	1.000000
268	5.350000	0.000000
269	5.300000	1.000000
270	5.400000	0.000000
271	5.400000	0.500000
272	5.350000	1.000000
273	5.450000	0.000000
274	5.400000	1.000000
275	5.500000	0.000000
276	5.500000	0.500000
277	5.450000	1.000000
278	5.550000	0.000000
279	5.500000	1.000000
280	5.600000	0.000000
281	5.600000	0.500000
282	5.550000	1.000000
283	5.650000	0.000000
284	5.600000	1.000000
285	5.700000	0.000000
286	5.700000	0.500000
287	5.650000	1.000000
288	5.750000	0.000000
289	5.700000	1.000000
290	5.800000	0.000000
291	5.800000	0.500000
292	5.750000	1.000000
293	5.850000	0.000000
294	5.800000	1.000000
295	5.900000	0.000000
296	5.900000	0.500000
297	5.850000	1.000000
298	5.950000	0.000000
299	5.900000	1.000000
300	6.000000	0.000000
301	6.000000	0.500000
302	5.950000	1.000000
303	6.050000	0.000000
304	6.000000	1.000000
305	6.100000	0.000000
306	6.100000	0.500000
307	6.050000	1.000000
308	6.150000	0.000000
309	6.100000	1.000000
310	6.200000	0.000000
311	6.200000	0.500000
312	6.150000	1.000000
313	6.250000	0.000000
314	6.200000	1.000000
315	6.300000	0.000000
316	6.300000	0.500000
317	6.250000	1.000000
318	6.350000	0.000000
319	6.300000	1.000000
320	6.400000	0.000000
321	6.400000	0.500000
322	6.350000	1.000000
323	6.450000	0.000000
324	6.400000	1.000000
325	6.500000	0.000000
326	6.500000	0.500000
327	6.450000	1.000000
328	6.550000	0.000000
329	6.500000	1.000000
330	6.600000	0.000000
331	6.600000	0.500000
332	6.550000	1.000000

333	6.650000	0.000000	410	8.200000	0.000000
334	6.600000	1.000000	411	8.150000	1.000000
335	6.700000	0.000000	412	8.200000	0.500000
336	6.700000	0.500000	413	8.250000	0.000000
337	6.650000	1.000000	414	8.200000	1.000000
338	6.750000	0.000000	415	8.300000	0.000000
339	6.700000	1.000000	416	8.250000	1.000000
340	6.800000	0.000000	417	8.300000	0.500000
341	6.800000	0.500000	418	8.350000	0.000000
342	6.750000	1.000000	419	8.300000	1.000000
343	6.850000	0.000000	420	8.400000	0.000000
344	6.800000	1.000000	421	8.350000	1.000000
345	6.900000	0.000000	422	8.400000	0.500000
346	6.900000	0.500000	423	8.450000	0.000000
347	6.850000	1.000000	424	8.400000	1.000000
348	6.950000	0.000000	425	8.500000	0.000000
349	6.900000	1.000000	426	8.450000	1.000000
350	7.000000	0.000000	427	8.500000	0.500000
351	7.000000	0.500000	428	8.550000	0.000000
352	6.950000	1.000000	429	8.500000	1.000000
353	7.050000	0.000000	430	8.600000	0.000000
354	7.000000	1.000000	431	8.550000	1.000000
355	7.100000	0.000000	432	8.600000	0.500000
356	7.100000	0.500000	433	8.650000	0.000000
357	7.050000	1.000000	434	8.600000	1.000000
358	7.150000	0.000000	435	8.700000	0.000000
359	7.100000	1.000000	436	8.650000	1.000000
360	7.200000	0.000000	437	8.700000	0.500000
361	7.200000	0.500000	438	8.750000	0.000000
362	7.150000	1.000000	439	8.700000	1.000000
363	7.250000	0.000000	440	8.800000	0.000000
364	7.200000	1.000000	441	8.750000	1.000000
365	7.300000	0.000000	442	8.800000	0.500000
366	7.300000	0.500000	443	8.850000	0.000000
367	7.250000	1.000000	444	8.800000	1.000000
368	7.350000	0.000000	445	8.900000	0.000000
369	7.300000	1.000000	446	8.850000	1.000000
370	7.400000	0.000000	447	8.900000	0.500000
371	7.400000	0.500000	448	8.950000	0.000000
372	7.350000	1.000000	449	8.900000	1.000000
373	7.450000	0.000000	450	9.000000	0.000000
374	7.400000	1.000000	451	8.950000	1.000000
375	7.500000	0.000000	452	9.000000	0.500000
376	7.500000	0.500000	453	9.050000	0.000000
377	7.450000	1.000000	454	9.000000	1.000000
378	7.550000	0.000000	455	9.100000	0.000000
379	7.500000	1.000000	456	9.050000	1.000000
380	7.600000	0.000000	457	9.100000	0.500000
381	7.550000	1.000000	458	9.150000	0.000000
382	7.600000	0.500000	459	9.100000	1.000000
383	7.650000	0.000000	460	9.200000	0.000000
384	7.600000	1.000000	461	9.150000	1.000000
385	7.700000	0.000000	462	9.200000	0.500000
386	7.650000	1.000000	463	9.250000	0.000000
387	7.700000	0.500000	464	9.200000	1.000000
388	7.750000	0.000000	465	9.300000	0.000000
389	7.700000	1.000000	466	9.250000	1.000000
390	7.800000	0.000000	467	9.300000	0.500000
391	7.750000	1.000000	468	9.350000	0.000000
392	7.800000	0.500000	469	9.300000	1.000000
393	7.850000	0.000000	470	9.400000	0.000000
394	7.800000	1.000000	471	9.350000	1.000000
395	7.900000	0.000000	472	9.400000	0.500000
396	7.850000	1.000000	473	9.450000	0.000000
397	7.900000	0.500000	474	9.400000	1.000000
398	7.950000	0.000000	475	9.500000	0.000000
399	7.900000	1.000000	476	9.450000	1.000000
400	8.000000	0.000000	477	9.500000	0.500000
401	7.950000	1.000000	478	9.550000	0.000000
402	8.000000	0.500000	479	9.500000	1.000000
403	8.050000	0.000000	480	9.600000	0.000000
404	8.000000	1.000000	481	9.550000	1.000000
405	8.100000	0.000000	482	9.600000	0.500000
406	8.050000	1.000000	483	9.650000	0.000000
407	8.100000	0.500000	484	9.600000	1.000000
408	8.150000	0.000000	485	9.700000	0.000000
409	8.100000	1.000000	486	9.650000	1.000000

487	9.700000	0.500000	546	10.900000	0.000000
488	9.750000	0.000000	547	10.900000	0.500000
489	9.700000	1.000000	548	10.900000	1.000000
490	9.800000	0.000000	549	10.950000	0.000000
491	9.750000	1.000000	550	10.950000	1.000000
492	9.800000	0.500000	551	11.000000	0.000000
493	9.850000	0.000000	552	11.000000	0.500000
494	9.800000	1.000000	553	11.000000	1.000000
495	9.900000	0.000000	554	11.050000	0.000000
496	9.850000	1.000000	555	11.050000	1.000000
497	9.900000	0.500000	556	11.100000	0.000000
498	9.950000	0.000000	557	11.100000	0.500000
499	9.900000	1.000000	558	11.100000	1.000000
500	10.000000	0.000000	559	11.150000	0.000000
501	9.950000	1.000000	560	11.150000	1.000000
502	10.000000	0.500000	561	11.200000	0.000000
503	10.000000	1.000000	562	11.200000	0.500000
504	10.050000	0.000000	563	11.200000	1.000000
505	10.050000	1.000000	564	11.250000	0.000000
506	10.100000	0.000000	565	11.250000	1.000000
507	10.100000	0.500000	566	11.300000	0.000000
508	10.100000	1.000000	567	11.300000	0.500000
509	10.150000	0.000000	568	11.300000	1.000000
510	10.150000	1.000000	569	11.350000	0.000000
511	10.200000	0.000000	570	11.350000	1.000000
512	10.200000	0.500000	571	11.400000	0.000000
513	10.200000	1.000000	572	11.400000	0.500000
514	10.250000	0.000000	573	11.400000	1.000000
515	10.250000	1.000000	574	11.450000	0.000000
516	10.300000	0.000000	575	11.450000	1.000000
517	10.300000	0.500000	576	11.500000	0.000000
518	10.300000	1.000000	577	11.500000	0.500000
519	10.350000	0.000000	578	11.500000	1.000000
520	10.350000	1.000000	579	11.550000	0.000000
521	10.400000	0.000000	580	11.550000	1.000000
522	10.400000	0.500000	581	11.600000	0.000000
523	10.400000	1.000000	582	11.600000	0.500000
524	10.450000	0.000000	583	11.600000	1.000000
525	10.450000	1.000000	584	11.650000	0.000000
526	10.500000	0.000000	585	11.650000	1.000000
527	10.500000	0.500000	586	11.700000	0.000000
528	10.500000	1.000000	587	11.700000	0.500000
529	10.550000	0.000000	588	11.700000	1.000000
530	10.550000	1.000000	589	11.750000	0.000000
531	10.600000	0.000000	590	11.750000	1.000000
532	10.600000	0.500000	591	11.800000	0.000000
533	10.600000	1.000000	592	11.800000	0.500000
534	10.650000	0.000000	593	11.800000	1.000000
535	10.650000	1.000000	594	11.850000	0.000000
536	10.700000	0.000000	595	11.850000	1.000000
537	10.700000	0.500000	596	11.900000	0.000000
538	10.700000	1.000000	597	11.900000	0.500000
539	10.750000	0.000000	598	11.900000	1.000000
540	10.750000	1.000000	599	11.950000	0.000000
541	10.800000	0.000000	600	11.950000	1.000000
542	10.800000	0.500000	601	12.000000	0.000000
543	10.800000	1.000000	602	12.000000	0.500000
544	10.850000	0.000000	603	12.000000	1.000000
545	10.850000	1.000000			

$ Connectivities and identifier of the element material

1	3	13	33	32	31	11	1	2	4
2	5	14	35	34	33	13	3	4	4
3	7	16	38	37	35	14	5	6	4
4	9	18	41	40	38	16	7	8	4
5	12	21	44	42	41	18	9	10	4
6	17	23	48	46	44	21	12	15	4
7	20	26	52	49	48	23	17	19	4
8	24	28	55	54	52	26	20	22	4
9	27	36	59	58	55	28	24	25	4
10	30	45	64	61	59	36	27	29	4
11	43	51	67	66	64	45	30	39	4
12	50	56	72	70	67	51	43	47	4
13	57	62	76	75	72	56	50	53	4
14	63	68	81	79	76	62	57	60	4
15	69	73	86	83	81	68	63	65	4
16	74	78	90	87	86	73	69	71	4
17	80	84	95	92	90	78	74	77	4

18	85	89	99	97	95	84	80	82	4
19	91	94	103	102	99	89	85	88	4
20	96	100	108	106	103	94	91	93	4
21	101	105	113	111	108	100	96	98	4
22	107	110	118	116	113	105	101	104	4
23	112	115	123	121	118	110	107	109	4
24	117	120	127	126	123	115	112	114	4
25	122	124	132	129	127	120	117	119	4
26	128	130	137	134	132	124	122	125	4
27	133	135	142	139	137	130	128	131	4
28	138	140	147	144	142	135	133	136	4
29	143	145	152	149	147	140	138	141	4
30	148	150	157	154	152	145	143	146	4
31	153	155	162	159	157	150	148	151	4
32	158	160	167	164	162	155	153	156	4
33	163	165	171	169	167	160	158	161	4
34	168	170	176	173	171	165	163	166	4
35	174	175	181	178	176	170	168	172	4
36	179	180	186	183	181	175	174	177	4
37	184	185	190	188	186	180	179	182	4
38	189	191	195	193	190	185	184	187	4
39	194	196	200	198	195	191	189	192	4
40	199	201	205	203	200	196	194	197	4
41	204	206	210	208	205	201	199	202	4
42	209	211	215	213	210	206	204	207	4
43	214	216	220	218	215	211	209	212	4
44	219	221	225	223	220	216	214	217	4
45	224	226	230	228	225	221	219	222	4
46	229	231	235	233	230	226	224	227	4
47	234	236	240	238	235	231	229	232	4
48	239	241	245	243	240	236	234	237	4
49	244	246	250	248	245	241	239	242	4
50	249	251	254	252	250	246	244	247	4
51	255	256	259	257	254	251	249	253	4
52	260	261	264	262	259	256	255	258	4
53	265	266	269	267	264	261	260	263	4
54	270	271	274	272	269	266	265	268	4
55	275	276	279	277	274	271	270	273	4
56	280	281	284	282	279	276	275	278	4
57	285	286	289	287	284	281	280	283	4
58	290	291	294	292	289	286	285	288	4
59	295	296	299	297	294	291	290	293	4
60	300	301	304	302	299	296	295	298	4
61	305	306	309	307	304	301	300	303	4
62	310	311	314	312	309	306	305	308	4
63	315	316	319	317	314	311	310	313	4
64	320	321	324	322	319	316	315	318	4
65	325	326	329	327	324	321	320	323	4
66	330	331	334	332	329	326	325	328	4
67	335	336	339	337	334	331	330	333	4
68	340	341	344	342	339	336	335	338	4
69	345	346	349	347	344	341	340	343	4
70	350	351	354	352	349	346	345	348	4
71	355	356	359	357	354	351	350	353	4
72	360	361	364	362	359	356	355	358	4
73	365	366	369	367	364	361	360	363	4
74	370	371	374	372	369	366	365	368	4
75	375	376	379	377	374	371	370	373	4
76	380	382	384	381	379	376	375	378	4
77	385	387	389	386	384	382	380	383	4
78	390	392	394	391	389	387	385	388	4
79	395	397	399	396	394	392	390	393	4
80	400	402	404	401	399	397	395	398	4
81	405	407	409	406	404	402	400	403	4
82	410	412	414	411	409	407	405	408	4
83	415	417	419	416	414	412	410	413	4
84	420	422	424	421	419	417	415	418	4
85	425	427	429	426	424	422	420	423	4
86	430	432	434	431	429	427	425	428	4
87	435	437	439	436	434	432	430	433	4
88	440	442	444	441	439	437	435	438	4
89	445	447	449	446	444	442	440	443	4
90	450	452	454	451	449	447	445	448	4
91	455	457	459	456	454	452	450	453	4
92	460	462	464	461	459	457	455	458	4
93	465	467	469	466	464	462	460	463	4
94	470	472	474	471	469	467	465	468	4

```
      95     475     477     479     476     474     472     470     473       4
      96     480     482     484     481     479     477     475     478       4
      97     485     487     489     486     484     482     480     483       4
      98     490     492     494     491     489     487     485     488       4
      99     495     497     499     496     494     492     490     493       4
     100     500     502     503     501     499     497     495     498       4
     101     506     507     508     505     503     502     500     504       4
     102     511     512     513     510     508     507     506     509       4
     103     516     517     518     515     513     512     511     514       4
     104     521     522     523     520     518     517     516     519       4
     105     526     527     528     525     523     522     521     524       4
     106     531     532     533     530     528     527     526     529       4
     107     536     537     538     535     533     532     531     534       4
     108     541     542     543     540     538     537     536     539       4
     109     546     547     548     545     543     542     541     544       4
     110     551     552     553     550     548     547     546     549       4
     111     556     557     558     555     553     552     551     554       4
     112     561     562     563     560     558     557     556     559       4
     113     566     567     568     565     563     562     561     564       4
     114     571     572     573     570     568     567     566     569       4
     115     576     577     578     575     573     572     571     574       4
     116     581     582     583     580     578     577     576     579       4
     117     586     587     588     585     583     582     581     584       4
     118     591     592     593     590     588     587     586     589       4
     119     596     597     598     595     593     592     591     594       4
     120     601     602     603     600     598     597     596     599       4
$ Initial conditions
101325,9.55319e7, 298.15, 0, 0
$ Boundary conditions
      4       1                                                  5       1       0.000000         0.000000
 1       1    101325.000000         0.000000                        4      31
 2       4      1300.000000         0.020000                1       1    101325.000000         0.000000
 3       4       298.150000        20.000000                2       4      1300.000000         0.020000
 5       1         0.000000         0.000000                3       4       298.150000        20.000000
      1       2                                                  5       1         0.000000         0.000000
 5       1         0.000000         0.000000                       1      32
      1       3                                                  5       1         0.000000         0.000000
 5       1         0.000000         0.000000                       1      33
      1       4                                                  5       1         0.000000         0.000000
 5       1         0.000000         0.000000                       1      34
      1       5                                                  5       1         0.000000         0.000000
 5       1         0.000000         0.000000                       1      35
      1       6                                                  5       1         0.000000         0.000000
 5       1         0.000000         0.000000                       1      37
      1       7                                                  5       1         0.000000         0.000000
 5       1         0.000000         0.000000                       1      38
      1       8                                                  5       1         0.000000         0.000000
 5       1         0.000000         0.000000                       1      39
      1       9                                                  5       1         0.000000         0.000000
 5       1         0.000000         0.000000                       1      40
      1      10                                                  5       1         0.000000         0.000000
 5       1         0.000000         0.000000                       1      41
      3      11                                                  5       1         0.000000         0.000000
 1       1    101325.000000         0.000000                       1      42
 2       4      1300.000000         0.020000                5       1         0.000000         0.000000
 3       4       298.150000        20.000000                      1      43
      1      12                                                  5       1         0.000000         0.000000
 5       1         0.000000         0.000000                       1      44
      1      15                                                  5       1         0.000000         0.000000
 5       1         0.000000         0.000000                       1      46
      1      17                                                  5       1         0.000000         0.000000
 5       1         0.000000         0.000000                       1      47
      1      19                                                  5       1         0.000000         0.000000
 5       1         0.000000         0.000000                       1      48
      1      20                                                  5       1         0.000000         0.000000
 5       1         0.000000         0.000000                       1      49
      1      22                                                  5       1         0.000000         0.000000
 5       1         0.000000         0.000000                       1      50
      1      24                                                  5       1         0.000000         0.000000
 5       1         0.000000         0.000000                       1      52
      1      25                                                  5       1         0.000000         0.000000
 5       1         0.000000         0.000000                       1      53
      1      27                                                  5       1         0.000000         0.000000
 5       1         0.000000         0.000000                       1      54
      1      29                                                  5       1         0.000000         0.000000
 5       1         0.000000         0.000000                       1      55
      1      30                                                  5       1         0.000000         0.000000
```

```
     1      57
5       1          0.000000          0.000000
     1      58
5       1          0.000000          0.000000
     1      59
5       1          0.000000          0.000000
     1      60
5       1          0.000000          0.000000
     1      61
5       1          0.000000          0.000000
     1      63
5       1          0.000000          0.000000
     1      64
5       1          0.000000          0.000000
     1      65
5       1          0.000000          0.000000
     1      66
5       1          0.000000          0.000000
     1      67
5       1          0.000000          0.000000
     1      69
5       1          0.000000          0.000000
     1      70
5       1          0.000000          0.000000
     1      71
5       1          0.000000          0.000000
     1      72
5       1          0.000000          0.000000
     1      74
5       1          0.000000          0.000000
     1      75
5       1          0.000000          0.000000
     1      76
5       1          0.000000          0.000000
     1      77
5       1          0.000000          0.000000
     1      79
5       1          0.000000          0.000000
     1      80
5       1          0.000000          0.000000
     1      81
5       1          0.000000          0.000000
     1      82
5       1          0.000000          0.000000
     1      83
5       1          0.000000          0.000000
     1      85
5       1          0.000000          0.000000
     1      86
5       1          0.000000          0.000000
     1      87
5       1          0.000000          0.000000
     1      88
5       1          0.000000          0.000000
     1      90
5       1          0.000000          0.000000
     1      91
5       1          0.000000          0.000000
     1      92
5       1          0.000000          0.000000
     1      93
5       1          0.000000          0.000000
     1      95
5       1          0.000000          0.000000
     1      96
5       1          0.000000          0.000000
     1      97
5       1          0.000000          0.000000
     1      98
5       1          0.000000          0.000000
     1      99
5       1          0.000000          0.000000
     1     101
5       1          0.000000          0.000000
     1     102
5       1          0.000000          0.000000
     1     103
5       1          0.000000          0.000000
     1     104
5       1          0.000000          0.000000
     1     106
5       1          0.000000          0.000000
     1     107
5       1          0.000000          0.000000
     1     108
5       1          0.000000          0.000000
     1     109
5       1          0.000000          0.000000
     1     111
5       1          0.000000          0.000000
     1     112
5       1          0.000000          0.000000
     1     113
5       1          0.000000          0.000000
     1     114
5       1          0.000000          0.000000
     1     116
5       1          0.000000          0.000000
     1     117
5       1          0.000000          0.000000
     1     118
5       1          0.000000          0.000000
     1     119
5       1          0.000000          0.000000
     1     121
5       1          0.000000          0.000000
     1     122
5       1          0.000000          0.000000
     1     123
5       1          0.000000          0.000000
     1     125
5       1          0.000000          0.000000
     1     126
5       1          0.000000          0.000000
     1     127
5       1          0.000000          0.000000
     1     128
5       1          0.000000          0.000000
     1     129
5       1          0.000000          0.000000
     1     131
5       1          0.000000          0.000000
     1     132
5       1          0.000000          0.000000
     1     133
5       1          0.000000          0.000000
     1     134
5       1          0.000000          0.000000
     1     136
5       1          0.000000          0.000000
     1     137
5       1          0.000000          0.000000
     1     138
5       1          0.000000          0.000000
     1     139
5       1          0.000000          0.000000
     1     141
5       1          0.000000          0.000000
     1     142
5       1          0.000000          0.000000
     1     143
5       1          0.000000          0.000000
     1     144
5       1          0.000000          0.000000
     1     146
5       1          0.000000          0.000000
     1     147
5       1          0.000000          0.000000
     1     148
5       1          0.000000          0.000000
     1     149
5       1          0.000000          0.000000
     1     151
5       1          0.000000          0.000000
```

5	1	1	152	0.000000	0.000000	5	1	1	200	0.000000	0.000000
5	1	1	153	0.000000	0.000000	5	1	1	202	0.000000	0.000000
5	1	1	154	0.000000	0.000000	5	1	1	203	0.000000	0.000000
5	1	1	156	0.000000	0.000000	5	1	1	204	0.000000	0.000000
5	1	1	157	0.000000	0.000000	5	1	1	205	0.000000	0.000000
5	1	1	158	0.000000	0.000000	5	1	1	207	0.000000	0.000000
5	1	1	159	0.000000	0.000000	5	1	1	208	0.000000	0.000000
5	1	1	161	0.000000	0.000000	5	1	1	209	0.000000	0.000000
5	1	1	162	0.000000	0.000000	5	1	1	210	0.000000	0.000000
5	1	1	163	0.000000	0.000000	5	1	1	212	0.000000	0.000000
5	1	1	164	0.000000	0.000000	5	1	1	213	0.000000	0.000000
5	1	1	166	0.000000	0.000000	5	1	1	214	0.000000	0.000000
5	1	1	167	0.000000	0.000000	5	1	1	215	0.000000	0.000000
5	1	1	168	0.000000	0.000000	5	1	1	217	0.000000	0.000000
5	1	1	169	0.000000	0.000000	5	1	1	218	0.000000	0.000000
5	1	1	171	0.000000	0.000000	5	1	1	219	0.000000	0.000000
5	1	1	172	0.000000	0.000000	5	1	1	220	0.000000	0.000000
5	1	1	173	0.000000	0.000000	5	1	1	222	0.000000	0.000000
5	1	1	174	0.000000	0.000000	5	1	1	223	0.000000	0.000000
5	1	1	176	0.000000	0.000000	5	1	1	224	0.000000	0.000000
5	1	1	177	0.000000	0.000000	5	1	1	225	0.000000	0.000000
5	1	1	178	0.000000	0.000000	5	1	1	227	0.000000	0.000000
5	1	1	179	0.000000	0.000000	5	1	1	228	0.000000	0.000000
5	1	1	181	0.000000	0.000000	5	1	1	229	0.000000	0.000000
5	1	1	182	0.000000	0.000000	5	1	1	230	0.000000	0.000000
5	1	1	183	0.000000	0.000000	5	1	1	232	0.000000	0.000000
5	1	1	184	0.000000	0.000000	5	1	1	233	0.000000	0.000000
5	1	1	186	0.000000	0.000000	5	1	1	234	0.000000	0.000000
5	1	1	187	0.000000	0.000000	5	1	1	235	0.000000	0.000000
5	1	1	188	0.000000	0.000000	5	1	1	237	0.000000	0.000000
5	1	1	189	0.000000	0.000000	5	1	1	238	0.000000	0.000000
5	1	1	190	0.000000	0.000000	5	1	1	239	0.000000	0.000000
5	1	1	192	0.000000	0.000000	5	1	1	240	0.000000	0.000000
5	1	1	193	0.000000	0.000000	5	1	1	242	0.000000	0.000000
5	1	1	194	0.000000	0.000000	5	1	1	243	0.000000	0.000000
5	1	1	195	0.000000	0.000000	5	1	1	244	0.000000	0.000000
5	1	1	197	0.000000	0.000000	5	1	1	245	0.000000	0.000000
5	1	1	198	0.000000	0.000000	5	1	1	247	0.000000	0.000000
5	1	1	199								

```
     1     248
5         1          0.000000          0.000000
     1     249
5         1          0.000000          0.000000
     1     250
5         1          0.000000          0.000000
     1     252
5         1          0.000000          0.000000
     1     253
5         1          0.000000          0.000000
     1     254
5         1          0.000000          0.000000
     1     255
5         1          0.000000          0.000000
     1     257
5         1          0.000000          0.000000
     1     258
5         1          0.000000          0.000000
     1     259
5         1          0.000000          0.000000
     1     260
5         1          0.000000          0.000000
     1     262
5         1          0.000000          0.000000
     1     263
5         1          0.000000          0.000000
     1     264
5         1          0.000000          0.000000
     1     265
5         1          0.000000          0.000000
     1     267
5         1          0.000000          0.000000
     1     268
5         1          0.000000          0.000000
     1     269
5         1          0.000000          0.000000
     1     270
5         1          0.000000          0.000000
     1     272
5         1          0.000000          0.000000
     1     273
5         1          0.000000          0.000000
     1     274
5         1          0.000000          0.000000
     1     275
5         1          0.000000          0.000000
     1     277
5         1          0.000000          0.000000
     1     278
5         1          0.000000          0.000000
     1     279
5         1          0.000000          0.000000
     1     280
5         1          0.000000          0.000000
     1     282
5         1          0.000000          0.000000
     1     283
5         1          0.000000          0.000000
     1     284
5         1          0.000000          0.000000
     1     285
5         1          0.000000          0.000000
     1     287
5         1          0.000000          0.000000
     1     288
5         1          0.000000          0.000000
     1     289
5         1          0.000000          0.000000
     1     290
5         1          0.000000          0.000000
     1     292
5         1          0.000000          0.000000
     1     293
5         1          0.000000          0.000000
     1     294
5         1          0.000000          0.000000
     1     295
5         1          0.000000          0.000000
     1     297
5         1          0.000000          0.000000
     1     298
5         1          0.000000          0.000000
     1     299
5         1          0.000000          0.000000
     1     300
5         1          0.000000          0.000000
     1     302
5         1          0.000000          0.000000
     1     303
5         1          0.000000          0.000000
     1     304
5         1          0.000000          0.000000
     1     305
5         1          0.000000          0.000000
     1     307
5         1          0.000000          0.000000
     1     308
5         1          0.000000          0.000000
     1     309
5         1          0.000000          0.000000
     1     310
5         1          0.000000          0.000000
     1     312
5         1          0.000000          0.000000
     1     313
5         1          0.000000          0.000000
     1     314
5         1          0.000000          0.000000
     1     315
5         1          0.000000          0.000000
     1     317
5         1          0.000000          0.000000
     1     318
5         1          0.000000          0.000000
     1     319
5         1          0.000000          0.000000
     1     320
5         1          0.000000          0.000000
     1     322
5         1          0.000000          0.000000
     1     323
5         1          0.000000          0.000000
     1     324
5         1          0.000000          0.000000
     1     325
5         1          0.000000          0.000000
     1     327
5         1          0.000000          0.000000
     1     328
5         1          0.000000          0.000000
     1     329
5         1          0.000000          0.000000
     1     330
5         1          0.000000          0.000000
     1     332
5         1          0.000000          0.000000
     1     333
5         1          0.000000          0.000000
     1     334
5         1          0.000000          0.000000
     1     335
5         1          0.000000          0.000000
     1     337
5         1          0.000000          0.000000
     1     338
5         1          0.000000          0.000000
     1     339
5         1          0.000000          0.000000
     1     340
5         1          0.000000          0.000000
     1     342
5         1          0.000000          0.000000
     1     343
5         1          0.000000          0.000000
```

```
     1     344
5       1          0.000000          0.000000
     1     345
5       1          0.000000          0.000000
     1     347
5       1          0.000000          0.000000
     1     348
5       1          0.000000          0.000000
     1     349
5       1          0.000000          0.000000
     1     350
5       1          0.000000          0.000000
     1     352
5       1          0.000000          0.000000
     1     353
5       1          0.000000          0.000000
     1     354
5       1          0.000000          0.000000
     1     355
5       1          0.000000          0.000000
     1     357
5       1          0.000000          0.000000
     1     358
5       1          0.000000          0.000000
     1     359
5       1          0.000000          0.000000
     1     360
5       1          0.000000          0.000000
     1     362
5       1          0.000000          0.000000
     1     363
5       1          0.000000          0.000000
     1     364
5       1          0.000000          0.000000
     1     365
5       1          0.000000          0.000000
     1     367
5       1          0.000000          0.000000
     1     368
5       1          0.000000          0.000000
     1     369
5       1          0.000000          0.000000
     1     370
5       1          0.000000          0.000000
     1     372
5       1          0.000000          0.000000
     1     373
5       1          0.000000          0.000000
     1     374
5       1          0.000000          0.000000
     1     375
5       1          0.000000          0.000000
     1     377
5       1          0.000000          0.000000
     1     378
5       1          0.000000          0.000000
     1     379
5       1          0.000000          0.000000
     1     380
5       1          0.000000          0.000000
     1     381
5       1          0.000000          0.000000
     1     383
5       1          0.000000          0.000000
     1     384
5       1          0.000000          0.000000
     1     385
5       1          0.000000          0.000000
     1     386
5       1          0.000000          0.000000
     1     388
5       1          0.000000          0.000000
     1     389
5       1          0.000000          0.000000
     1     390
5       1          0.000000          0.000000
     1     391
5       1          0.000000          0.000000
     1     393
5       1          0.000000          0.000000
     1     394
5       1          0.000000          0.000000
     1     395
5       1          0.000000          0.000000
     1     396
5       1          0.000000          0.000000
     1     398
5       1          0.000000          0.000000
     1     399
5       1          0.000000          0.000000
     1     400
5       1          0.000000          0.000000
     1     401
5       1          0.000000          0.000000
     1     403
5       1          0.000000          0.000000
     1     404
5       1          0.000000          0.000000
     1     405
5       1          0.000000          0.000000
     1     406
5       1          0.000000          0.000000
     1     408
5       1          0.000000          0.000000
     1     409
5       1          0.000000          0.000000
     1     410
5       1          0.000000          0.000000
     1     411
5       1          0.000000          0.000000
     1     413
5       1          0.000000          0.000000
     1     414
5       1          0.000000          0.000000
     1     415
5       1          0.000000          0.000000
     1     416
5       1          0.000000          0.000000
     1     418
5       1          0.000000          0.000000
     1     419
5       1          0.000000          0.000000
     1     420
5       1          0.000000          0.000000
     1     421
5       1          0.000000          0.000000
     1     423
5       1          0.000000          0.000000
     1     424
5       1          0.000000          0.000000
     1     425
5       1          0.000000          0.000000
     1     426
5       1          0.000000          0.000000
     1     428
5       1          0.000000          0.000000
     1     429
5       1          0.000000          0.000000
     1     430
5       1          0.000000          0.000000
     1     431
5       1          0.000000          0.000000
     1     433
5       1          0.000000          0.000000
     1     434
5       1          0.000000          0.000000
     1     435
5       1          0.000000          0.000000
     1     436
5       1          0.000000          0.000000
     1     438
5       1          0.000000          0.000000
     1     439
5       1          0.000000          0.000000
```

```
     1     440
5         1          0.000000          0.000000
     1     441
5         1          0.000000          0.000000
     1     443
5         1          0.000000          0.000000
     1     444
5         1          0.000000          0.000000
     1     445
5         1          0.000000          0.000000
     1     446
5         1          0.000000          0.000000
     1     448
5         1          0.000000          0.000000
     1     449
5         1          0.000000          0.000000
     1     450
5         1          0.000000          0.000000
     1     451
5         1          0.000000          0.000000
     1     453
5         1          0.000000          0.000000
     1     454
5         1          0.000000          0.000000
     1     455
5         1          0.000000          0.000000
     1     456
5         1          0.000000          0.000000
     1     458
5         1          0.000000          0.000000
     1     459
5         1          0.000000          0.000000
     1     460
5         1          0.000000          0.000000
     1     461
5         1          0.000000          0.000000
     1     463
5         1          0.000000          0.000000
     1     464
5         1          0.000000          0.000000
     1     465
5         1          0.000000          0.000000
     1     466
5         1          0.000000          0.000000
     1     468
5         1          0.000000          0.000000
     1     469
5         1          0.000000          0.000000
     1     470
5         1          0.000000          0.000000
     1     471
5         1          0.000000          0.000000
     1     473
5         1          0.000000          0.000000
     1     474
5         1          0.000000          0.000000
     1     475
5         1          0.000000          0.000000
     1     476
5         1          0.000000          0.000000
     1     478
5         1          0.000000          0.000000
     1     479
5         1          0.000000          0.000000
     1     480
5         1          0.000000          0.000000
     1     481
5         1          0.000000          0.000000
     1     483
5         1          0.000000          0.000000
     1     484
5         1          0.000000          0.000000
     1     485
5         1          0.000000          0.000000
     1     486
5         1          0.000000          0.000000
     1     488
5         1          0.000000          0.000000
     1     489
5         1          0.000000          0.000000
     1     490
5         1          0.000000          0.000000
     1     491
5         1          0.000000          0.000000
     1     493
5         1          0.000000          0.000000
     1     494
5         1          0.000000          0.000000
     1     495
5         1          0.000000          0.000000
     1     496
5         1          0.000000          0.000000
     1     498
5         1          0.000000          0.000000
     1     499
5         1          0.000000          0.000000
     1     500
5         1          0.000000          0.000000
     1     501
5         1          0.000000          0.000000
     1     503
5         1          0.000000          0.000000
     1     504
5         1          0.000000          0.000000
     1     505
5         1          0.000000          0.000000
     1     506
5         1          0.000000          0.000000
     1     508
5         1          0.000000          0.000000
     1     509
5         1          0.000000          0.000000
     1     510
5         1          0.000000          0.000000
     1     511
5         1          0.000000          0.000000
     1     513
5         1          0.000000          0.000000
     1     514
5         1          0.000000          0.000000
     1     515
5         1          0.000000          0.000000
     1     516
5         1          0.000000          0.000000
     1     518
5         1          0.000000          0.000000
     1     519
5         1          0.000000          0.000000
     1     520
5         1          0.000000          0.000000
     1     521
5         1          0.000000          0.000000
     1     523
5         1          0.000000          0.000000
     1     524
5         1          0.000000          0.000000
     1     525
5         1          0.000000          0.000000
     1     526
5         1          0.000000          0.000000
     1     528
5         1          0.000000          0.000000
     1     529
5         1          0.000000          0.000000
     1     530
5         1          0.000000          0.000000
     1     531
5         1          0.000000          0.000000
     1     533
5         1          0.000000          0.000000
     1     534
5         1          0.000000          0.000000
     1     535
5         1          0.000000          0.000000
```

```
     1     536
5       1          0.000000          0.000000
     1     538
5       1          0.000000          0.000000
     1     539
5       1          0.000000          0.000000
     1     540
5       1          0.000000          0.000000
     1     541
5       1          0.000000          0.000000
     1     543
5       1          0.000000          0.000000
     1     544
5       1          0.000000          0.000000
     1     545
5       1          0.000000          0.000000
     1     546
5       1          0.000000          0.000000
     1     548
5       1          0.000000          0.000000
     1     549
5       1          0.000000          0.000000
     1     550
5       1          0.000000          0.000000
     1     551
5       1          0.000000          0.000000
     1     553
5       1          0.000000          0.000000
     1     554
5       1          0.000000          0.000000
     1     555
5       1          0.000000          0.000000
     1     556
5       1          0.000000          0.000000
     1     558
5       1          0.000000          0.000000
     1     559
5       1          0.000000          0.000000
     1     560
5       1          0.000000          0.000000
     1     561
5       1          0.000000          0.000000
     1     563
5       1          0.000000          0.000000
     1     564
5       1          0.000000          0.000000
     1     565
5       1          0.000000          0.000000
     1     566
5       1          0.000000          0.000000
     1     568
5       1          0.000000          0.000000
     1     569
5       1          0.000000          0.000000
     1     570
5       1          0.000000          0.000000
     1     571
5       1          0.000000          0.000000
     1     573
5       1          0.000000          0.000000
     1     574
5       1          0.000000          0.000000
     1     575
5       1          0.000000          0.000000
     1     576
5       1          0.000000          0.000000
     1     578
5       1          0.000000          0.000000
     1     579
5       1          0.000000          0.000000
     1     580
5       1          0.000000          0.000000
     1     581
5       1          0.000000          0.000000
     1     583
5       1          0.000000          0.000000
     1     584
5       1          0.000000          0.000000
     1     585
5       1          0.000000          0.000000
     1     586
5       1          0.000000          0.000000
     1     588
5       1          0.000000          0.000000
     1     589
5       1          0.000000          0.000000
     1     590
5       1          0.000000          0.000000
     1     591
5       1          0.000000          0.000000
     1     593
5       1          0.000000          0.000000
     1     594
5       1          0.000000          0.000000
     1     595
5       1          0.000000          0.000000
     1     596
5       1          0.000000          0.000000
     1     598
5       1          0.000000          0.000000
     1     599
5       1          0.000000          0.000000
     1     600
5       1          0.000000          0.000000
     5     601
1       1     101325.000000          0.000000
2       3          0.500000          0.005000
3       3       -298.150000         -5.000000
4       1          0.000000          0.000000
5       1          0.000000          0.000000
     4     602
1       1     101325.000000          0.000000
2       3          0.500000          0.005000
3       3       -298.150000         -5.000000
4       1          0.000000          0.000000
     5     603
1       1     101325.000000          0.000000
2       3          0.500000          0.005000
3       3       -298.150000         -5.000000
4       1          0.000000          0.000000
5       1          0.000000          0.000000
$ Stop input data file
```

Appendix 4C

Appendix 4C.1 ACCEPTED PUBLICATIONS RELATED TO THIS CHAPTER

In this Appendix are included the publications concerning the subjects dealt in this chapter that, up to the date of this Thesis writing, have been accepted in specialized congresses related to the topics involved herein. Find enclosed the brochure of the Congress, the abstract submitted for its acceptance and the confirmation of its acceptance:

Brochure of the Congress where the abstract was submitted (Page I of II).

COUPLED PROBLEMS 2009

8-11 June 2009, Ischia Island, Spain

How to register and submit contributions

Authors are invited to submit their contributions on any of the conference topics. Submission of contributions and conference registration should be performed electronically via the conference web site.

http://congress.cimne.upc.es/coupled09

Conference Chairmen

B. Schrefler Università degli Studi di Padova, Italy
E. Oñate Universitat Politècnica de Catalunya, Spain
M. Papadrakakis National Technical University of Athens, Greece

Technical Advisory Panel

C. Agelet de Saracibar, *Spain*
M.H. Alibadi, *UK*
F. Armero, *US*
M. Arroyo, *Spain*
K.-J. Bathe, *USA*
G. Beer, *Austria*
M. Casteleiro, *Spain*
M. Cervera, *Spain*
M. Chiumenti, *Spain*
F. Chinesta, *France*
R. Codina, *Spain*
J.-P. Coyette, *Belgium*
M. Dobbiare, *Spain*
C. Farhat, *USA*
C. Felippa, *USA*
J. Fish, *USA*
L. Gastaldi, *Italy*
J.M. Goicolea, *Spain*
A. Guerrero, *Spain*
A. Huerta, *Spain*
T.J.R. Hughes, *USA*
J.M. Huyghes, *The Netherlands*
S. Idelsohn, *Argentina*
H. Irschik, *Austria*
G.E. Kamiadakis, *USA*
A.J. Kassab, *USA*
P. Ladeveze, *France*
R. Lerch, *Germany*
R.W. Lewis, *U.K.*
W.K. Liu, *USA*
C. Majorana, *Italy*
J. Mora, *Spain*
H. Muhlhaus, *Australia*
R. Ohayon, *France*
R. Owen, *U.K.*
K. C. Park, *USA*
J. Periaux, *France*
G. Pijaudier-Cabot, *France*
P.M. Pinsky, *USA*
E. Ramm, *Germany*
E. Rank, *Germany*
K. Runesson, *Sweden*
A. Tadeu, *Portugal*
T. Tezduyar, *USA*
O. von Estorff, *Germany*
W. Wall, *Germany*
N.-E. Wiberg, *Sweden*
P. Wriggers, *Germany*

View of Ischia Island

Important Dates

Deadline for presenting one page abstract	30 October 2008
Acceptance of the contributions and instruction	28 November 2008
Deadline for submitting the final contribution and early payment	27 February 2009
Hotel booking	available at the congress site

Objectives

The increasing necessity to solve complex problems in science and engineering accounting for all the coupling occurring on the different scales of the problem requires the development of new ideas and methods which can effectively provide accurate numerical solutions in affordable computing times.

The objective of Coupled Problems 2009 is to present and discuss state of the art, mathematical methods, numerical methods and computational techniques for solving coupling problems of multidisciplinary character in science and engineering. Emphasis will be given on showing the potential of new computational methods for solving practical multidisciplinary problems of industrial interest.

Previous editions on the conference were held in the Island of Santorini, Greece (2005) and Ibiza, Spain (2007). Coupled Problems 2007 attracted somie 180 participants. The goal of COUPLED PROBLEMS 2009 is to make a step forwards in the formulation and solution of real life problems with a multidisciplinary vision accounting for all the complex couplings involved in the physical description of the problem.

Conference Topics

Papers are welcomed in one of the following topics (the list is not exhaustive):

- Mathematical formulation of multidisciplinary, multiphysics problems
- Numerical methods for coupled problems: finite elements, finite volume, finite differences, meshless methods, etc.
- Coupled solution strategies. Loose and strong coupling schemes.
- Computational methods for multiscale problems
- Distributed computing methods. Grid computing technologies.
- Optimum design in multi-disciplinary problems
- Applications in science and engineering: thermo-mechanical problems, soil-structure-interaction, electro-magnetic-dynamic problems, aero-acoustic, geomechanics, etc.

Location

The conference will take place at the Hotel Continental Terme in the island of Ischia in Italy (http://www.continentaleterme.it). Ischia is one of the most appealing islands in the Mediterranean sea with beautiful beaches and landscapes, and interesting cultural heritage and exselent cuisine.

Brochure of the Congress where the abstract was submitted (Page II of II).
Remark: Note that the author is included in the Technical Advisory Panel of the Congress.

SPALLING NOMOGRAMS IN HIGH-STRENGTH CONCRETE STRUCTURES OF HIGH-RISE BUILDINGS UNDER NATURAL FIRE

ANGEL GUERRERO[*], FRANCESCO PESAVENTO[†] AND FREDERIC MARIMON[*]

[*] Dept. of Materials Resistance and Structures in Engineering
Universitat Politècnica de Catalunya
Av. Diagonal 647, 08028 Barcelona - Spain
email: gptcce_guerrero@teleline.es, frederic.marimon@upc.edu

[†] Dept. of Structural and Transportation Engineering
University of Padova
Via F. Marzolo 9, 34131 Padova – Italy
email: pesa@dic.unipd.it

Key words: Concrete, Coupled model, Hitecosp, Spalling, Natural Fire, High-Rise building, Nomogram, Eurocode 1 Part 1-2

The first aim of this paper is to expose a spectrum of spalling nomograms recently developed from an amount of 91 cases analyzed by means of Hitecosp software[1] and addressed, as an starting point, to evaluate the sensitivity of the hygro-thermo-chemo-mechanical processes involved on the High-Strength concretes behaviour under a natural fire to some relevant parameters whose values may be chosen from a very early stage of High-Rise Buildings design or already known in case of existing High-Rise Buildings, such as the initial moisture content of concrete, its intrinsic permeability, the rate of temperature increase (fire intensity), the porosity, compressive strength, type of aggregate and, in general, the whole set of hygro-thermo-chemical properties of concrete, and the dimensions of the structural element. As it will be described, the spalling nomograms will show, as a first overall conclusion, that a high initial moisture content, a high heating rate, a low concrete porosity (hence also permeability), an additional compressive load parallel to the heated surface, and the use of aggregates with high thermal expansion are in general factors favouring Thermal Spalling.

The second but not less important aim of the spalling nomograms described herein, is to analyse if spalling is energetically possible and, hence, the spalling risk in every of the 91 sets of conditions so both Designers and Fire Fighting Services may have a valuable information in order to take decisions about design and about the expectable consequences of fire fighting actions from a really intuitive, graphical and immediate point of view.

An essential contribution of this work is to discern what is the energetic contribution, within spalling process, of both the compressed gas (the build-up of high pore pressure close to the heated concrete surface as a result of rapid evaporation of the moisture) and the constrained elastic energy (due to the thermal stresses resulting from high values of restrained strains caused by temperature gradients). As it will be explained later on, for the highest levels of the Intrinsic Permeability, the main contributor is the constrained elastic energy ΔU whilst for its lowest levels the main contributor is the compressed gas W. Furthermore, in general the Initial Saturation Degree does not affect significantly, within the considered range of values, to the relative energetic contribution of both factors.

Some parallel and also relevant contributions of the work presented in this paper are related to the type of spalling that is expectable in each situation (either violent and explosive or slow in nature), to the extent of the spalling and, even more relevant, to the instant when spalling is expected. For example, referring only to the cases with heating curves ranging from the slowest Parametric Heating curves admitted in Eurocode 1, Part 1-2 up to the fast ISO834 Heating curve, the case with the highest average velocity of the spalled-off pieces is that corresponding to an Initial Saturation Degree at 60%, an Intrinsic Permeability value of 10^{-19} m^2, an ISO834 heating curve and a C60 material. The mean velocity of the spalled-off pieces considering only the spalling cases not related to Hydrocarbon heating curves is 7,1 m/s and its median value is 4,8 m/s.

REFERENCES

[1] Brite Euram III BRPR-CT95-0065 HITECO, *Understanding and industrial application of High Performance Concrete in High Temperature Environment – Final report*, 1999.

Abstract submitted to the Congress and currently accepted.

De: *coupled09@cimne.upc.edu [mailto:coupled09@cimne.upc.edu]*
Enviado el: *viernes, 28 de noviembre de 2008 16:22*
Para: *aguerrero*
Asunto: *Notification of Acceptance and General Guidelines*

Paper Ref: 124 Title: Spalling Nomograms in High-Strength Concrete Structures of High-Rise Buildings under Natural Fires

Dear Eng. Angel Guerrero Castells

We are pleased to notify you that your paper ***has been accepted*** *for presentation at the III International Conference on Computational Methods for Coupled Problems in Science and Engineering - COUPLED PROBLEMS 2009.*

The following instructions will hopefully clarify the procedure for submitting the extended abstract and for the registration to the Conference.

Extended Abstract Submission

Authors are invited ! to submit electronically, through the web site of the Conference http://congress.cimne.upc.es/coupled09 , before February 27, 2009 the Extended Abstract to be published in the Proceedings to be distributed to all participants at the Conference.

Full instructions for writing and submitting the extended abstract can be found in the Instructions for Authors on the conference web site http://congress.cimne.upc.es/coupled09/frontal/Autor.asp

Authors are asked to submit the files in .pdf format. Other formats are not accepted by the system.

About Registration to COUPLED PROBLEMS 2009

Please note that acceptance of papers for presentation is conditional to receiving the final version of the Extended Abstract in publication format, and the payment of the speaker's congress registration fee, during the advance period (before February 27th, 2009) . Only one presentation per author is allowed.

We thank you for your participation in COUPLED PROBLEMS 2009 and look forward to meeting you in Ischia, Italy, on June 8 - 10 2009.

Sincerely yours,

Bernhard Schrefler
Eugenio Oñate
Manolis Papadrakakis
COUPLED PROBLEMS 2009 Chairmen

Acceptance of the Abstract submitted to the Congress.

Chapter 5

PRELIMINARY AND SIMPLIFIED ANALYSIS OF COOLING EFFECT ON HSCs SPALLING BEHAVIOUR

THIS PAGE IS INTENTIONALLY
LEFT BLANK

Chapter 5

PRELIMINARY AND SIMPLIFIED ANALYSIS OF COOLING EFFECT ON HSCs SPALLING BEHAVIOUR

The first aim of this chapter is to establish a methodology for a preliminary and simplified analysis of the effect of a forced cooling on the spalling behaviour of High Strength (and Very High Strength) Concretes in order to evaluate if it is significant enough to justify a relevant, greater and deeper work concerning this matter. A secondary aim of this chapter is to formulate some preliminary conclusions that may help to orientate better the analysis to be done later on models of a much higher complexity and requiring huge computational and postprocessing efforts.

5.1 METHODOLOGY FOR THE PRELIMINARY AND SIMPLIFIED ANALYSIS OF COOLING EFFECT ON HSC SPALLING BEHAVIOUR

As explained in the chapter concerning the historical evolution of spalling evaluation methodologies, to assess the thermal spalling risk several authors [1-7] have discussed some quantitative criteria based on different physical phenomena leading to thermal spalling of concrete layers of pieces from a heated surface.

However, most of these criteria were based on an experimental basis only, often in the form of diagrams showing 'area of the spalling risk' as a function of several concrete properties like permeability or tensile strength, being their validity limited to the materials and element geometries used in the tests they were based on. There were also formulated some analytical criteria, using limit state analysis [4,6], but they were usually based on simplified models of concrete performance during heating, by evaluating the thermally induced stress and/or vapour pressures. Mainly, criteria presented in the past fall into three categories [8]:

1. Criteria based on pore pressure prediction, which consider the pore pressure as responsible for thermal spalling [7]. Usually, the models employed for the description of the hygral state of concrete are rather simple. For example, mass transport in concrete pores is considered as a purely diffusive phenomenon [6,9], or pore pressure is directly evaluated by using an idealized spherical model for the pores of the material [5]. In some cases the so-called ''moisture clog'' is indicated as the main cause of spalling [3].
2. Criteria based on thermal stresses. These are the simplest ones and are related to the non-uniform thermal stresses that can reach the maximum compressive strength of concrete for a given temperature, e.g. [2].
3. Criteria based on combined action of thermal stresses and pore pressure. This class of spalling criteria encompasses the criteria by Zhukov [4] and Connelly [6]. The first author proposed a method for the evaluation of the strain energy density in the direction of the heated surface W_x, taking into account the stresses due to external mechanical load, thermal field and pore pressure acting on a slab heated on one face. The spalling occurs when the strain energy density W_x in x-direction equals the rupture energy density defined on the basis of tensile strength of concrete. Connelly [6] extended Zhukov's model considering pore pressure stresses as acting simultaneously in the three directions x, y, z. The critical state for spalling was hence defined in a way similar to Zhukov's approach.

These criteria omitted the complexity of hygro-thermal and chemo-physical processes in concrete at high temperature so they were not able to give a realistic evaluation of the thermal spalling risk.

Gawin, Pesavento and Schrefler [8] have recently developed simplified models of thermal spalling used to define special indexes aiming for quantitative assessment of its risk, considering both effects of pore pressure build-up and the accumulated strain energy, together with thermo-chemical material degradation and cracking, namely:

1. Pressure-induced shear model, which predicts the 'plastic' failure of the material constraints for the external layer, leading to a spalling index called I_{s1}.
2. Buckling model considering gas pressure, involving the hypothesis of buckling of a zone which is initially delaminated from the rest of the structure, leading to a spalling index called I_{s2}.
3. And, finally, a simplified fracture mechanics model, where the main mechanism considered for the compressive failure is the sideways propagation of a band of parallel axial splitting cracks, leading to a spalling index called I_{s3}.

Although these three models have been tested for the results of numerical simulations based on an experimental test described in the following paragraphs, showing their usefulness in the prediction of both the time and position of concrete rupture, a fourth spalling index [8] called 'intuitive' or I_{s4}, based on the analysis of physical phenomena during heating of concrete and leading to thermal spalling, will be selected for these evaluation since, as it will be explained later, it showed the best correlation against tests.

The selected spalling index is obtained choosing the following factors favouring thermal spalling: high local values of gas overpressure, p^g- p_{atm}, and mechanical damage parameter, d, high values of averaged transversal traction stresses, σ_{th}, and constrained elastic energy $\overline{U}$ .The considered factors impeding thermal spalling are high average values of traction strength, $\overline{f}_t$, and specific fracture energy, $\overline{G}f$, for the material layer between a current position and the heated surface. Additionally, to obtain a non-dimensional quantity, [8] introduced a reference pressure (assume as equal to atmospheric pressure, p_{atm}) and a characteristic element dimension L (e.g. thickness for a wall, radius for a cylindrical specimen). Finally, internal geometrical parameters involved are unknown and are jointly described by a scaling factor, C_s, which is a non-dimensional parameter. Therefore, the fourth spalling index selected herein, I_{s4}, is given by the following relation:

$$I_{s4} = \frac{\overline{\sigma}_{th} \cdot \overline{U} \cdot d}{\overline{f}_t \cdot \overline{G}_f} \cdot \frac{p^g - p_{atm}}{p_{atm}} \cdot L \cdot C_s \tag{5.1}$$

Before using this spalling index to analyse, through a preliminary and simplified methodology, the effect of cooling on HSCs spalling behaviour, on the next paragraphs is shown the capability of I_{s4} to predict spalling behaviour through a selected experimental case.

5.1.1 Selection and development of the case for the evaluation of the I_{s4} spalling index capabilities

5.1.1.1 THE CRITERIA FOR THE SELECTION OF THE CASE FOR THE EVALUATION OF THE I_{S4} SPALLING INDEX

In the next paragraphs, an experimental case dealt by [8] to test the spalling index I_{s4} for the numerical results done at NIST for a C-90 concrete (with a compressive strength at ambient temperature of 98,2 MPa) exposed to the temperature of 450 ºC [10-13] is presented. These results are particularly suitable for this purpose because during the developed tests all three cylindrical specimens of the concrete, called MIX 1, experienced thermal spalling at a thickness of about 2 cm from the heated surface.

It is also suitable for the purpose of this chapter because both the mechanical and thermal properties of the MIX 1 concrete and others describing its main thermo-hygral-chemo-mechanical behaviour are known after the tests.

5.1.1.2 THE SETUP OF THE CASE SELECTED FOR THE EVALUATION OF THE I_{S4} SPALLING INDEX

The main aim of the tests carried out at NIST laboratories [10-13] was to evaluate the thermo-mechanical behaviour of concrete exposed to high temperature, in particular the measurement of Young's modulus and compressive strength as function of temperature for four different HPCs of different mixture composition. The cylindrical specimens, all of them with diameter of 100 mm and height of 200 mm, were tested using different test methods and target temperature of 450 ºC for the concrete indicated as MIX1 (with f_c = 98,2 MPa, w/c = 0,22, 10% of cement mass replaced by silica fume). All specimens of the mixture experienced explosive spalling, being that the main reason for the present selection of this test results as the evaluation case of I_{S4} capability to predict spalling behaviour and, after that, for the preliminary and simplified analysis of the cooling effect on HSCs spalling behaviour.

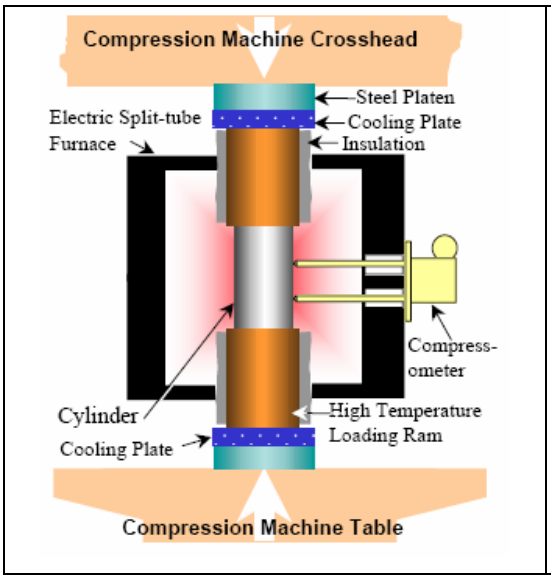

Figure 5-1. *Mechanical Property test setup (both figures excerpt from [14])*

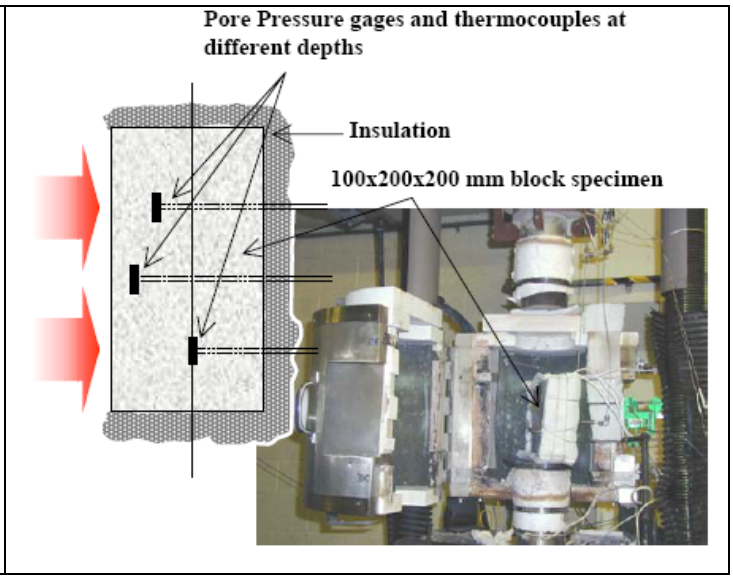

Figure 5-2. *Pore pressure specimen and test setup*

During the test, heating rate was initially equal to 5 K/min and heating was stopped when the temperature in the centre of the specimen was within 10 K of the target temperature T, and the difference between the surface and centre temperatures of the concrete specimen was less than 10 K. For further details concerning the mix compositions and test procedures, see [10-13].

Basic material parameters of MIX1, used in the following simulations by [8], are next summarised:

Table 5-1. Main properties of MIX 1 concrete at 20 ºC

Material property	MIX 1 value
Water / binder ratio, w/b [-]	0,22
Binder content [kg/m^3]	OPC: 596 + micro-silica: 65,7
Aggregate type and size	Limestone, max. size of 13 mm
MIP porosity, n[%]	7.7
Water intrinsic permeability, k_0 [m^2]	2 x 10^{-19}
Young modulus, E [GPa]	36,7
Poisson's ratio, ν [-]	0,18
Thermal Conductiviy, χ [W/m K]	2,5
Specific heat, C_p [J/kg K]	800

(For a more extensive description of MIX 1 properties and their evolution with temperature, see Chapter 4)

5.1.1.3 THE MAIN EXPERIMENTAL RESULTS OBTAINED FOR THE CASE SELECTED FOR THE EVALUATION OF THE I_{S4} SPALLING INDEX

Figures 5-3 and 5-4 show both the temperature development during tests at different depths of the Mixture 1 cylinder and the temperature difference, DT, between the surface and the centre of the specimens measured during the tests. A remark about the initial phase of heating must be done since the experimental profile shows that temperature difference between core and surface is practically zero for more than one hour, what was probably caused by some temperature measurement problems.

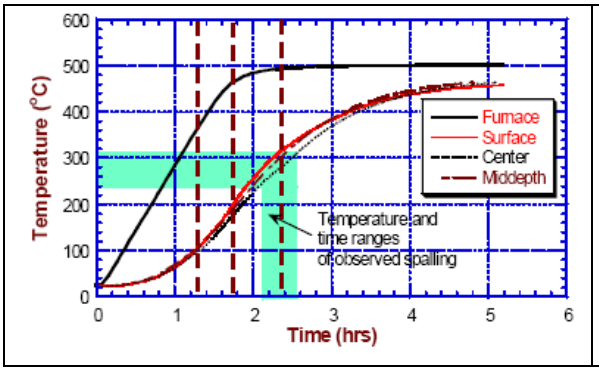

Figure 5-3. *Temperature development on Mixture 1 cylinder (excerpt from [14])*

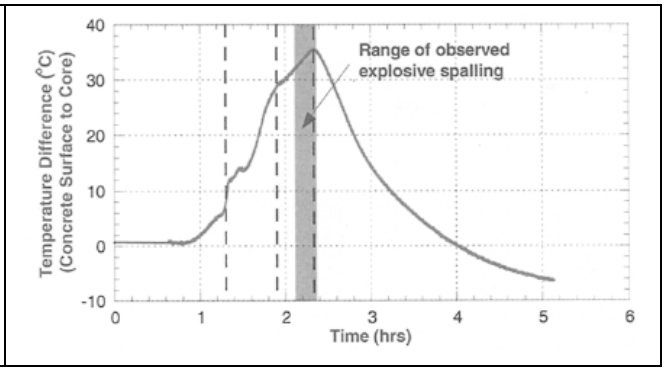

Figure 5-4. *Thermal gradient between surface and core of Mixture 1 cylinder (excerpt from [12])*

Figure 5-5. *Remnants of an exploded cylinder and rendering of fracture formation (excerpt from [14])*

As shown in these figures, the temperature distribution inside the specimen has a complex history compared with the furnace air temperature. There were observed 'perturbations' in the rates of temperature rise that occurred at different times during heating. In general, three types of perturbations were observed with increasing temperature:

1. A sudden decrease in the rate of temperature rise at the centre;
2. An increase in the rate of temperature rise on the surface and beginning of a simultaneous decrease in the temperature rise at the centre; and
3. An increase in the rate of temperature rise at the centre.

Examples of these perturbations are marked in the figures 5-3 and 5-4 by vertical dashed lines. It is believed that these perturbations are related to different stages of the moisture transformation and transport process (vaporization and movement of free and chemically bound water) that occur in the specimen during heating. The first two perturbations in the rates of temperature rise at the centre and the surface of the specimen coincided with concrete temperatures of about 100 °C and 180 °C (see figure 5-3). At slightly above 100 °C, free water in the concrete begins to evaporate rapidly. A moisture front is driven by the heat towards the centre of the specimen, causing a decrease in the rate of temperature rise at the specimen centre and thus an increase in the temperature difference between the cylinder's surface and centre. When the centre reaches about 180 °C, a significant amount chemically bound water is released. This caused a similar decrease in the rate of temperature rise at centre. In addition, the rate of temperature rise on the surface increases, presumably due to a reduction in the evaporative cooling effect, as marked by the second vertical dashed line in both 5-3 and 5-4 figures.

The temperature difference between the surface and centre reaches a maximum of 36 °C at a corresponding centre temperature of 270 °C. This coincides the third major perturbation in the rates of temperature rise in the cylinder. In this case there is a rapid increase in the rate of temperature rise at centre (third vertical dashed line). After this point, the rate of temperature rise on the concrete surface is lower than that of the centre, causing the temperature difference to decrease as shown in figure 5-4.

Examination of exploded cylinders showed that typically there was a large intact core, measured approximately 70 x 120 mm, which was surrounded by an approximately 20 mm-thick outer concrete shell (see figure 5-5). It appears that explosive spalling of the cylinders occurs by separation of the 20 mm thick shell from the core. This is consistent with the notion that explosive failure results (partially) from the build-up of internal vapour pressure. All cylinders of mixture I exploded while being heated to 450 °C.

The mean concrete temperatures (at 25 mm deep in the cylinder) when explosive spalling occurred was about 250 °C, with an approximate range of ± 50 °C (see figures 5-3 and 5-4). As can be seen in the figure 5-4, the temperature range in which explosive spalling occurred coincides with the time of high thermal gradient between the surface and centre. This suggests that, while internal pore pressure may be one of the primary causes for the explosive spalling of the specimens, the build-up of thermally induced strains might also have an important role in this failure.

5.1.1.4 THE NUMERICAL SIMULATION DEVELOPED FOR THE CASE SELECTED FOR THE EVALUATION OF THE I_{S4} SPALLING INDEX

The mesh needed for the numerical simulation of the experimental case described on previous paragraphs must be defined with enough refinement to show the sharp differences in the radial distribution of parameters such as gas pressure that were observed during tests.

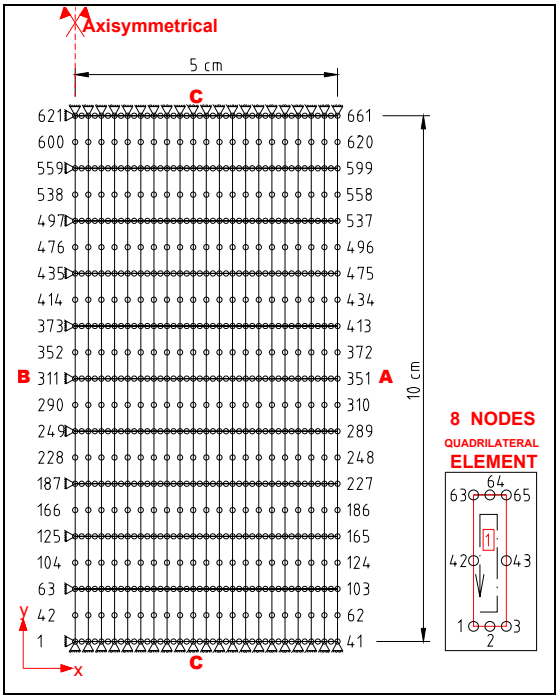

Figure 5-6. *Axisymmetric model, figures and element detail*

Side	Variables	Values and coefficients
A	u_x	$u_x = 0$
	u_y	$u_y = 0$
	p^g	$p^g = 101.325$ Pa
	p^c	$p^c = 1000$ Pa, β_c = variable
	T: convective	T = See figure 5-7, α_c = variable
	T: radiative	$e\sigma_0 = 5{,}1 \times 10^{-8}$ W m^{-2} K^{-1}
B	u_x	$u_x = 0$
	p^g	$q^g = 0$ (dry air flux = 0)
	p^c	$q^{gw} = q^w = 0$ (vapour flux = 0)
	T	$q^T = 0$ (heat flux = 0)
C	u_y	$u_y = 0$
	p^g	$q^g = 0$
	p^c	$q^{gw} = q^w = 0$
	T	$q^T = 0$

Table 5-2. *Boundary conditions used in the numerical simulation of the NIST case*

Due to the nature of the test developed, an axisymmetric model with a total number of 200 eight-nodes quadrilateral elements, with 40 degrees of freedom and a 3x3 order of integration, and 661 nodes, and the boundary conditions exposed on the table 5-2 has been implemented.

According to the different stages of the heating curve defined in the test, curve which is shown in the figure 5-7, the simulation has been divided into the following five stages with different time steps and frequency of results recording:

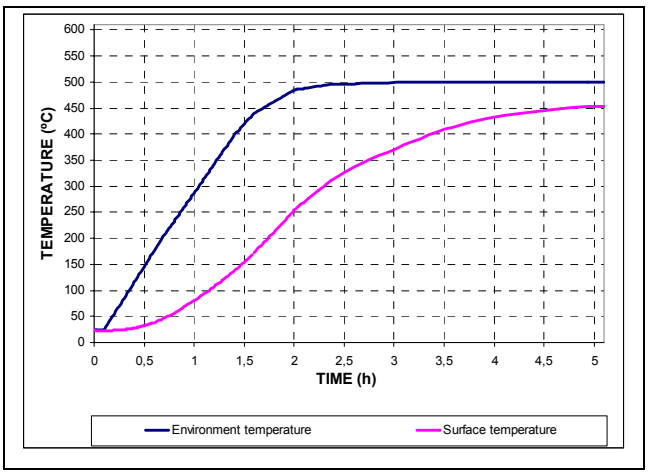

Input file name	Initial time (s)	Time step (s)	Number of time steps	Freq. results record (time steps)	Final time (s)
C90NIST1_01	0	1E-6	10	10	1E-5
C90NIST1_02	1E-5	0,5	720	120	360
C90NIST1_03	360	6	1.200	10	7.560
C90NIST1_04	7.560	12	600	50	14.760
C90NIST1_05	14.760	12	300	50	18.360

Table 5-3. *Time history of the simulation stages*

Figure 5-7. *Environment and surface Temperature time history*

Time evolution and radial distributions of the parameters necessary to compare the values of the I_{s4} spalling index against the experimental spalling behaviour will be extracted both from the simulation and from available literature as it will be explained on next paragraph.

5.1.1.5 THE RESULTS OF THE NUMERICAL SIMULATION AND THEIR COMPARISON AGAINST EXPERIMENTAL RESULTS

The surface of the concrete cylinder is heated both by a convective flux and by a radiation flux, what results in a gradual increase of the element temperature, starting from the surface zone (see figure 5-8).

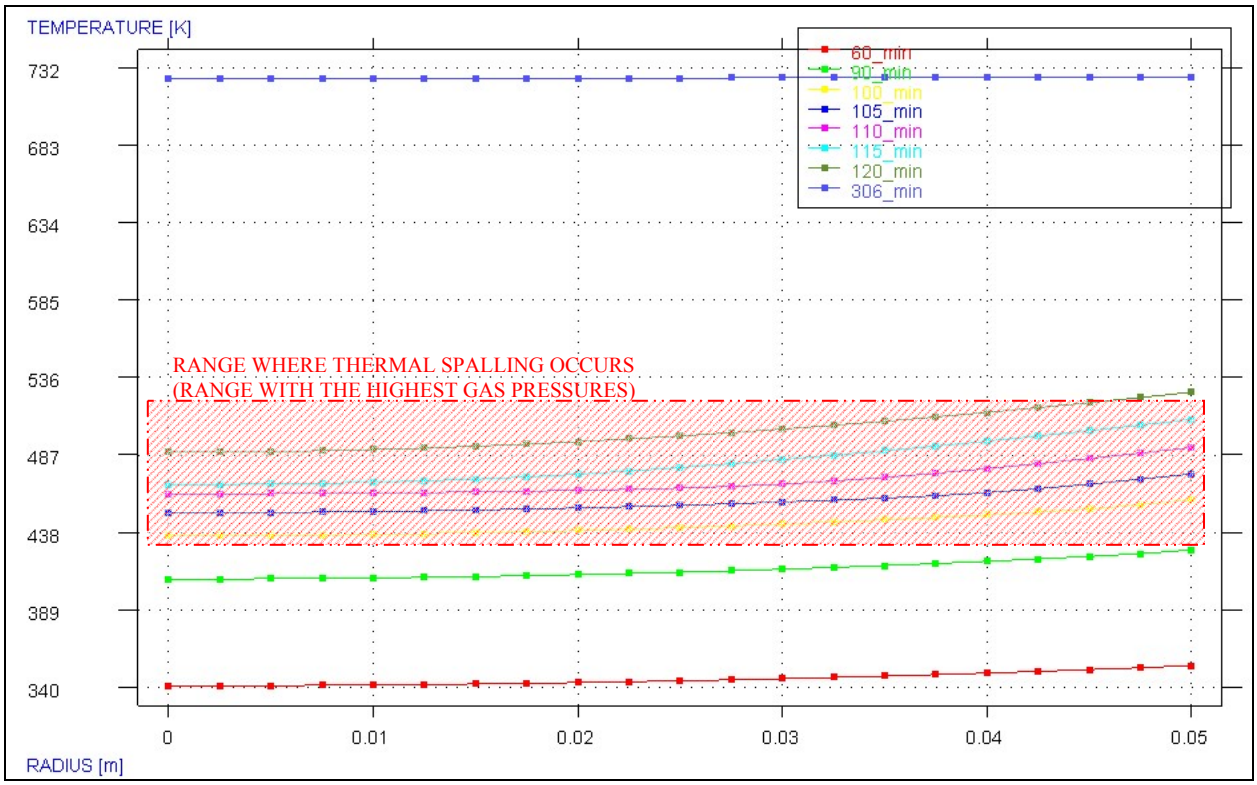

Figure 5-8. *Radial distribution of temperature (right side: surface; left side: cylinder axis)*

The temperature gradients appear, in part, because almost all moisture must evaporate in the temperature range of 100-200ºC before a further temperature increase, what requires a

considerable amount of energy. Figure 5-9 shows the temperature difference, DT, between the surface and the centre of the specimens measured during the tests and the corresponding numerical value.

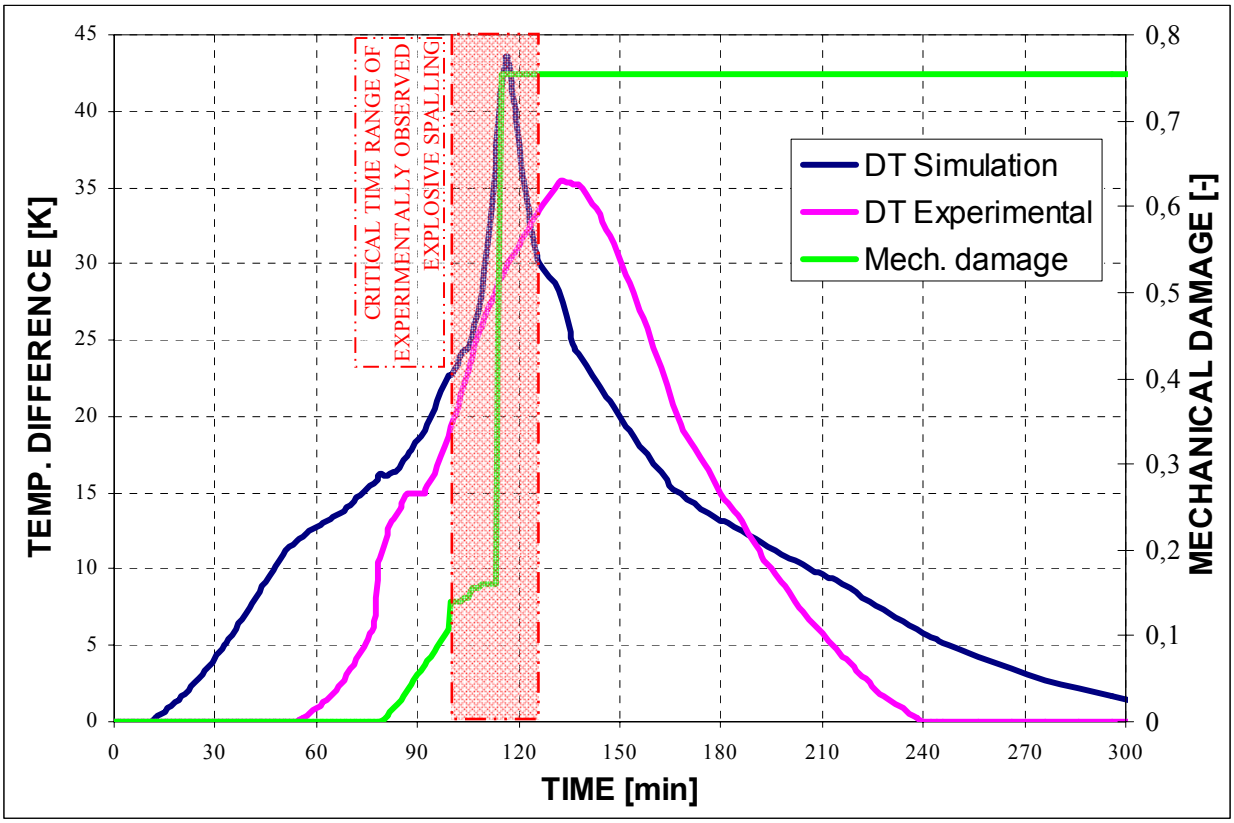

Figure 5-9: *Temperature difference between the surface and the cylinder axis, and mechanical damage at middle of the radius.*

The accordance between numerical and experimental results is quite good, except of the initial phase of heating, when the experimental profile shows that temperature difference between core and surface is practically zero for more than one hour, what was probably caused by some temperature measurement problems. In this case, since the heating process is rather slow if compared for example with an ISO fire, the phenomena observed next in the results are not so sharp and sudden as it might be in other real fire cases.

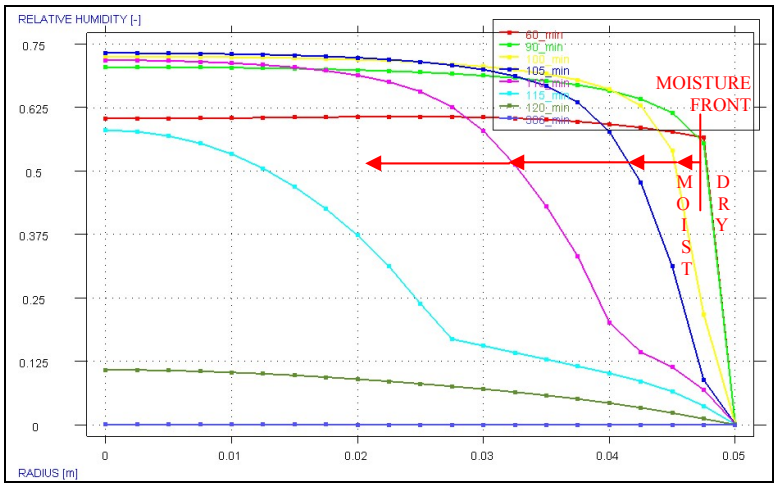

Figure 5-10: *Radial distribution of Relative Humidity (right side: surface; left side: cylinder axis).*

Due to moisture evaporation, the relative humidity in the surface zone (initially 50% for this case) decreases to a very low value, figure 5-10, and an initially sharp front, separating the moist and dry material, moves inwards. At this front intensive evaporation takes place, increasing considerably the vapour pressure (see figure 5-11). The maximum values of vapour and gas pressures (figures 5-11 and 5-12 respectively) increase initially, then they remain almost constant as the surface temperature increases and the front moves inwards.

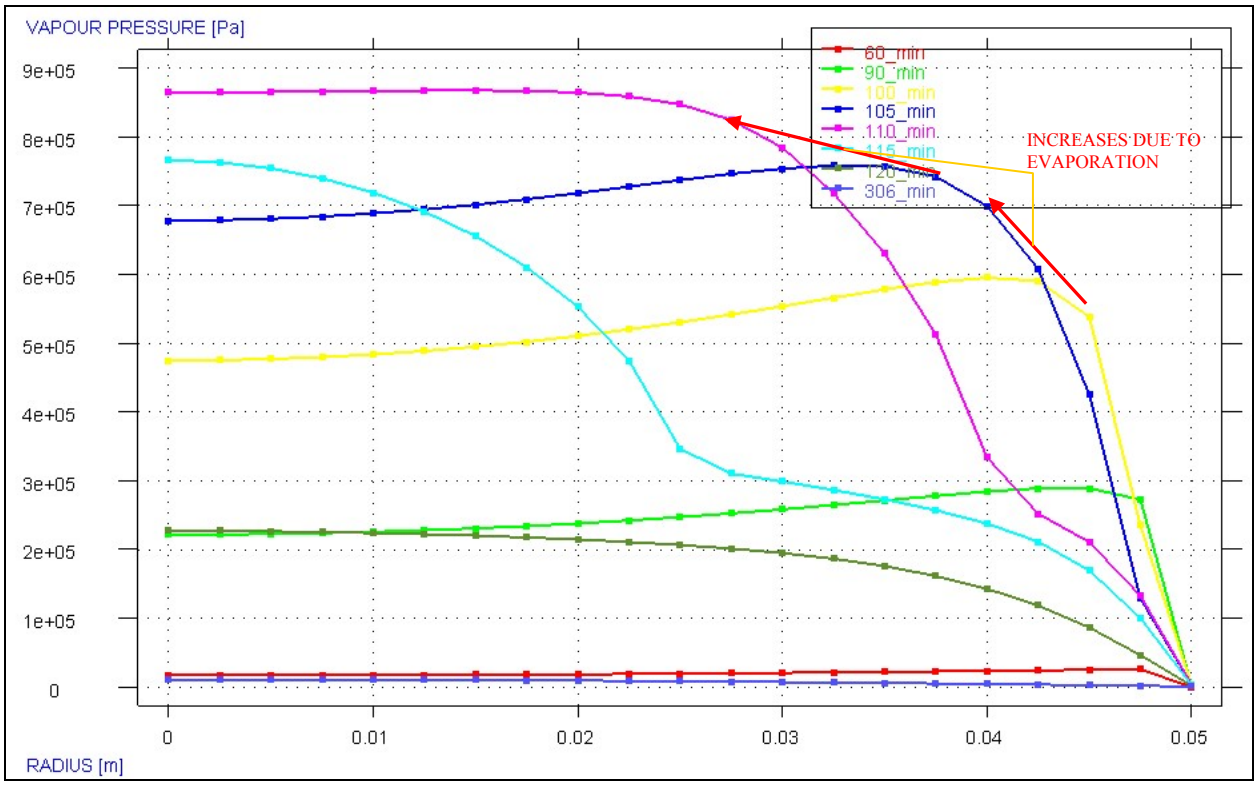

Figure 5-11: *Radial distribution of Vapour Pressure (right side: surface; left side: cylinder axis).*

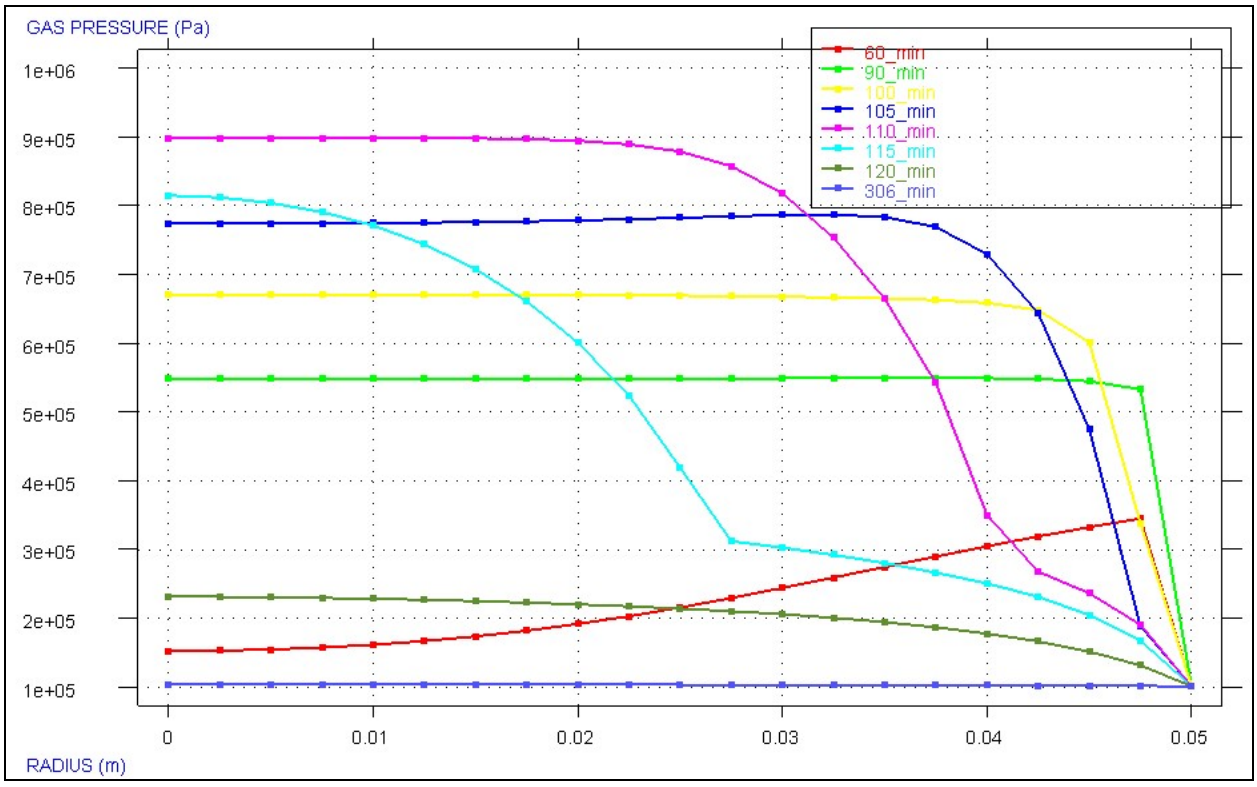

Figure 5-12: *Radial distribution of Gas pressure (right side: surface; left side: cylinder axis).*

The maximum value of gas pressure usually coincides with the position where the temperature of approximately 200ºC occurs. In the regions with lower temperature, below about 130ºC, the gas pressure increase is caused mainly by a growth of the dry air pressure due to heating, achieving the maximum value of 0,25 – 0,4 MPa at the position with a temperature of about 100ºC. In the regions with higher temperature, the effect of a rapid increase of vapour

pressure due to heating and temperature-dependence of the saturation vapour pressure dominate. At temperatures 200-300 ºC the gas in the material pores consists mainly of water vapour and the gradients of vapour pressure cause the vapour flow both towards the surface and inwards. The latter mass flow results in vapour condensation when the hot vapour inflows colder – internal layers of the concrete element – and in an increase of the relative humidity (see figure 5-10) above the initial value, often referred to as "moisture clog" or "saturation plug". An additional increase of the liquid water volume in the material pores is due to the water thermal dilatation, which is particularly important above the temperature of about 160ºC. A significant decrease of the gas permeability may be observed due to these effects, resulting in a decrease of the pore space available for the gas phase.

Increasing temperature causes the material dilatation of the aggregate which in part is due to concrete dehydration (products of the chemical reactions have greater volume than the initial volume of a concrete), in part due to material cracking and progressive crack opening, and finally due to "normal" thermal dilatation of the material skeleton. The concrete cracking during heating is caused by an incompatibility of thermal dilatation of the aggregate and the cement paste, resulting in high traction stresses in the Inter-Phase Transition Zones and development of local micro-cracks. Due to these cracks and chemical transformations of concrete (dehydration), the concrete strength properties and Young's modulus degrade gradually, what can be expressed [8] in terms of the so-called thermo-chemical damage parameter (see figure 5-13).

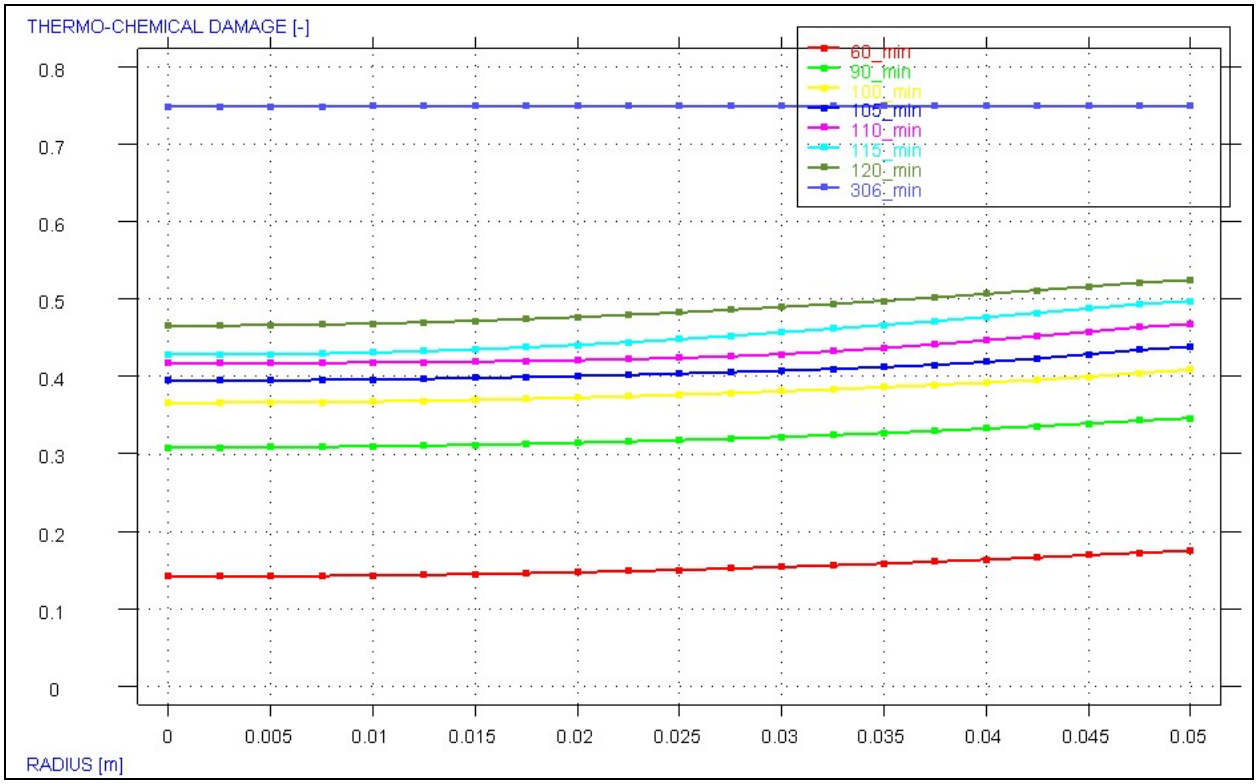

Figure 5-13: *Radial distribution of Thermo – Chemical Damage (right side: surface; left side: cylinder axis).*

A thermal dilatation of the external layers of a heated element is constrained by the core material which has lower temperature (figure 5-8). This causes macro-stresses in the external layers of the element, compression in the direction parallel to the surface (figure 5-14) and traction in the direction perpendicular to it (figure 5-15), as well as accumulation of the elastic strain energy (figure 5-16). The tensile stresses may cause further development of cracks and fractures, parallel to the element surface, resulting in subsequent degradation of the material strength properties in the surface zone (figures 5-17 and 5-18). An additional, external compressive load parallel to the element surface can intensify the aforementioned phenomena.

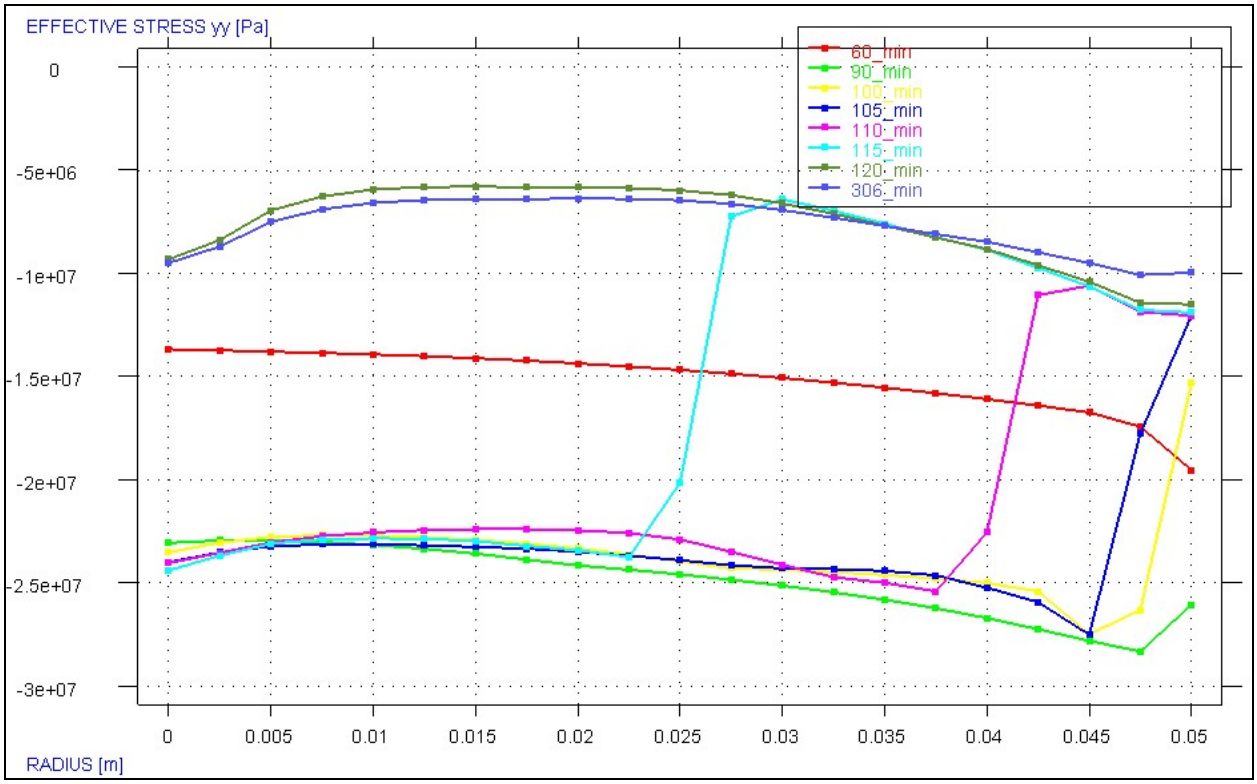

Figure 5-14: *Radial distribution of macro-stresses parallel to surface (right side: surface; left side: cylinder axis).*

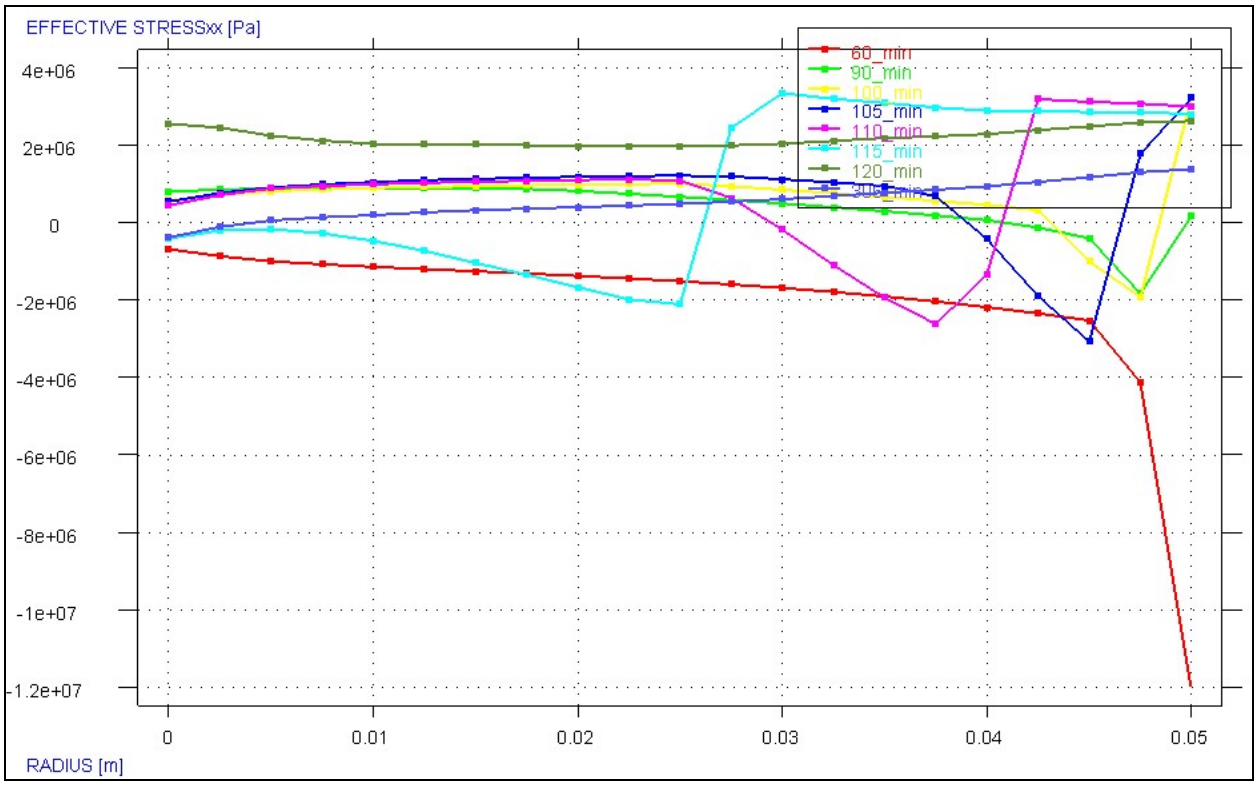

Figure 5-15: *Radial distribution of macro-stresses perpendicular to surface (right side: surface; left side: cylinder axis).*

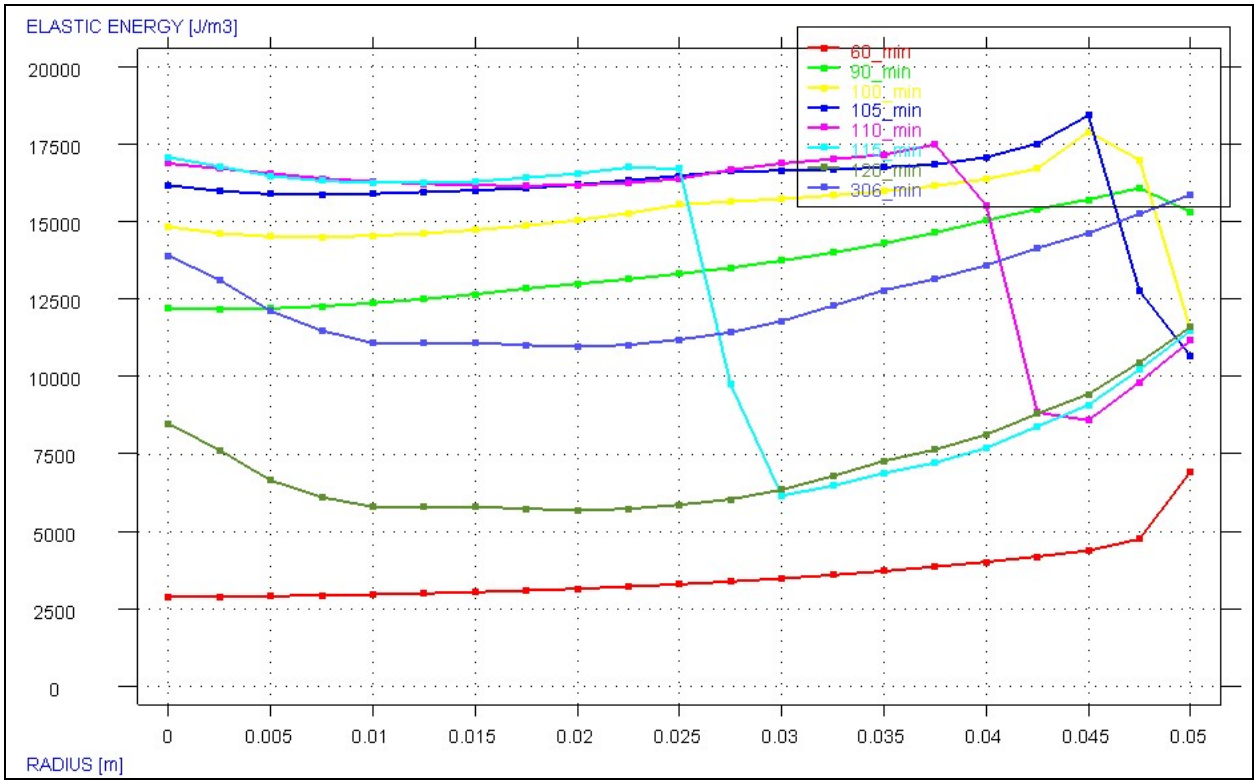

Figure 5-16: *Radial distribution of Elastic energy (right side: surface; left side: cylinder axis).*

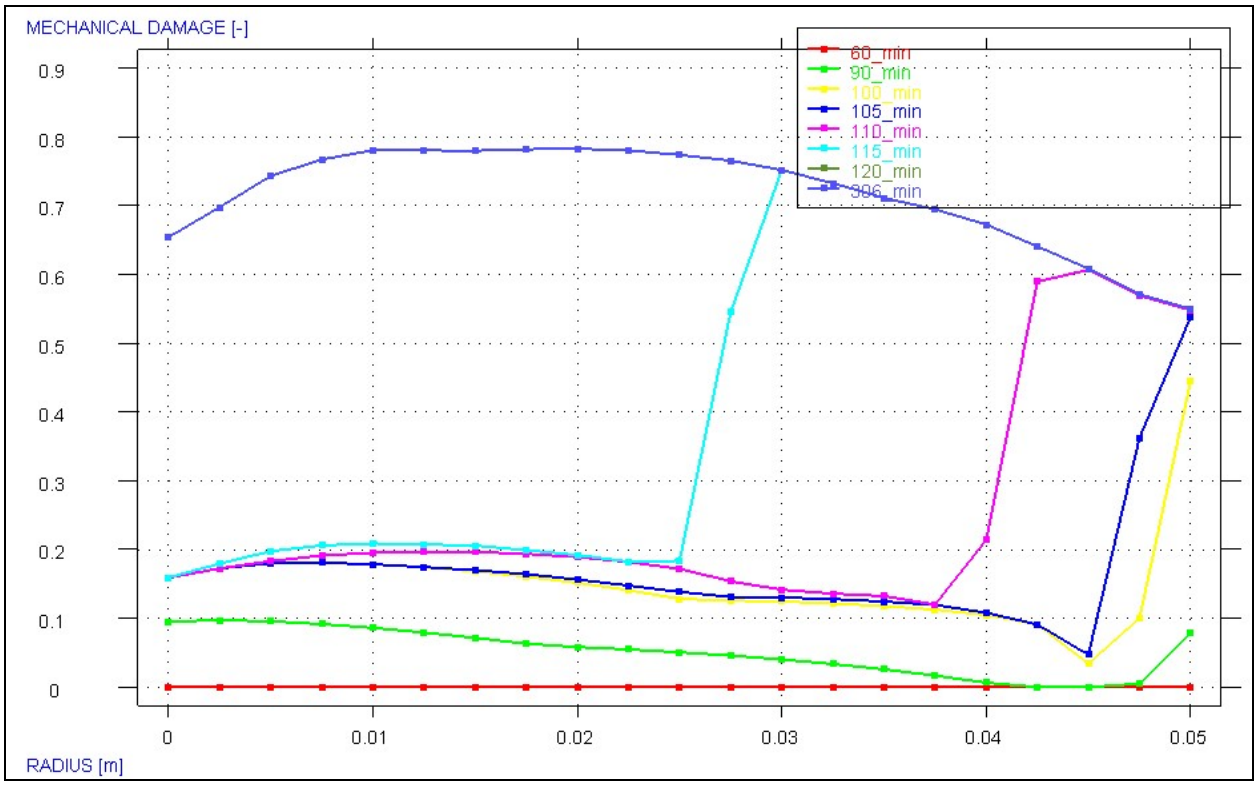

Figure 5-17: *Radial distribution of Mechanical Damage (right side: surface; left side: cylinder axis).*

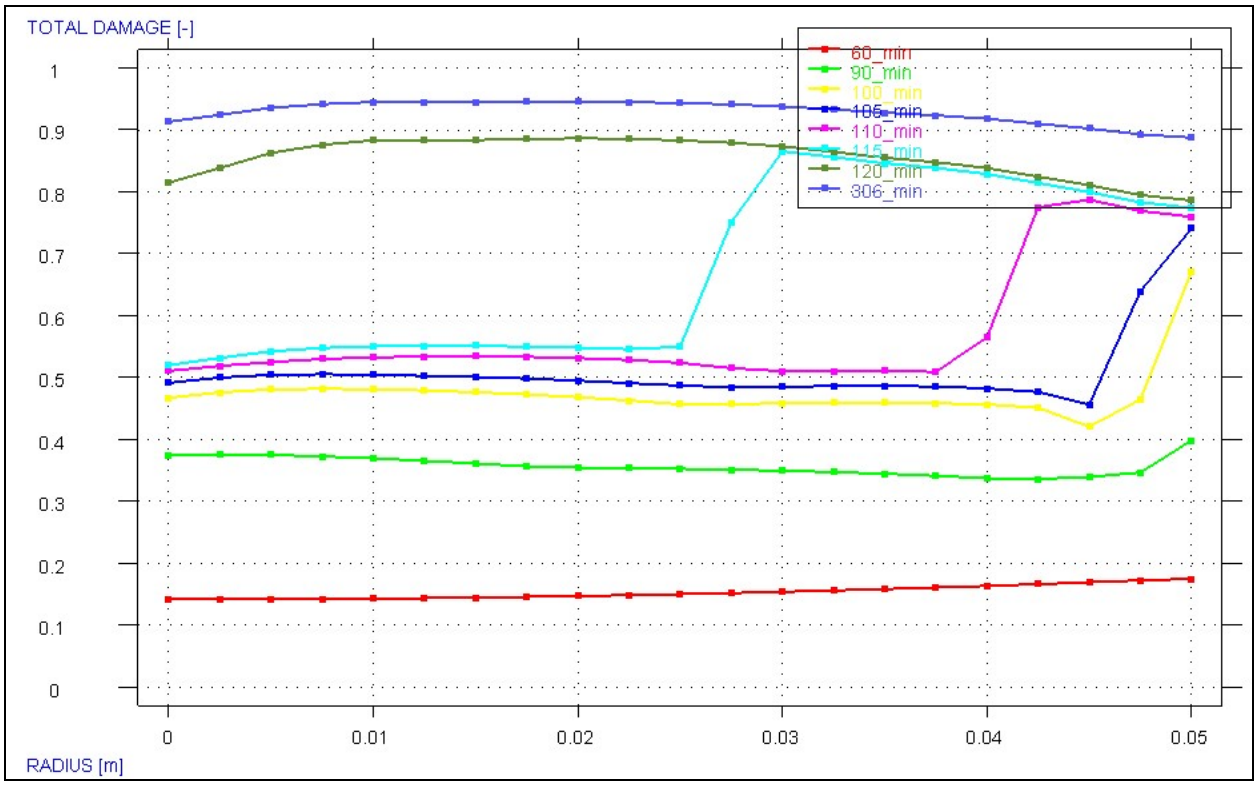

Figure 5-18: *Radial distribution of Total Damage (right side: surface; left side: cylinder axis).*

Development of the cracks, both of thermo-chemical origin and the macro-stresses induced ones, causes a considerable increase of the material intrinsic permeability, and thereupon gas pressure decreases in the external layers where high temperatures are observed (see figure 5-9 and 5-12, where after the sharp increase of mechanical damage in the middle of the radius around 105 and 115 minutes – see figures 5-19 and 5-20 – coinciding with the peak of gas pressure, gas pressure decreases rapidly being at the end of the simulation (after 300 minutes) equal to the atmospheric pressure in the whole specimen, indicating that concrete is almost completely damaged, which is also observed from the almost uniform radial distribution of the mechanical and total damage parameters at the final time, figures 5-17 and 5-18).

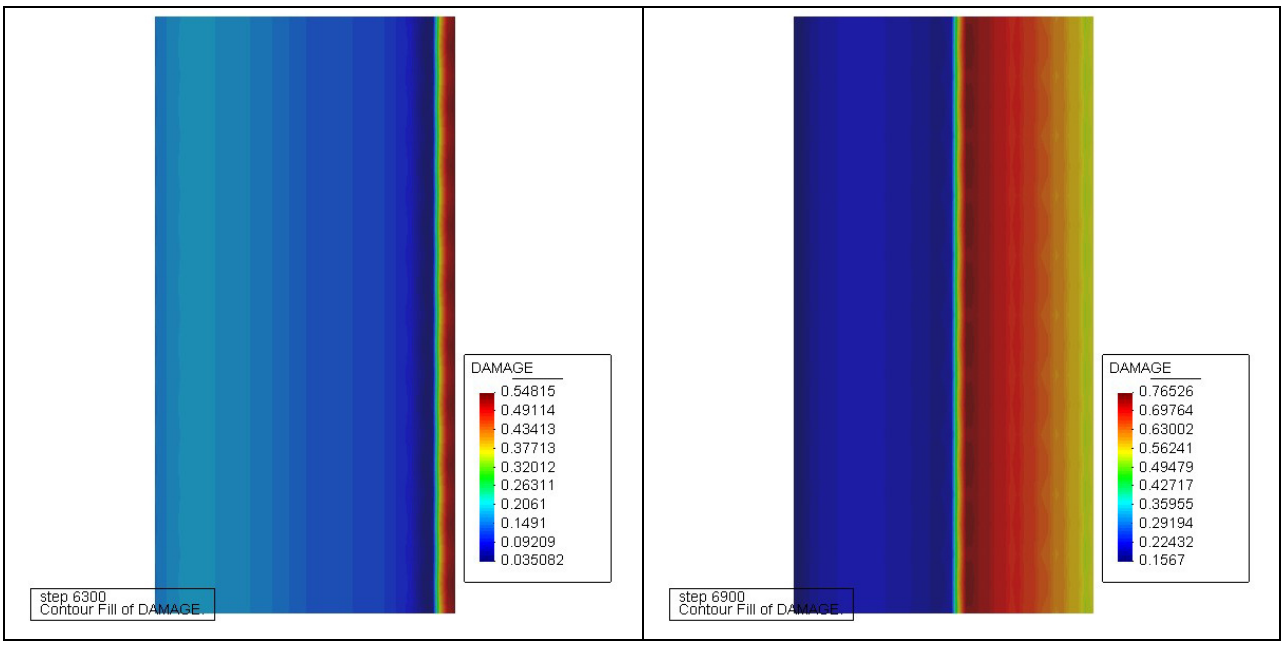

Figure 5-19: *Mechanical damage at 105 minutes*

Figure 5-20: *Mechanical damage at 115 minutes*

As it has been seen on previous figures, the highest values of gas pressure usually correspond to the temperature 150-250 ºC (time range from 105 to 115 minutes), and this is also the range where the so-called thermal spalling of concrete usually occurs (when elastic strain energy of constrained thermal dilatation, accumulated in the surface layer and then rapidly released after concrete fracture is considerable, the thermal spalling can be violent and explosive in nature as it was observed during the experimental tests developed).

The reconstruction of the exploded specimens (figure 5-5), by means of rendering technique, showed that, in the all cases of spalling, the specimen core which measured approximately 70 mm at maximum width, was the largest remaining piece of concrete. The core was surrounded by an approximately 20 mm thick outer shell of concrete, what probably corresponded to the location of the primary fracture. The numerical results obtained show a similar behaviour.

5.1.1.6 THE I_{S4} SPALLING INDEX EVALUATION FROM THE RESULTS OF THE NUMERICAL SIMULATION AND ITS COMPARISON AGAINST EXPERIMENTAL RESULTS

As it has been explained on previous paragraphs, to predict both the time and position of concrete rupture a spalling index developed by [8] and called 'intuitive' or I_{s4} has been selected, being its capabilities analysed in this paragraph.

The selected spalling index [8] is obtained choosing the following factors favouring thermal spalling: high local values of gas overpressure, p^g- p_{atm}, and mechanical damage parameter, d, high values of averaged transversal traction stresses, $\overline{\sigma}_{th}$, and constrained elastic energy $\overline{U}$ .The considered factors impeding thermal spalling are high average values of traction strength, $\overline{f}_t$, and specific fracture energy, $\overline{G}f$, for the material layer between a current position and the heated surface. Additionally, to obtain a non-dimensional quantity, [8] introduced a reference pressure (assume as equal to atmospheric pressure, p_{atm}) and a characteristic element dimension L (e.g. thickness for a wall, radius for a cylindrical specimen). Finally, internal geometrical parameters involved are unknown and are jointly described by a scaling factor, C_s, which is a non-dimensional parameter. Therefore, the fourth spalling index selected herein, I_{s4}, is given by the following relation:

$$I_{s4} = \frac{\overline{\sigma}_{th} \cdot \overline{U} \cdot d}{\overline{f}_t \cdot \overline{G}_f} \cdot \frac{p^g - p_{atm}}{p_{atm}} \cdot L \cdot C_s \tag{5.2}$$

Herein,

- The values of $\overline{\sigma}_{th}$, d, $\overline{U}$, p^g and the temperatures at each position are obtained from Hitecosp software [15] and then averaged for the material layer between a current position and the heated surface.
- The values of the specific fracture energy are obtained from experimental tests [16].
- The value of $\overline{f}_t$ is obtained from the material tensile strength equation for the temperature at each temperature and then averaged as described.

The results obtained applying in this equation the values obtained from the analysed case, results shown on previous figures 5-8 to 5-18, are shown on figure 5-21.

In figure 5-21 it is clearly observed that the instant with a maximum risk of suffering spalling, according to I_{s4} definition, is 115 minutes and the position of the main concrete rupture is at 2 centimetres from surface.

This prediction matches qualitative and quantitatively with the results of the experimental tests already described on paragraph 5.1.1.3 and shown on figure 5-5, where the examination of exploded cylinders showed that typically there was a large intact core, measured approximately 70 x 120 mm, which was surrounded by an approximately 20 mm-thick outer concrete shell. At 115 minutes, the calculated mean concrete temperature (at 25 mm deep in the cylinder) was 205 ºC (within the approximate range of 250 °C ± 50 °C measured during experimental tests).

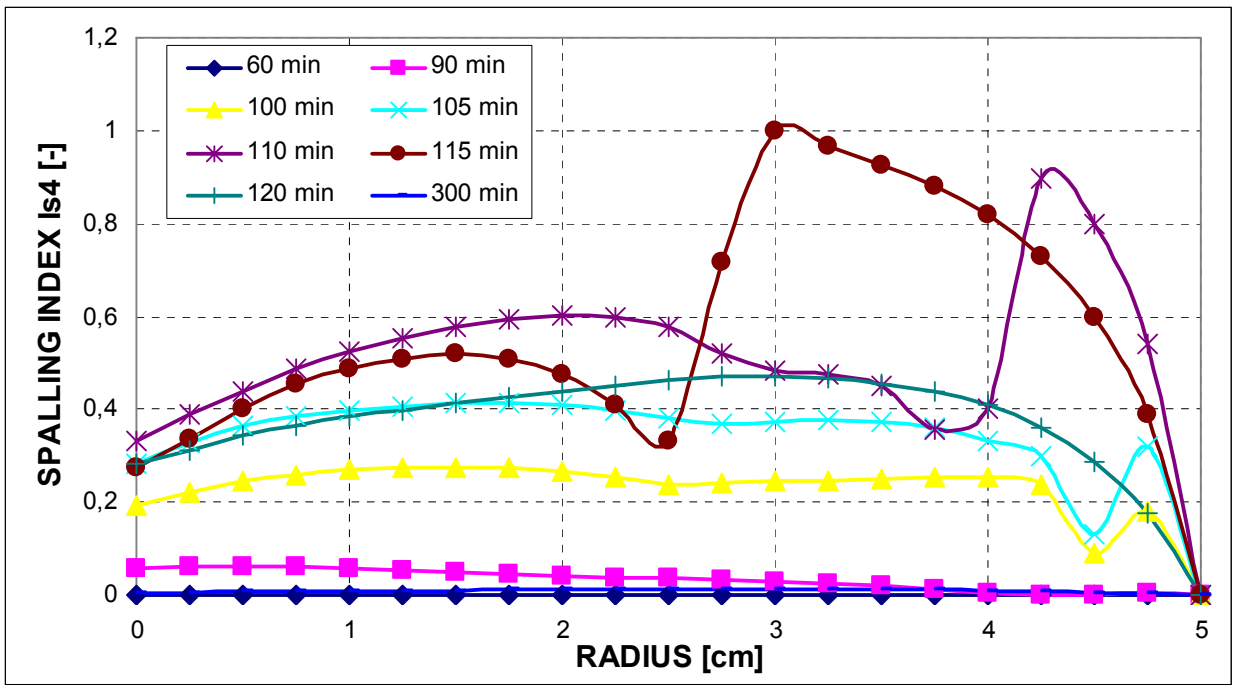

Figure 5-21: *Radial distribution of Spalling Index I_{s4} (right side: surface; left side: cylinder axis).*

Hence, from these results it is observed that although this criterion developed by [8] is not based on any particular physical model, but on a general analysis of factors favouring and impeding thermal spalling, without associating with them any "weighting" factors, gives precise indications concerning the time and position of concrete rupture for the analysed case, in a good agreement with the NIST experiments. This also suggests that explanation of the thermal spalling causes should consider rather a joint action of the pore pressure build-up and the elastic energy of constrained thermal dilatation strains, than indicate one of these as a decisive one.

Of course, one cannot expect that the geometrical (or scaling) parameters evaluated from the NIST tests' results have a universal character and will be valid for any situation, because they depend on several factors, like for example the size and shape of a heated element, concrete composition, etc.

Nevertheless, they can be useful as a first approximation for analysis of thermal spalling risk in heated concrete elements, and in particular to determine the position of the main fracture, corresponding to the highest value of the spalling index. Having this value, it is then possible to perform a simplified analysis of fracture energy and stored elastic energy to determine if concrete spalling is energetically possible, being I_{s4} spalling index therefore especially suitable to compare how different boundary conditions will affect the risk of thermal spalling where no experimental results are available, capability that is essential to develop the following tasks.

Beyond this conclusion, once determined the position of the main fracture it must be analysed, at least through a simplified methodology, if concrete spalling is energetically possible through the comparison of the fracture energy and the stored elastic energy similarly as it was already done in [8]:

Parameter	**Source / equation**	**Value obtained**
Possible thickness of the ruptured layer of concrete (corresponding to the highest value of the spalling index), Δx	From figure 5-21	2 cm
Released elastic energy, ΔU	Integrating a curve of the elastic energy density (figure 5-16) for the instant showing the highest value of the spalling index an in the range of the coordinates corresponding to this layer $\sum_{r1}^{r3} u_i(x) \cdot (x_i - x_{i-1}) \cdot 2 \cdot \pi \cdot (\frac{r_1 + r_3}{2}) \cdot H$ Where $r_1 = 0{,}03$ m, from figure 5-21; $r_3 = 0{,}05$ m, from figure 5-21; $H = 0{,}2$ m	x_i [m] / u_i (x) [J/m^3]: 0,03 / 6.135,01; 0,0325 / 6.439,93; 0,035 / 6.849,58; 0,0375 / 7.299,80; 0,04 / 7.754,62; 0,0425 / 8.418,29; 0,045 / 9.088,56; 0,0475 / 10.093,90; 0,05 / 10.581,70; ΔU = 9,1 J
Total mass of spalled concrete, Δm	$\rho \cdot \pi \cdot (r_3^2 - r_1^2) \cdot H$	2,63 Kg
Total Area of rupture, ΔA_{fr}	Assuming certain average dimensions of the spalled pieces of concrete: $2 \cdot \pi \cdot r_1 \cdot H$	0,03768 m^2
Energy dispersed for fracturing, ΔE_{fr}	$\Delta E_{fr} = \Delta A_{fr} \cdot G_f$ Where Gf is the specific fracture energy obtained from experimental tests [16], 180 J/m^2	6,1 J
Rough estimation for the kinetic energy, ΔE_k	$\Delta E_k = \Delta U - \Delta E_{fr}$	3 J

Since the kinetic energy value is positive (i.e. the stored elastic energy is greater than the energy needed for the rupture), the concrete spalling at 115 minutes is energetically possible (either explosive or progressive spalling depending on ΔE_k value, the mass of spalled concrete and the gas pressure, the latter with a direct influence on the work performed by the gas during its adiabatic expansion to the atmospheric pressure).

So, in conclusion, this demonstrates the capability of both the numerical model and the proposed spalling criteria I_{s4} to assess the risk of thermal spalling in High Strength Concrete structures exposed to elevated temperatures where no experimental results are available.

It must be noticed that if thermal creep had not been considered within the calculations of the I_{s4} spalling index (see figure 5-22 on next page), its maximum value would have been as low as 0,3313 (instead of the unity) taking into account the real value of the scaling factor involved in the 'intuitive criterion' ($C_s = 4{,}86$).

In that case the main fracture would appear around 10 minutes earlier than if thermal creep was considered and just 2,5 millimetres away from the surface instead of the 2 centimetres gap observed on previous paragraphs.

These values of the I_{s4} spalling index are important for comparative reasons because the simulations shown next do not consider thermal creep since, up to the date of this preliminary and simplified analysis of the cooling effect on the High Strength Concrete behaviour, there are not any software releases available capable to predict hygro-thermo-chemo-mechanical

behaviour considering thermal creep during a cooling process (and, obviously, it makes no sense on developing that release until one has the certainty that cooling will have a significant (and unfavourable) effect on thermal spalling risk, certainty which is precisely the aim of this chapter as it was explained on its first paragraph).

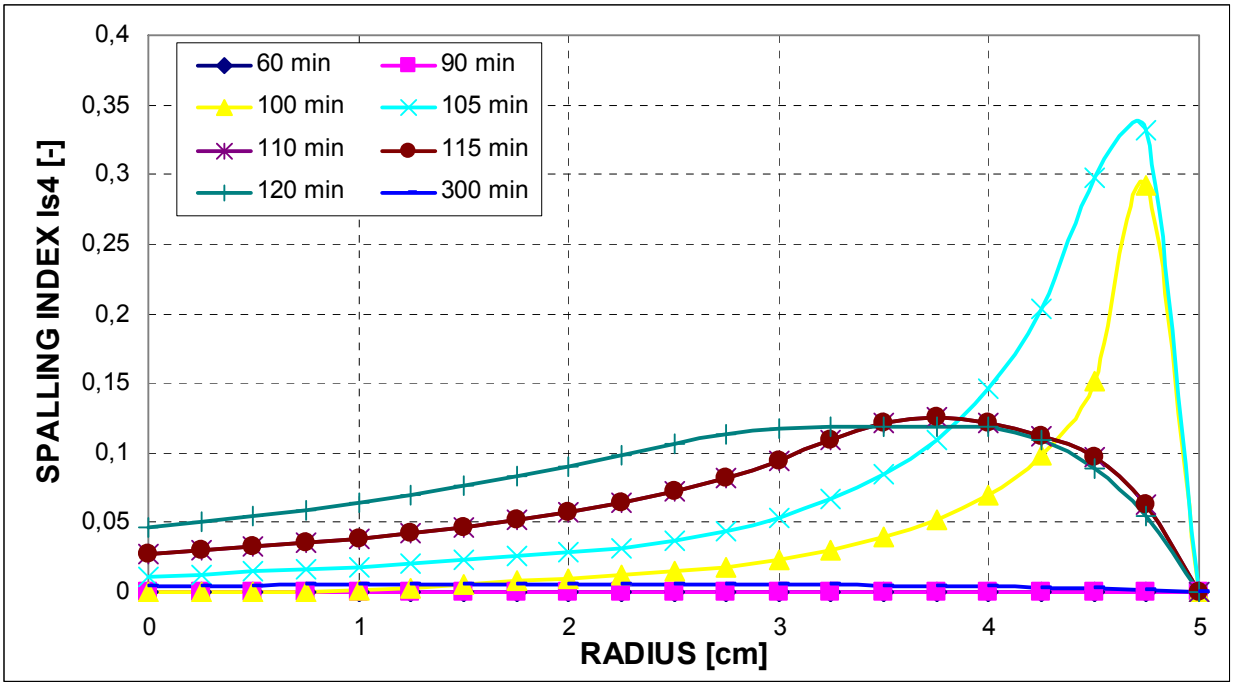

Figure 5-22: *Radial distribution of Spalling Index I_{s4} (right side: surface; left side: cylinder axis if Thermal Creep is not considered (right side: surface; left side: cylinder axis).*

5.2 PRELIMINARY AND SIMPLIFIED ANALYSIS OF COOLING EFFECT ON HSC SPALLING BEHAVIOUR

The methodology described previously on this chapter will now be applied to the same axisymmetric cylinder model, since it is an experimentally validated case both for the numerical analysis and for the evaluation of the I_{s4} spalling index, and for two different types of materials, these are the so-called MIX1 or C-90 material already described on table 5-1 and the C-60 material (with a compressive strength at ambient temperature of about 60 MPa) whose basic material parameters are next summarised (see table 5-4), during several cooling processes. Selecting these two materials, the main range of commercial High Strength Concretes is covered from the lowest compressive stress, 60 MPa, up to the highest one, 98 MPa, so it will be also possible to discern the relevancy of the effect of the material on the thermal spalling risk.

Table 5-4. Main properties of C60 concrete at 20 ºC

Material property	C60 value
Water / binder ratio, w/b [-]	0,36
Binder content [kg/m^3]	OPC: 450
Aggregate type and size	Limestone, max. size of 20 mm
MIP porosity, n[%]	10,385
Water intrinsic permeability, k_0 [m^2]	2 x 10^{-18}
Young modulus, E [GPa]	35,604
Poisson's ratio, ν [-]	0,18
Thermal Conductiviy, χ [W/m K]	1,8079
Specific heat, C_p [J/kg K]	855,25758

(For a more extensive description of C60 properties and their evolution with temperature, see the Material Properties Annex)

On next paragraphs, first of all it is defined a heating and "natural" cooling curve, as it is explained in detail next, under which the spalling index I_{s4} is evaluated as a reference situation where none action of the fire fighting services is taken into account.

Next, several types of realistic "forced" cooling curves are implemented and the spalling index I_{s4} is evaluated again for each situation (and for each material) so preliminary conclusions about the effect of forced cooling on the spalling behaviour of High Strength (and Very High Strength) Concretes are derived so it is possible to evaluate if this effect is significant enough to justify a relevant, greater and deeper work concerning this matter.

5.2.1 Selection of the heating and "natural" cooling curves for the preliminary and simplified analysis

Since the temperature evolution in a HSC concrete element has an essential influence on the thermal spalling risk [14], the heating and cooling curves selected for this preliminary and simplified analysis need to be chosen within the most realistic ones corresponding to High-Rise Buildings rooms and/or offices. Therefore, the heating curves adopted must be clearly representative of the temperature distributions during real fires so time-temperature parametric curves will be selected and implemented as defined in the Eurocode 1, Part 1-2 [17], definition that will be briefly described and applied for a particular High-Rise Building case next, since this is an European regulation widely spread and prestigious document where parametric curves have been defined on an experimental bases:

The time-temperature curves shown next are valid for fire sectors with a built surface not higher than 500 square meters, without holes at the roof and with a maximum height of 4 meters, assuming a complete combustion of the fire load.

The time-temperature curves in the *heating* stage are defined by:

$$\Theta_g = 20 + 1.325 \cdot (1 - 0{,}324 \cdot e^{-0{,}2 \cdot t^*} - 0{,}204 \cdot e^{-1{,}7 \cdot t^*} - 0{,}472 \cdot e^{-19 \cdot t^*}) \qquad (5.3)$$

Where,

Θ_g	is the air temperature within the fire sector	[ºC]
t^*	$= t \cdot \Gamma$	[h]
Γ	$= [O/b]^2 / (0{,}04 / 1.160)^2$	[-]
b	$= \sqrt{\rho \cdot c \cdot \lambda}$ with the following limits: 100<= b <=2.200	[J/m^{3}s$^{1/2}$K]
ρ	is the density of the element closing the fire sector (At ambient temperature)	[Kg/m^3]
c	is the specific heat of the element closing the fire sector (At ambient temperature)	[J/KgK]
λ	is the thermal conductivity of the element closing the fire sector (At ambient temperature)	[W/mK]
O	is the opening coefficient: $A_v \cdot \sqrt{h_{eq}} / A_t$ with the following limits: 0,02 <= O <= 0,20	[m$^{1/2}$]
A_v	is the total surface of the vertical openings at all of the walls	[m^2]
h_{eq}	is the averaged height of the windows at all of the walls	[m]
A_t	is the total surface closing the fire sector, including openings	[m^2]

The time-temperature curves in the *cooling* stage are defined by:

$$\Theta_g = \Theta_{\max} - 625 \cdot (t^* - t^*_{\max}) \qquad for \quad t^*_{\max} \le 0{,}5$$
$$\Theta_g = \Theta_{\max} - 250 \cdot (3 - t^*_{\max}) \cdot (t^* - t^*_{\max} \cdot x) \qquad for \quad 0{,}5 \le t^*_{\max} \le 2$$
$$\Theta_g = \Theta_{\max} - 250 \cdot (t^* - t^*_{\max} \cdot x) \qquad for \quad t^*_{\max} \ge 2,$$
$$where \qquad t^* = t \cdot \Gamma \tag{5.4}$$
$$t^*_{\max} = (0{,}2 \cdot 10^{-3} \cdot q_{t,d} / O) \cdot \Gamma$$
$$x = 1{,}0 \; if \; t_{\max} > t_{\lim}, or \; x = t_{\lim} \cdot \Gamma / t^*_{\max} \; if \; t_{\max} = t_{\lim}$$

(*where* $t_{\lim}$ *is* 25 min *for slow fires*, 20 min *for medium fires and* 15 min *for fast fires*)

The criteria assumed to select the particular case to apply these equations are, mainly, both that they represent a fire in a real 100 m^2 High-Rise open office and that the temperature evolution in the cylinder surface is not so different than that temperature profiles seen in previous paragraphs, so similar thermal spalling phenomena may be expected. The main parameters defining the selected case are the following ones:

Table 5-5. Parameters used to define the parametric heating and cooling curves according to Eurocode 1, Part 1-2

Parameter	Value
Office width [m]	10 m
Office depth [m]	10 m
Office height [m]	3 m
Vertical openings unitary height [m]	2 m
Vertical openings unitary width [m]	1 m
Number of vertical openings	2
Density of the element closing the fire sector [Kg/m^3]	2.621
Specific heat of the element closing the fire sector [J/KgK]	940,2
Thermal conductivity of element closing fire sector [W/mK]	1,386
Fire load (Office, Annex E of Eurocode 1,part 1-2)	511 MJ/m^2
Fire Spread Speed	Slow

Therefore, the heating and lets call "natural" cooling curves defined for this case are:

- Heating curve:

$$\Theta_{g,heating}[K] = 293{,}15 + 1.325 \cdot (1 - 0{,}324 \cdot e^{-0{,}0077 \cdot t[s]/3.600} - 0{,}204 \cdot e^{-0{,}06545 \cdot t[s]/3.600} - 0{,}472 \cdot e^{-0{,}7315 \cdot t[s]/3.600}) \tag{5.5}$$

- "Natural" cooling curve:

$$\Theta_{g,cooling}[K] = 871{,}45 - 625 \cdot \left(\frac{0{,}0385 \cdot t[s]}{3.600} - 0{,}0983 \right) \tag{5.6}$$

while the heat exchange coefficient will be selected, within the reasonable range of values for natural convection on air [5-20] W/m^{2}K, as the average value considered in the simulation of the NIST case previously reported, this is 7,6 W/m^{2}K.

Figure 5-23 shows the graphical representation of these heating and "natural" cooling parametric curves for the selected case.

As it can be observed on this figure, although a quite long fire (heating + cooling) simulation time has been selected (5 hours) it is not enough to make the temperature at the surface of the concrete element decrease for the environment cooling curve defined. On the contrary, on next paragraphs there will be observed sudden decreases of the surface temperature when a "forced" cooling of the environment is defined.

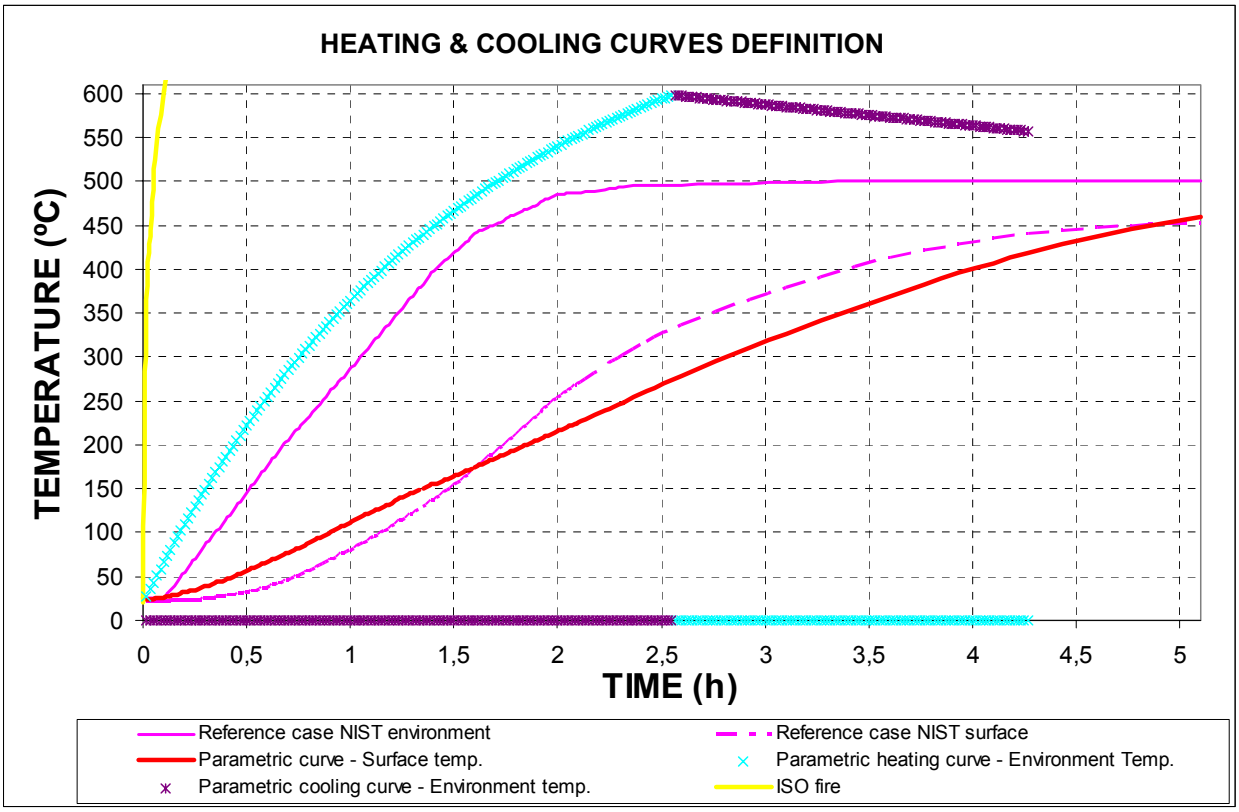

Figure 5-23: *a) ISO fire curve is represented to show it has been discarded because of its excessive heating rate if compared to real fires. b) The NIST cylinder heating curves (both environment and surface temperature curves) are taken as a reference. c) Parametric heating and "natural" cooling curves are discussed hereon (Note: The parametric Surface temperature shown corresponds to the C90 material).*

5.2.2 Results from the C-90 simulations.

5.2.2.1 RESULTS FROM THE C-90 PARAMETRIC HEATING AND "NATURAL" COOLING SIMULATIONS.

5.2.2.1.1 Direct results from the simulation

Figure 5-24 shows the main results obtained for the reference case where the parametric heating and "natural" cooling curves described on last paragraph (figure 5-23) have been implemented. These results, which represent a set of reference results corresponding to a case where none action of the fire fighting services is taken into account, are used not only to evaluate I_{s4} spalling index, but also to define a range of starting instants for the "forced" cooling processes in such a way that conclusions can be achieved concerning their effect on the thermal spalling behaviour of a HSC concrete element coinciding with different relevant stages of its hygro-thermo-chemo-mechanical behaviour.

Input file name	Initial time (s)	Time step (s)	Number of time steps	Freq. results record (# steps)	Final time (s)
ACT1ST2N_01	0	1E-6	10	10	1E-5
ACT1ST2N_02	1E-5	0,5	720	120	360
ACT1ST2N_03	360	6	1.200	10	7.560
ACT1ST2N_04	7.560	12	600	50	14.760
ACT1ST2N_05	14.760	12	300	50	18.360

Table 5-6. *Time history of the simulation stages*

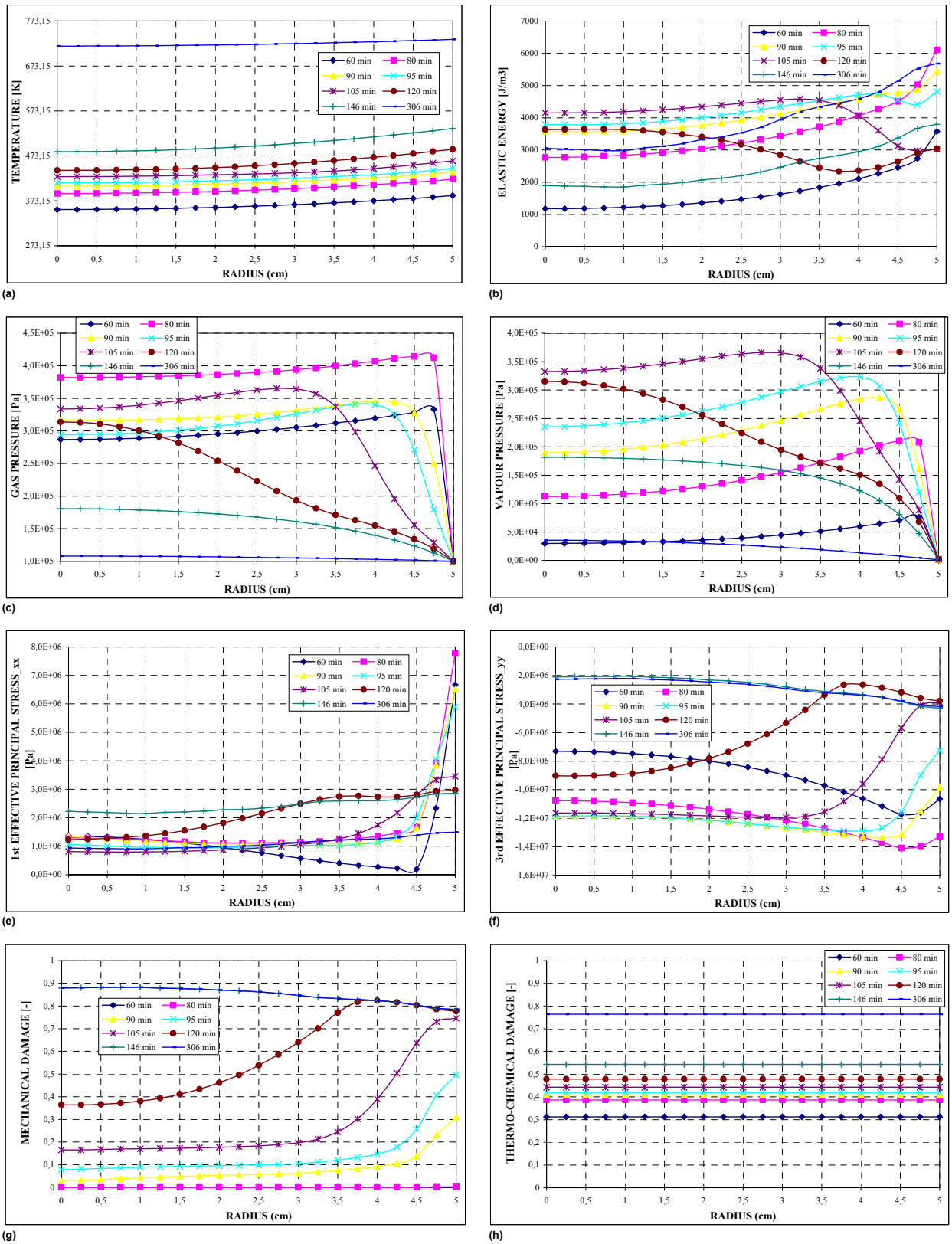

Figure 5-24: Heating and "natural" cooling results. *Radial distributions of the following fields: a) Temperature; (b) Elastic Energy; (c) Gas pressure; (d) Vapour pressure; (e) 1st principal stress_xx; (f) 3rd principal stress_yy; (g) Mechanical damage; (h) Thermo-chemical damage. Right side: cylinder heated surface; Left side: Cylinder axis.*

Figure 5-25 shows the information needed to define a range of starting instants for the "forced" cooling processes in different relevant stages of the concrete hygro-thermo-chemo-mechanical behaviour:

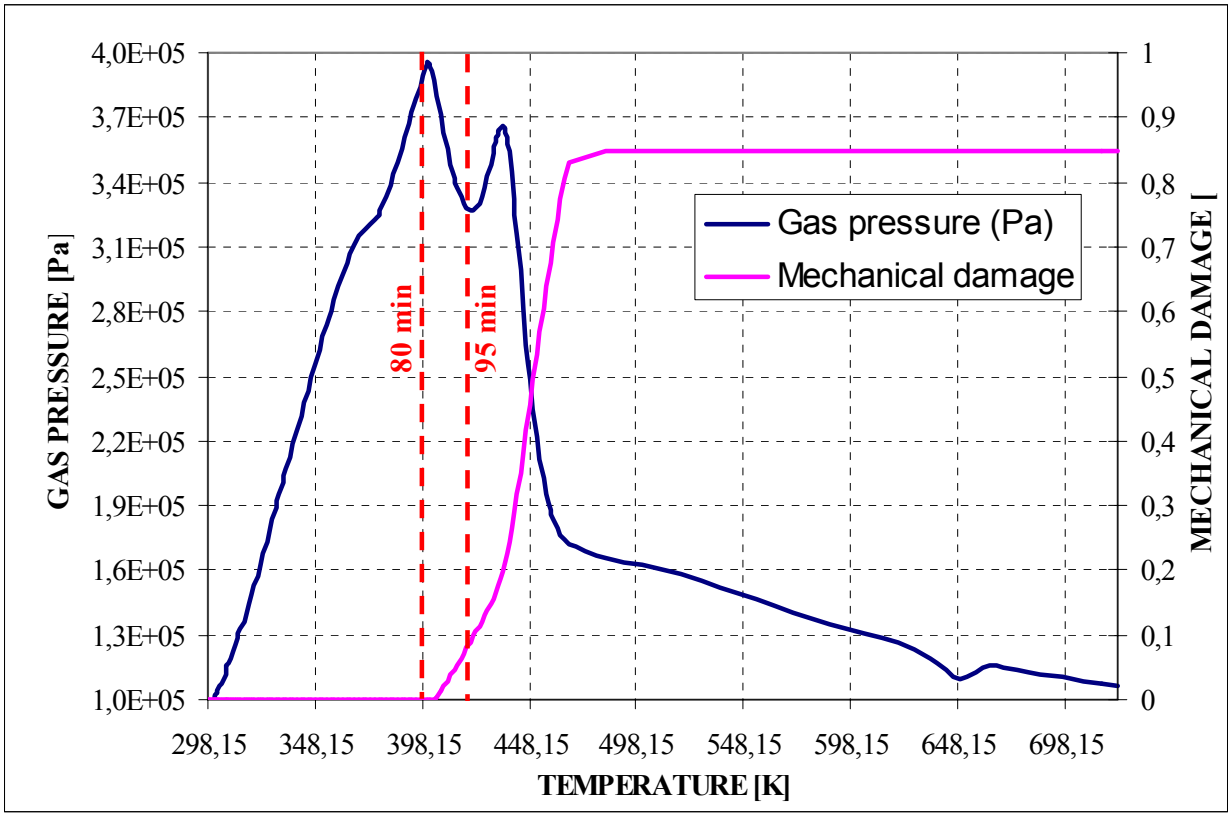

Figure 5-25: *Evolution with temperature of Gas Pressure and Mechanical Damage at 2 cm from surface.*

As it can be observed, after 80 minutes of heating mechanical damage at 3 cm from surface begins to increase coinciding with the gas pressure peak and the highest first principal stress value (figure 5-24.f). For this reason, this is the first instant selected (lets say Point A) to start a "forced" cooling process. Fifteen minutes later, gas pressure that had decreased from its maximum sharply, begins to increase again, being this instant the second starting point selected for the "forced" cooling process (lets say Point B).

For each of these two starting instants of "forced" cooling actions, two types of cooling processes are defined, namely, a so-called "slow" cooling, which consists on a decrease of the environment temperature down to the initial one (298,15 K) in a total time of 40 to 44 minutes (depending on how high is the environment temperature at the starting of the cooling process, in order to keep the same cooling ratio – $\Delta T/t$ – for both processes), and "fast" cooling, which represents the application of the water from a Hose-Nozzle directly on the cylinder surface through a decrease of the surface temperature to the initial one (298,15 K) in only 10 to 12 seconds (depending on how high is the surface temperature at the starting of the cooling process, in order again to keep the same cooling ratio – $\Delta T/t$ – for both processes). The definition of this "fast" kind of cooling processes leans on Computational Fluid Dynamics simulations which are explained on the corresponding chapter.

One must remember that this is only a preliminary and simplified analysis and, as it will be seen later, when a deeper and more representative analysis is to be done, the selection of these starting instants for the "forced" cooling processes will be done taking also into account how much time the fire fighting services use to last to begin their cooling actions in High-Rise Buildings by means of hose-nozzles.

Figure 5-26 shows all of the heating and cooling curves selected for the simulations developed on C-90 material within this and following paragraphs.

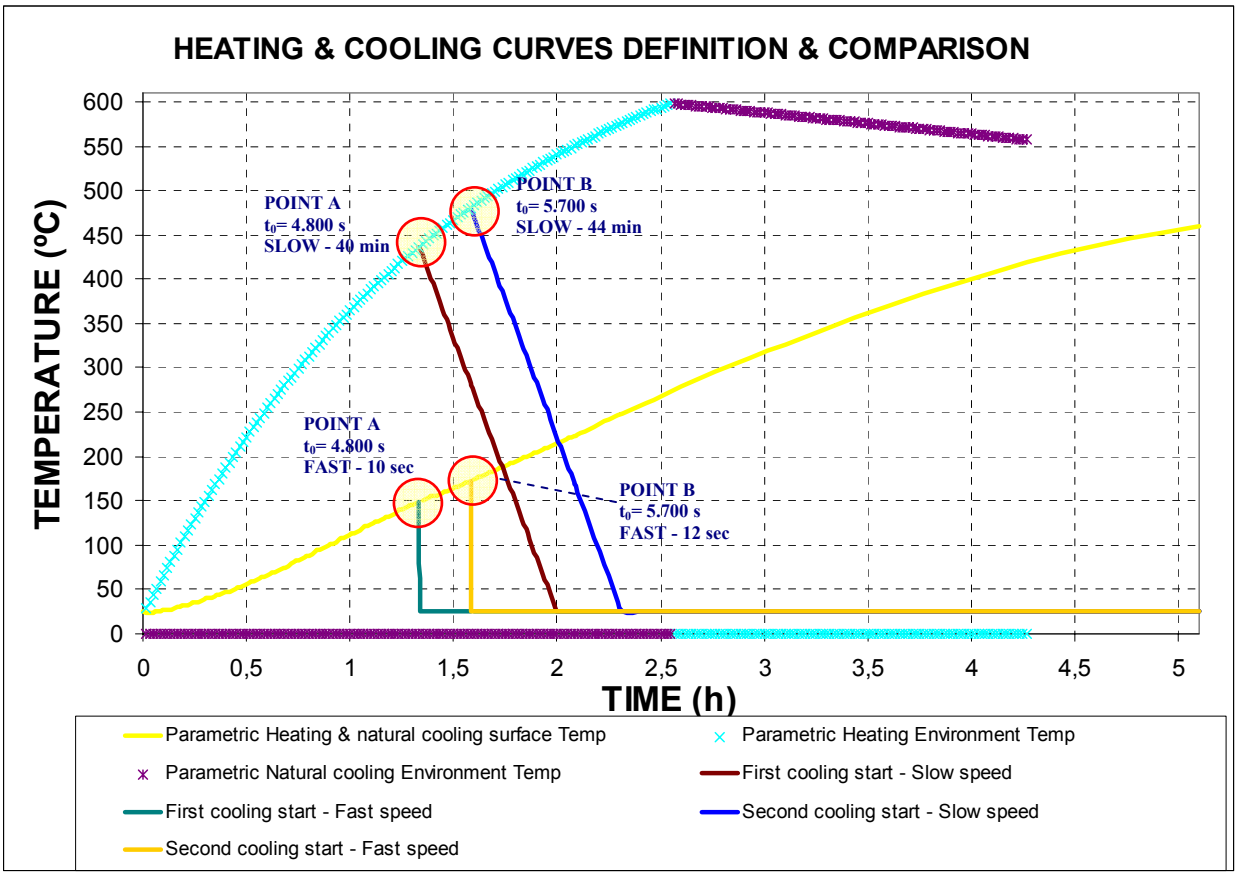

Figure 5-26: *Heating and cooling curves corresponding to the simulations described for C-90 material on this and later paragraphs.*

Of course, it must be remarked that beyond these preliminary analysis, several adjusts will have to been done to the typology of the cooling curves since, for example, following the end of a "fast" cooling process, for example at 4.810 seconds, cooling which is developed decreasing the surface temperature down to the initial one, a probably still much higher temperature of the environment will have to be taken into account, not being therefore constant the surface temperature from the end of the application of the Hose-Nozzle onwards. However, this initial definition of the cooling curves will be useful to obtain preliminary conclusions about cooling effect significance.

5.2.2.1.2 Evaluation of the I_{s4} spalling index

If we apply the same procedure defined on paragraph 5.1.1.6 for the NIST case, to the results obtained from the reference case dealt on this paragraph corresponding to the parametric heating and "natural" cooling curves shown on figure 5.23, the results of the evaluation of the I_{s4} spalling index for this case are shown next on figure 5-27.

The maximum spalling index value obtained for this case using the real value of the scaling factor involved in the 'intuitive criterion' (C_s = 4,86) is 0,2654 (slightly lower than that corresponding to the NIST case when not considering Thermal Creep effect). This value gives a preliminary idea of the probability of suffering spalling if compared to that of NIST experiments previously reported. From this figure it can also be observed that the expected position of the main fracture is at only 2,5 millimetres from surface (much more superficial than in the NIST case when considering thermal creep), while the instant showing the maximum value of the spalling index I_{s4} is 90 minutes.

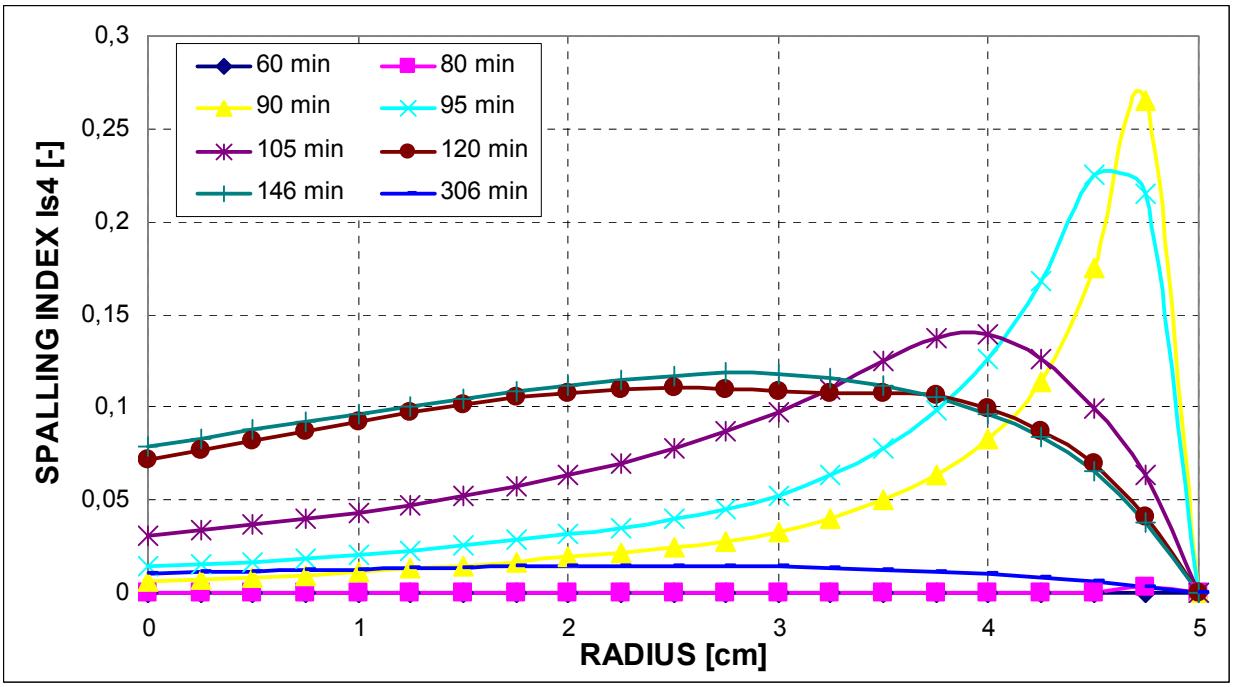

Figure 5-27: *Radial distribution of Spalling Index I_{s4} (right side: surface; left side: cylinder axis).*

5.2.2.1.3 Simplified analysis to determine if concrete spalling is energetically possible

As it has been already done within previous paragraphs, next it is analysed if concrete spalling is energetically possible through the comparison of the fracture energy and the stored elastic energy:

Parameter	**Source / equation**	**Value obtained**
Possible thickness of the ruptured layer of concrete (corresponding to the highest value of the spalling index), Δx	From figure 5-27	0,025 cm
Released elastic energy, ΔU	Integrating a curve of the elastic energy density (figure 5-24.b) for the instant showing the highest value of the spalling index an in the range of the coordinates corresponding to this layer $\sum_{r1}^{r3} u_i(x)\cdot(x_i - x_{i-1})\cdot 2\cdot\pi\cdot(\frac{r_1+r_3}{2})\cdot H$ Where r_1 = 0,0475 m, from figure 5-27 r_3 = 0,05 m, from figure 5-27 H = 0,2 m	x_i [m] / u_i (x) [J/m^3] 0,0475 / 4.880,69 0,05 / 5.451,52 ΔU = 1,582 J
Total mass of spalled concrete, Δm	$\rho\cdot\pi\cdot(r_3^2 - r_1^2)\cdot H$	0,401 Kg
Total Area of rupture, ΔA_{fr}	Assuming certain average dimensions of the spalled pieces of concrete: $2\cdot\pi\cdot r_1\cdot H$	0,05969 m^2
Energy dispersed for fracturing, ΔE_{fr}	$\Delta E_{fr} = \Delta A_{fr}\cdot G_f$ Where Gf is the specific fracture energy obtained from experimental tests [16], 177 J/m^2	10,56 J
Rough estimation for the kinetic energy, ΔE_k	$\Delta E_k = \Delta U - \Delta E_{fr}$	< 0

Since the kinetic energy value is negative (i.e. the stored elastic energy is smaller than the energy needed for the rupture), the concrete spalling at 90 minutes is not energetically possible.

5.2.2.2 RESULTS FROM THE C-90 PARAMETRIC HEATING AND "FORCED" COOLING SIMULATIONS (FIRST STARTING POINT –POINT A–, SLOW COOLING).

5.2.2.2.1 Direct results from the simulation

Figure 5-28 (next page) shows the main results obtained for this case where the parametric heating and the Point A (First cooling start) – Slow speed "forced" cooling curves described on last paragraph (figure 5-26) have been implemented.

It must be remarked that the calculations detailed on table 5-7 went out of convergence before the expected end, at a time of 9.486 seconds (approximately at 158 minutes) mainly due to extremely high values of Mechanical Damage (higher than 0,92) and Total Damage (higher than 0,95) coinciding with very high values of capillary pressure, so the last results available correspond to a time of 158 minutes.

Input file name	Initial time (s)	Time step (s)	Number of time steps	Freq. results record (time steps)	Final time (s)
ACT1ST2S_01	0	1E-6	10	10	1E-5
ACT1ST2S_02	1E-5	0,5	720	120	360
ACT1ST2S_03	360	6	740	10	4.800
ACT1ST2S_04	4.800	1	2.400	20	7.200
ACT1ST2S_05	7.200	6	60	20	7.560
ACT1ST2S_06	7.560	12	150	50	9.360
ACT1ST2S_07	9.360	6	1.500	1	18.360

Table 5-7. *Time history of the simulation stages*

Figure 5-29 shows that, although after 106 minutes the temperature at 2 centimetres from surface begins to decrease, Mechanical Damage increases uninterruptedly until the end of the simulation.

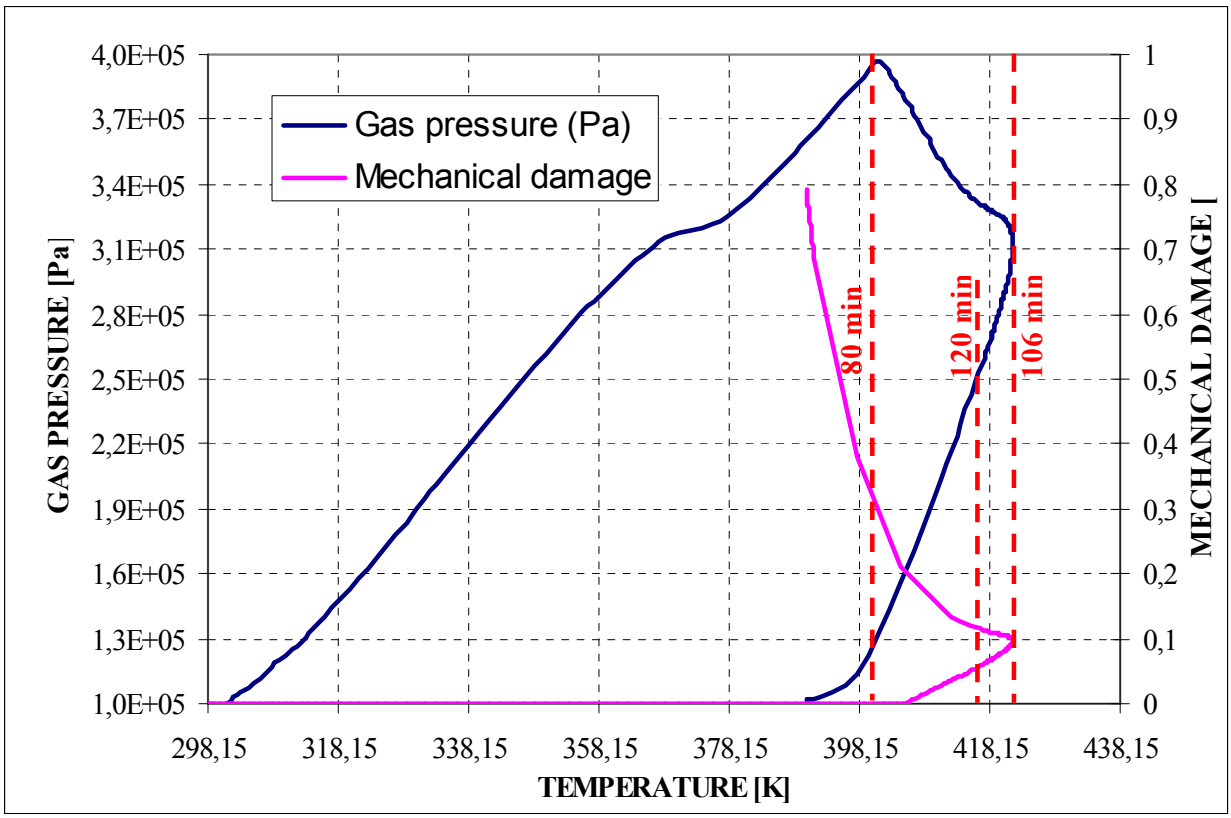

Figure 5-29: *Evolution with temperature of Gas Pressure and Mechanical Damage at 2 cm from surface.*

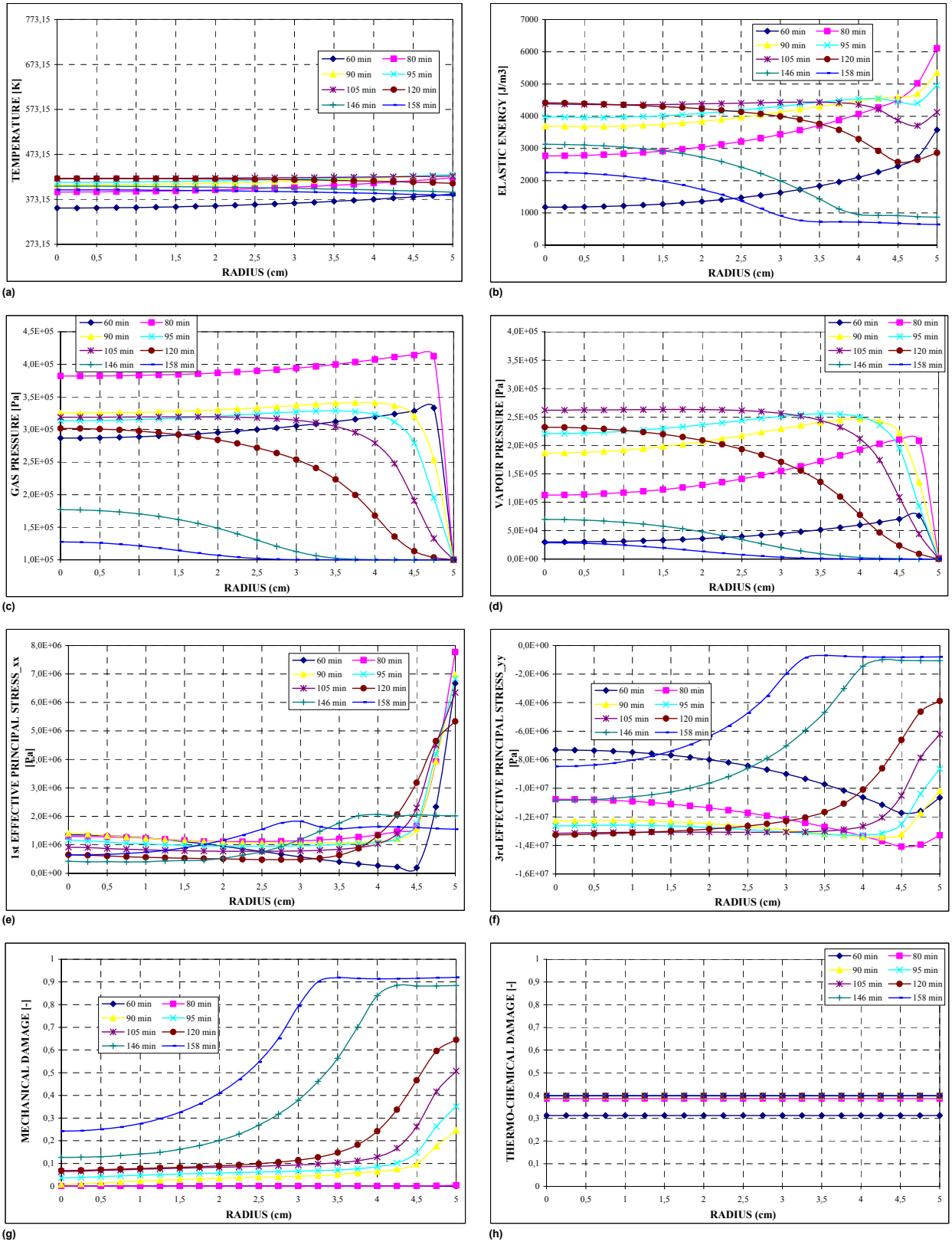

Figure 5-28: Heating and Point A (First cooling start) – Slow speed "forced" cooling results. *Radial distributions of the following fields: a) Temperature; (b) Elastic Energy; (c) Gas pressure; (d) Vapour pressure; (e) 1st principal stress_xx; (f) 3rd principal stress_yy; (g) Mechanical damage; (h) Thermo-chemical damage. Right side: cylinder heated surface; Left side: Cylinder axis.*

In this way, the maximum value achieved by the Total Damage parameter, so high as 0,954, corresponds to a situation where concrete element can be almost completely deteriorated due to stress- and temperature-induced cracking, as well as thermo-chemical degradation.

A kind of "critical value" of the Total Damage parameter has been estimated by [8] within D ≈ 0,90-0,95.

5.2.2.2.2 Evaluation of the I_{s4} spalling index

If we apply the same procedure defined on paragraph 5.1.1.6 for the NIST case, to the results obtained from the case dealt on this paragraph corresponding to the parametric heating and the Point A (First cooling start) – Slow speed "forced" cooling curves described on previous paragraphs (figure 5-26), the results of the evaluation of the I_{s4} spalling index for this case are shown on figure 5-30:

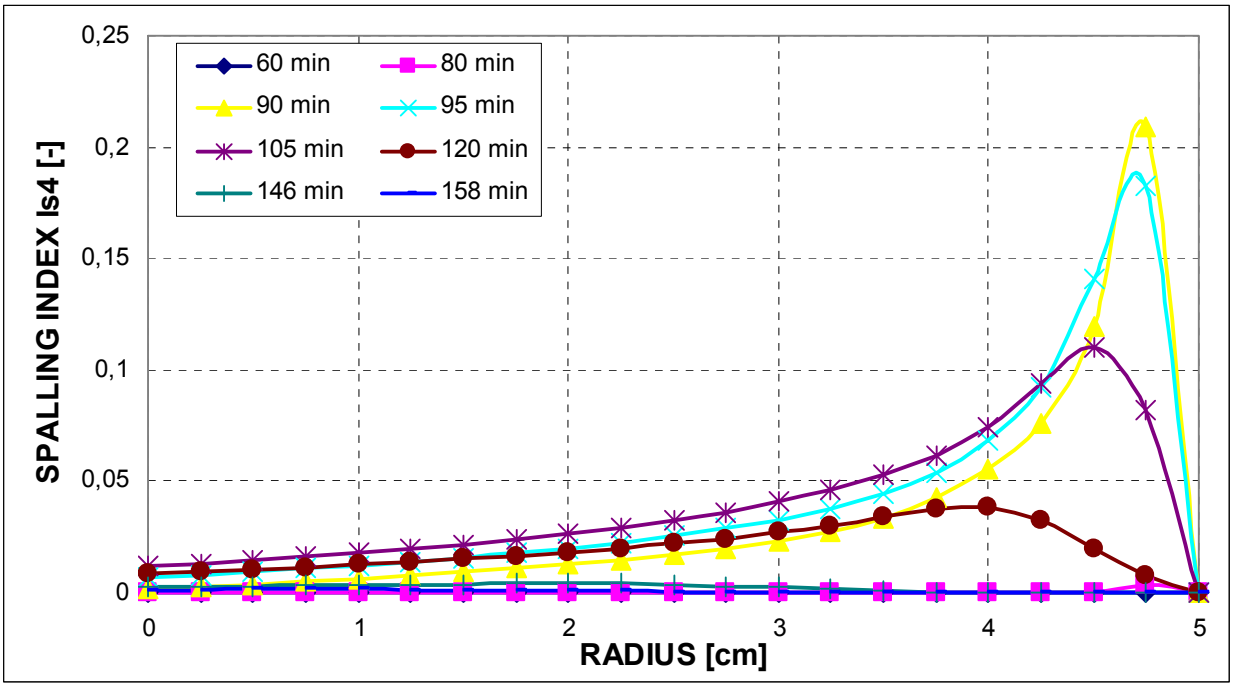

Figure 5-30: *Radial distribution of Spalling Index I_{s4} (right side: surface; left side: cylinder axis).*

The maximum spalling index value obtained for this case using the real value of the scaling factor involved in the 'intuitive criterion' (C_s = 4,86) is 0,2087. This value again gives a preliminary idea of the probability of suffering spalling if compared to that of NIST experiments previously reported.

From this figure it can also be observed that the expected position of the main fracture is at 2,5 millimetres from surface while the instant showing the maximum value of the spalling index I_{s4} is again 90 minutes (before "forced" slow cooling process starts).

5.2.2.2.3 Simplified analysis to determine if concrete spalling is energetically possible

As it has been already done within previous paragraphs, next it is analysed if concrete spalling is energetically possible through the comparison of the fracture energy and the stored elastic energy:

Parameter	Source / equation	Value obtained
Possible thickness of the ruptured layer of concrete (corresponding to the highest value of the spalling index), Δx	From figure 5-30	0,025 cm

Released elastic energy, ΔU	Integrating a curve of the elastic energy density (figure 5-28.b) for the instant showing the highest value of the spalling index an in the range of the coordinates corresponding to this layer $\sum_{r1}^{r3} u_i(x) \cdot (x_i - x_{i-1}) \cdot 2 \cdot \pi \cdot (\frac{r_1 + r_3}{2}) \cdot H$ Where r_1 = 0,0475 m, from figure 5-30 r_3 = 0,05 m, from figure 5-30 H = 0,2 m	x_i [m] / u_i (x) [J/m^3] 0,0475 / 4.702,39 0,05 / 5.357,04 ΔU = 1,541 J
Total mass of spalled concrete, Δm	$\rho \cdot \pi \cdot (r_3^2 - r_1^2) \cdot H$	0,401 Kg
Total Area of rupture, ΔA_{fr}	Assuming certain average dimensions of the spalled pieces of concrete: $2 \cdot \pi \cdot r_1 \cdot H$	0,05969 m^2
Energy dispersed for fracturing, ΔE_{fr}	$\Delta E_{fr} = \Delta A_{fr} \cdot G_f$ Where Gf is the specific fracture energy obtained from experimental tests [16], 177 J/m^2	10,56 J
Rough estimation for the kinetic energy, ΔE_k	$\Delta E_k = \Delta U - \Delta E_{fr}$	< 0

Since the kinetic energy value is negative (i.e. the stored elastic energy is smaller than the energy needed for the rupture), the concrete spalling at 90 minutes is not energetically possible.

5.2.2.3 RESULTS FROM THE C-90 PARAMETRIC HEATING AND "FORCED" COOLING SIMULATIONS (FIRST STARTING POINT –POINT A–, FAST COOLING).

5.2.2.3.1 Direct results from the simulation

Figure 5-31 shows the main results obtained for this case where the parametric heating and the Point A (First cooling start) – Fast speed "forced" cooling curves described on last paragraph (figure 5-26) have been implemented.

It must be remarked that the calculations detailed on table 5-8 went out of convergence before the expected end, at a time of 4.809,95 seconds (approximately 10 seconds after the beginning of the fast cooling process), mainly due to very sharp variations of gas pressure and mechanical damage, so the last results available correspond to a time of 80 minutes plus 9,95 seconds.

Input file name	**Initial time (s)**	**Time step (s)**	**Number of time steps**	Freq. results record (time steps)	**Final time (s)**
ACT1ST2F_01	0	1E-6	10	10	1E-5
ACT1ST2F_02	1E-5	0,5	720	120	360
ACT1ST2F_03	360	6	740	10	4.800
ACT1ST2F_04	4.800	0,1	240	5	4.824*
ACT1ST2F_04b	4.809,5	0,0001	15.000	500	4.811*
ACT1ST2F_05	4.824	6	396	4	7.200
ACT1ST2F_06	7.200	12	930	30	18.360

Table 5-8. *Time history of the simulation stages*

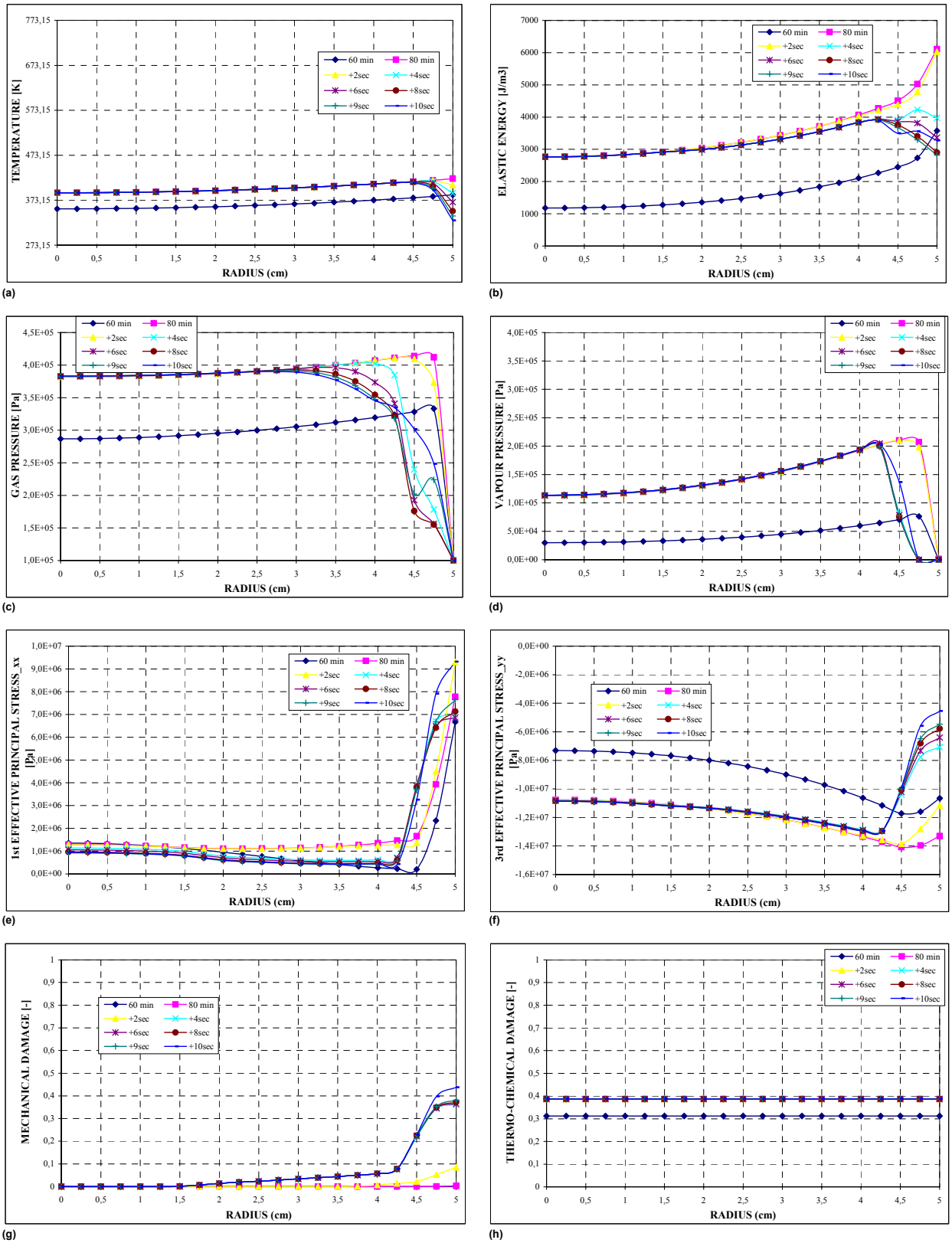

Figure 5-31: Heating and Point A (First cooling start) – Fast speed "forced" cooling results. *Radial distributions of the following fields: a) Temperature; (b) Elastic Energy; (c) Gas pressure; (d) Vapour pressure; (e) 1st principal stress_xx; (f) 3rd principal stress_yy; (g) Mechanical damage; (h) Thermo-chemical damage. Right side: cylinder heated surface; Left side: Cylinder axis.*

Figures 5-32 and 5-33 show that during the first 10 seconds of cooling process simulation, Mechanical Damage (at 0,25 cm from the surface) increases uninterruptedly (clearly beyond the

values obtained for the cases with "natural" and "forced-slow" cooling processes) until the end of the simulation while gas pressure at this same point shows high increases and decreases.

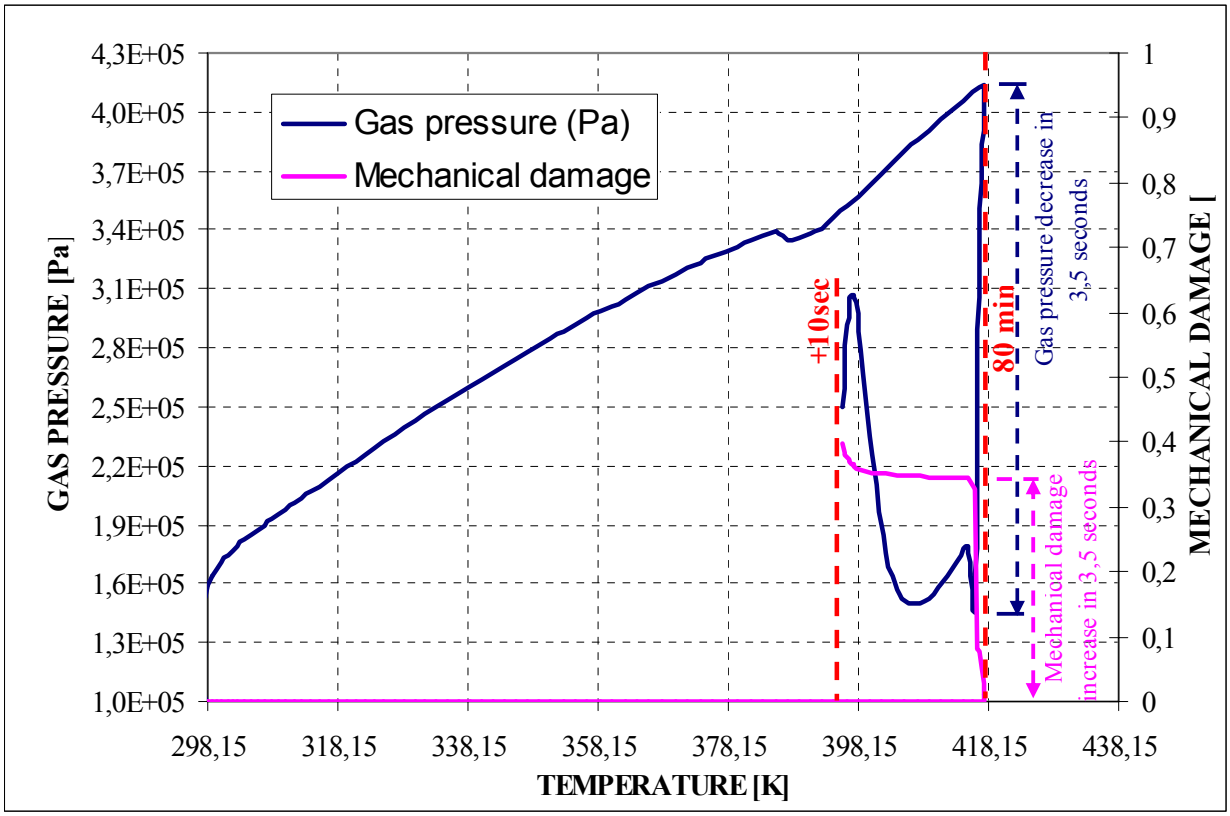

Figure 5-32: *Evolution with temperature of Gas Pressure and Mechanical Damage at 0,25 cm from surface.*

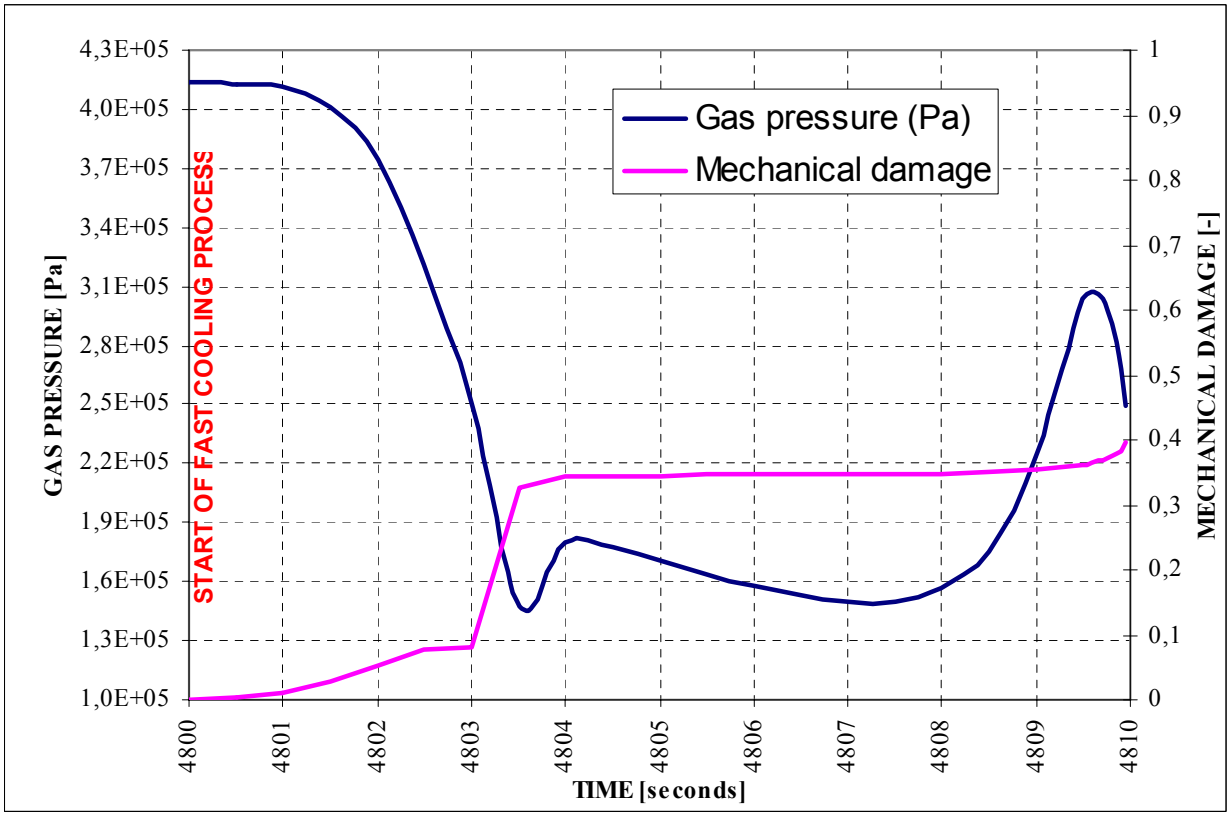

Figure 5-33: *Evolution with time of Gas Pressure and Mechanical Damage at 0,25 cm from surface during the 10 seconds of "forced" fast cooling.*

5.2.2.3.2 Evaluation of the I_{s4} spalling index

If we apply the same procedure defined on paragraph 5.1.1.6 for the NIST case, to the results obtained from the case dealt on this paragraph corresponding to the parametric heating and the Point A (First cooling start) – Fast speed "forced" cooling curves described on previous paragraphs (figure 5-26), the results of the evaluation of the I_{s4} spalling index for this case are shown on figure 5-34:

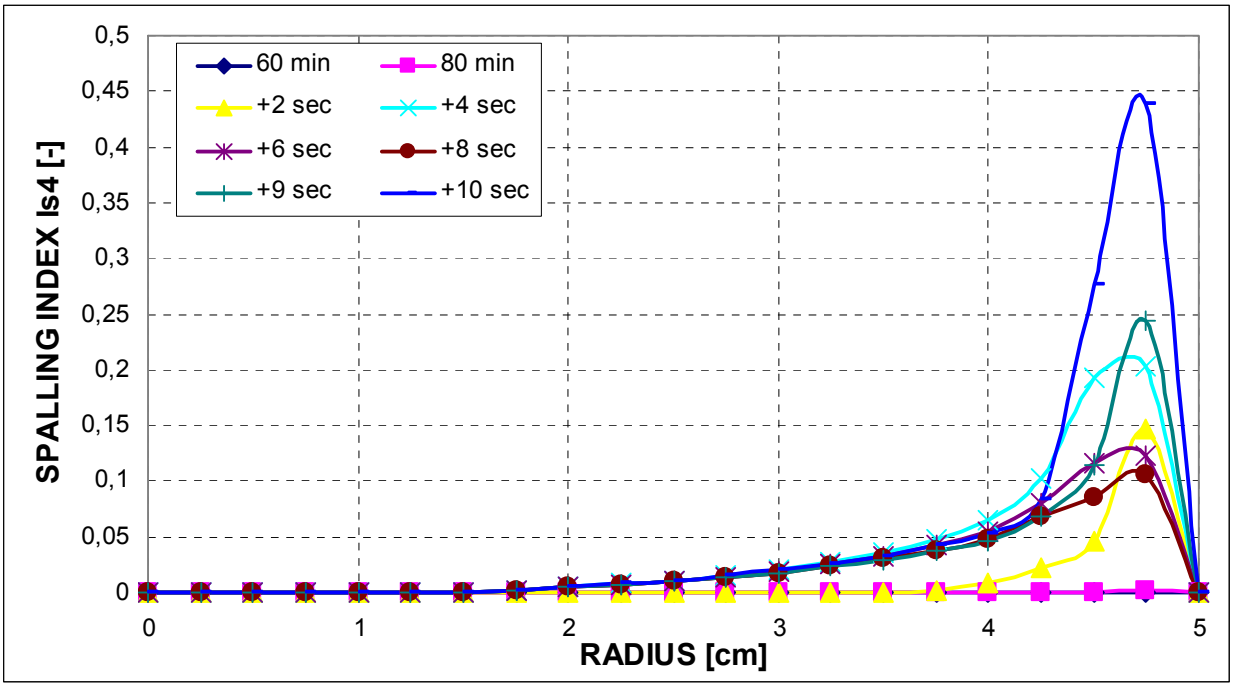

Figure 5-34: *Radial distribution of Spalling Index I_{s4} (right side: surface; left side: cylinder axis).*

The maximum spalling index value obtained for this case using the real value of the scaling factor involved in the 'intuitive criterion' (C_s = 4,86) approximately doubles that corresponding to previous cases (0,4379) – and, furthermore, it is much higher than that obtained for the NIST case without considering thermal creep). This fact, explained in detail in later paragraphs, gives a preliminary idea of a clearly unfavourable effect of a fast "forced" cooling (as short as only 10 seconds) o on the likelihood f a High-Strength concrete element to experiment thermal spalling.

From this figure it can also be observed that, once more, the expected position of the main fracture is at 2,5 millimetres from surface while the instant showing the maximum value of the spalling index I_{s4} is 10 seconds after the "forced" fast cooling process starts taking into account that the calculation stopped at that moment (perhaps a longer simulation would show that spalling risk would increase later on).

5.2.2.3.3 Simplified analysis to determine if concrete spalling is energetically possible

As it has been already done within previous paragraphs, next it is analysed if concrete spalling is energetically possible through the comparison of the fracture energy and the stored elastic energy:

Parameter	**Source / equation**	**Value obtained**	
Possible thickness of the ruptured layer of concrete (corresponding to the highest value of the spalling index), Δx	From figure 5-34	0,025 cm	
Released elastic energy, ΔU	Integrating a curve of the elastic energy density (figure 5-31.b) for the instant	x_i [m]	u_i (x) [J/m^3]
		0,0475	3.558,30

	showing the highest value of the spalling index an in the range of the coordinates corresponding to this layer $\sum_{r1}^{r3} u_i(x) \cdot (x_i - x_{i-1}) \cdot 2 \cdot \pi \cdot (\frac{r_1 + r_3}{2}) \cdot H$ Where r_1 = 0,0475 m, from figure 5-34 r_3 = 0,05 m, from figure 5-34 H = 0,2 m	0,05 3.271,10 ΔU = 1,046 J
Total mass of spalled concrete, Δm	$\rho \cdot \pi \cdot (r_3^2 - r_1^2) \cdot H$	0,401 Kg
Total Area of rupture, ΔA_{fr}	Assuming certain average dimensions of the spalled pieces of concrete: $2 \cdot \pi \cdot r_1 \cdot H$	0,05969 m^2
Energy dispersed for fracturing, ΔE_{fr}	$\Delta E_{fr} = \Delta A_{fr} \cdot G_f$ Where Gf is the specific fracture energy obtained from experimental tests [16], 177 J/m^2	10,56 J
Rough estimation for the kinetic energy, ΔE_k	$\Delta E_k = \Delta U - \Delta E_{fr}$	< 0

Since the kinetic energy value is negative (i.e. the stored elastic energy is smaller than the energy needed for the rupture), the concrete spalling at 80 minutes + 10 seconds is not energetically possible but one must remember that:

- These results correspond only to the first 10 seconds of simulation of the fast "forced" cooling process.
- If thermal creep had been taken into account the values of the released elastic energy would be much higher, as it happened on paragraph 5.1.1.6 for the NIST case.

5.2.2.4 COMPARISON OF THE I_{S4} SPALLING INDEX VALUES OBTAINED FOR DIFFERENT TYPOLOGIES OF COOLING PROCESSES.

The first achievement of this chapter has been to establish a methodology for a preliminary and simplified analysis of the effect of a forced cooling on the spalling behaviour of High Strength (and Very High Strength) Concretes in order to discern that this effect is definitely significant enough to justify a relevant, greater and deeper work concerning this matter. This methodology has been based on the previous works developed and reported by D. Gawin, F. Pesavento, B.A. Schrefler in their article [8] and, as it will be explained later in this paragraph, it has proved to be correlated against experimental tests and according to what it can be expected from the understanding of the hygro-thermo-chemo-mechanical processes involved on the High-Strength concretes behaviour.

On figure 5-35 are shown the values obtained for the Spalling Index I_{s4} from the simulations reported on previous paragraphs involving different typologies of the cooling processes: a "natural" cooling, and two "forced" cooling processes, namely, a Slow one developed in forty minutes and a fast one developed in ten seconds.

The first preliminary conclusion is that the main features of the cooling process (specially its speed and starting time) have a significant influence on the thermal spalling probability, since their effect on the values of the chosen Spalling Index makes them vary, for example, more than a 100 per cent between those corresponding to a slow "forced" cooling (with a maximum of about 0,21) and to a fast "forced" cooling (with a maximum of about 0,44).

It must be taken into account that since the fast "forced" cooling simulation has been only possible, up to this point, for a time period of 10 seconds after the start of the cooling, the results corresponding to this type of cooling may be much worse (never more favourable because of the irreversibility of cracking process) when taking into account the rest of the cooling process.

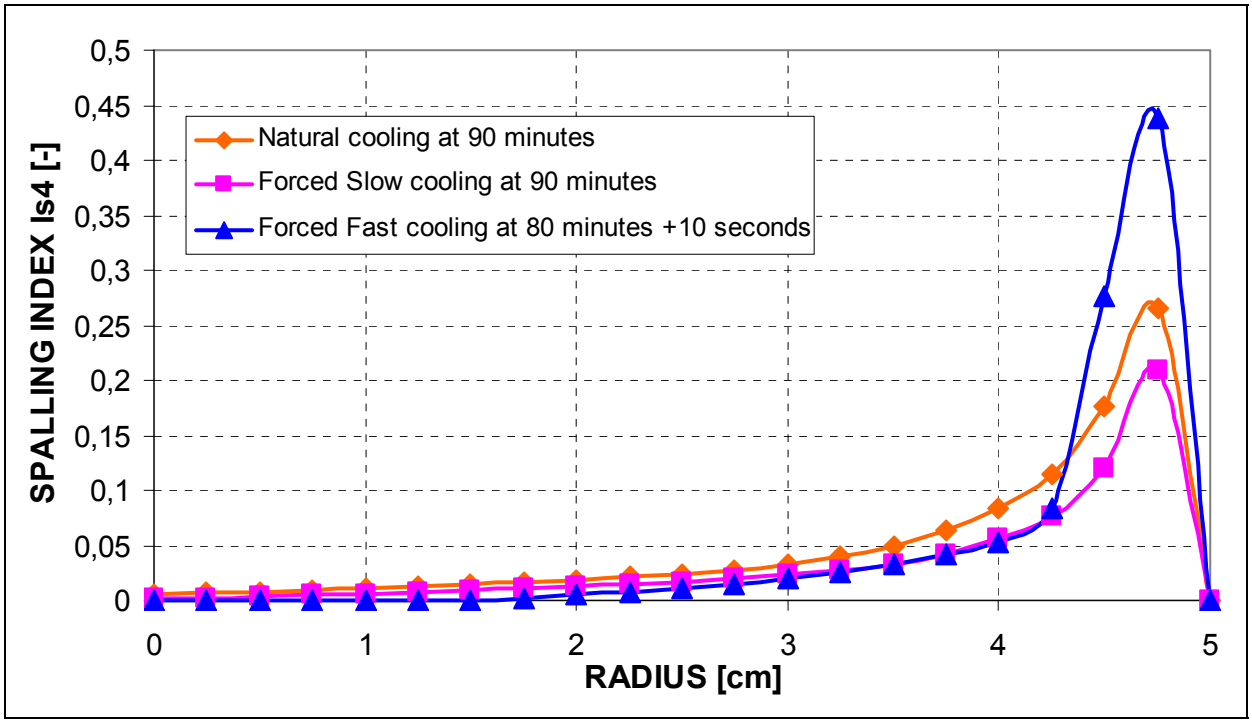

Figure 5-35: *Radial distribution of Spalling Index I_{s4} for different types of "natural" and "forced" cooling processes*

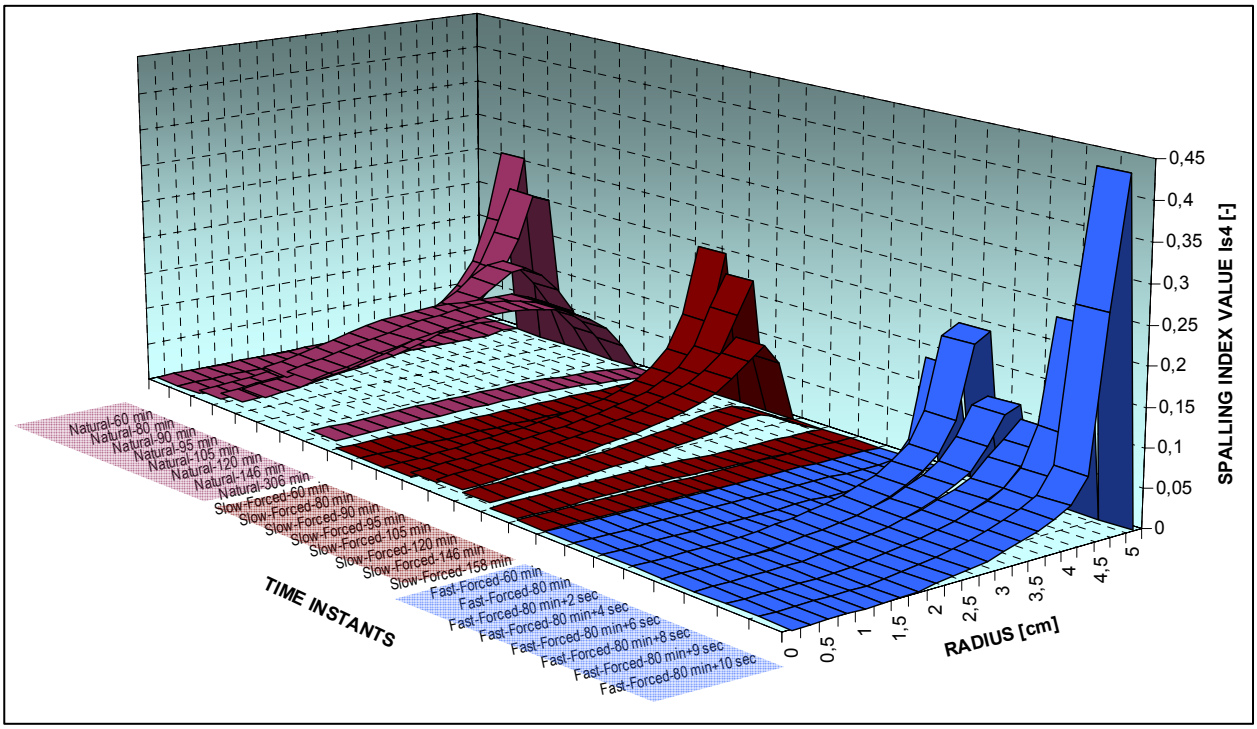

Figure 5-36: *Radial distribution of Spalling Index I_{s4} for different types of "natural" and "forced" cooling processes*

Figure 5-36 shows the complete evolution of the Spalling Index I_{s4} for each of the types of cooling processes adopted.

The second and relevant conclusion is that the Spalling Index I_{s4} obtained for the "forced" fast cooling process are much higher that those corresponding to a "natural" cooling process despite the latter makes the concrete element to remain at high temperatures much more time, so an unfavourable effect of the direct application of the water jet of a hose-nozzle from the fire fighting services (taking also into account that the lasting of the surface temperature decrease arisen from its application may be much faster than 10 seconds). In that sense, for this case the values of the Spalling Index I_{s4} obtained for the fast "forced" cooling (with a maximum of about 0,44) are a 62 per cent higher than those corresponding to the "natural" cooling (with a maximum of about 0,27).

It is true that the stored elastic energy corresponding to the fast "forced" cooling is slightly lower to that corresponding to the "natural" cooling process, but if we take into account that both the Spalling Index I_{s4}, the first principal stress and the mechanical damage (see figures 5-37 and 5-38) values obtained from the fast "forced" cooling are higher than those corresponding to the NIST case calculated without considering thermal creep (with only ten seconds of the fast cooling simulation), it is expectable that thermal spalling may take place (however, it must be reminded that these are just simplified and preliminary conclusions). Also the starting time of the cooling process may have a significant influence on the thermal spalling probability, so a higher synergic effect may be found when the fast "forced" cooling process starts later.

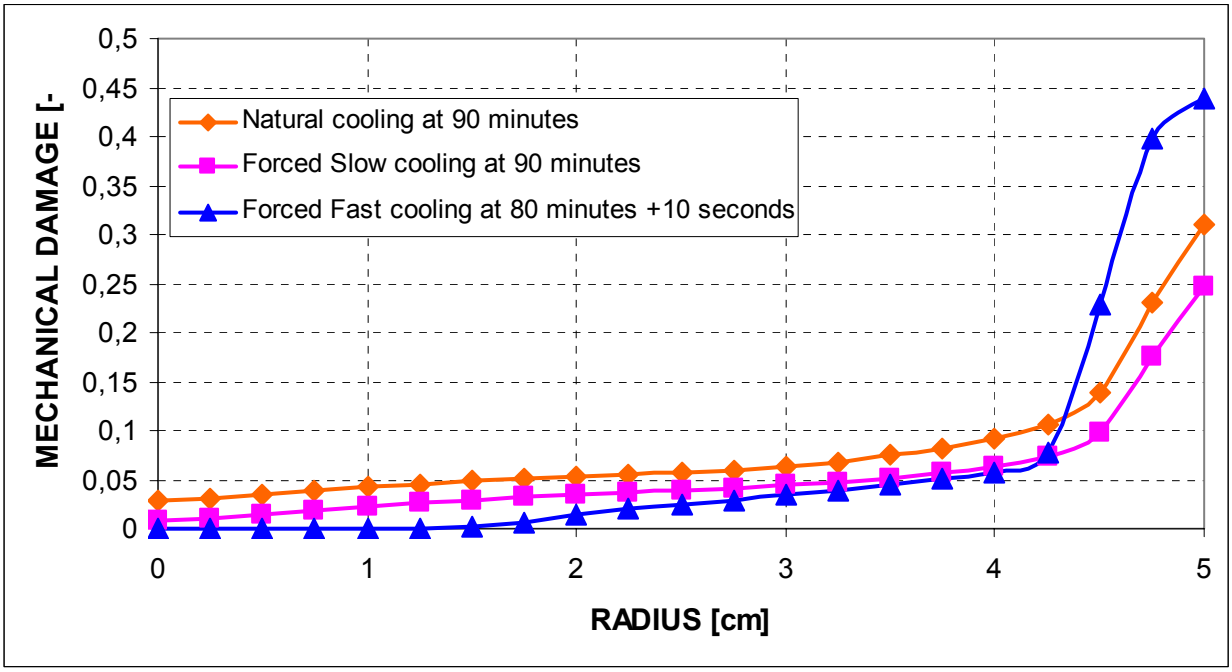

Figure 5-37: *Radial distribution of the mechanical damage for different types of "natural" and "forced" cooling processes.*

In conclusion, it has been found that the methodology shown herein for the preliminary and simplified analysis of the effect of a forced cooling on the spalling behaviour of High Strength (and Very High Strength) Concretes is reliable and that the results obtained show clearly that a fast "forced" cooling – at least –may have an unfavourable effect which is definitely significant enough to justify a relevant, greater and deeper work concerning this matter. However, this is only a preliminary and simplified conclusion that might change completely when introducing extremely relevant considerations such as the fact that some of the material properties whose definition is necessary to accomplish the hygro-thermo-chemo mechanical calculations developed herein do not show a 'reversible' trend when temperature cycles are applied to structural elements so must be taking into account through an 'irreversible' definition, considerations included within the advanced analyses developed in Chapter 6.

As a secondary conclusion of this chapter, it has been worked out that the models developed for the simulations will necessarily have to be defined with a high-order finite elements mesh and a design developed from the physical knowledge of the processes involved of the models developed for the simulations, since it has been observed that – specially with fast "forced" coolings – huge gradients of the variables may appear during calculations. This fact will surely lead to higher computational times and resources needs.

A third and final conclusion, is that thermal creep has a significant effect on the results dealt in this chapter to develop the conclusions exposed herein. For this reason, without considering thermal creep the values of the I_{s4} spalling index are important from a comparative point of view or for structural elements where thermal creep might not be significant (mainly cases where no strong constraints are applied). Since up to the date of this preliminary and simplified analysis there are not any software releases available capable to predict hygro-thermo-chemo-mechanical behaviour considering thermal creep during a cooling process (and, obviously, it made no sense on developing that release until one had the certainty that cooling will have a significant (and unfavourable) effect on thermal spalling risk) a release including this phenomena (and avoiding numerical difficulties) is a need that will have to be met in other research works beyond the scope of this thesis to enable the development of the same analyses described in Chapter 6 for structural elements with strong restraints.

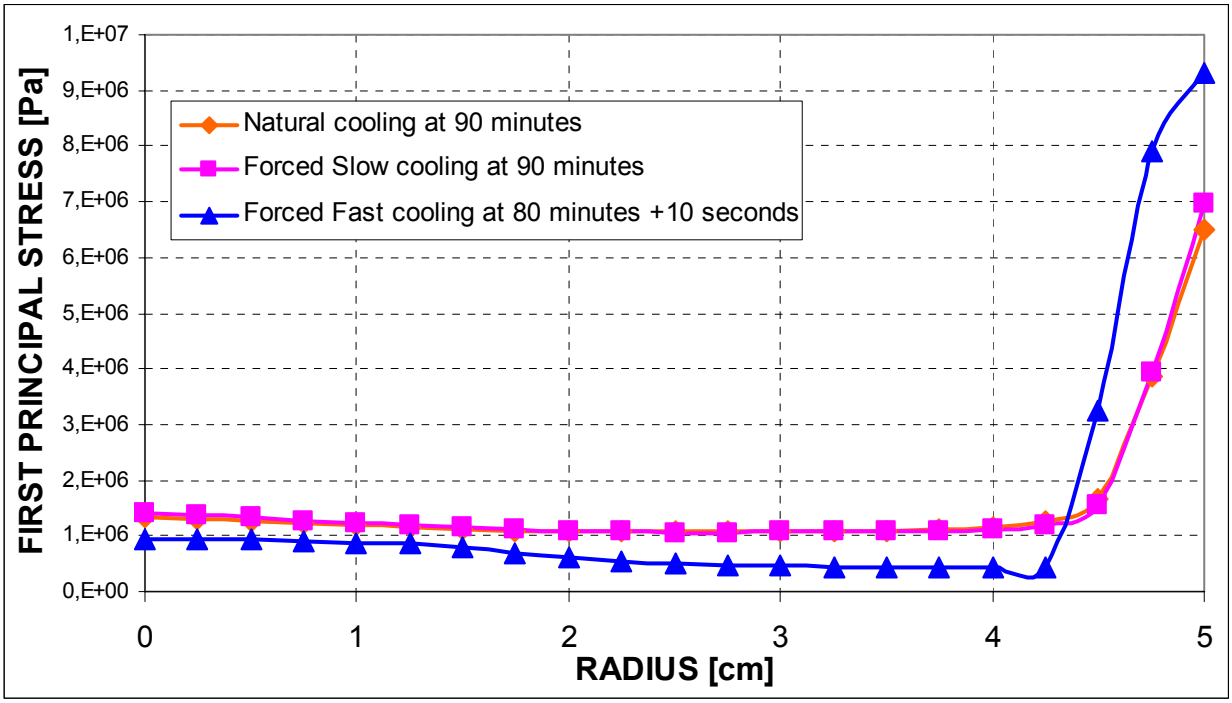

Figure 5-38: *Radial distribution of the first principal stress for different types of "natural" and "forced" cooling processes.*

5.3 BIBLIOGRAPHY OF THE CHAPTER

[1] G.W. Shorter, T.Z. Harmathy, *Moisture clog spalling*, Proc. Instit. Civil Engr. 20 (1965) 75-90.

[2] H. Saito, *Explosive spalling of prestressed concrete in fire*, Internal Report No 22, Building Research Institute, Japan, 1965.

[3] T.Z. Harmathy, *Effect of moisture on the fire endurance of building elements*, ASTM special technical publication 385, Philadelphia, 1965.

[4] V.V. Zhukov, *Explosive failure of concrete during a fire* (in Russian). Translation No. DT 2124, Joint Fire Research Organization, Borehamwood, 1975.

[5] P.J. Sullivan, A.A. Akhtaruzzaman, *Explosive spalling of concrete exposed to high temperature*, in: Proc. Of First International on Structural Mechanics in Reactor Technology, Berlin, 1971

[6] R.J. Connelly, *The spalling of concrete in fires*, Ph.D. thesis, Aston University, 1995, pp. 294

[7] N. Khoylou, *Modelling of moisture migration and spalling behaviour in non-uniformly heated concrete*, Ph.D. thesis, Imperial College, London, 1997, pp.1147.

[8] D. Gawin, F. Pesavento, B.A. Schrefler, *Towards prediction of the thermal spalling risk through a multi-phase porous media model of concrete*, Comput. Methods Appl. Mech. Engrg . 195 (2006) 5707-5729.

[9] Z.P. Bazant, W. Thonguthai, *Pore pressure and drying of concrete at high temperature*, J. Engrg. Mech. ASCE 104 (1978) 1059-1079.

[10] L.T. Phan, *Fire performance of high-strength concrete: a report of the state-of-the-art*, Res. Report NISTIR 5934, pp 105, National Institute of Standards and Technology, Gaitherburg, 1996.

[11] L.T. Phan, N.J. Carino, D. Duthinh, E. Garboczi (Eds.), Proc. Int. Workshop on Fire Performance of High-Strength Concrete, Gaitherburg, MD. USA, February 13-14, 1997, NIST Special Publication 919, NIST, 1997.

[12] L.T. Phan, J.R. Lawson, F.L. Davis, *Effects of elevated temperature exposure on heating characteristics, spalling and residual properties of high performance concrete*, Mater. Structu. 34 (March) (2001) 83-91.

[13] L.T. Phan, N.J. Carino, *Effects of test conditions and mixture proportions on behaviour of high-strength concrete exposed to high temperature*, ACI Mater. J. 99 (1) (2002) 54-66.

[14] L.T. Phan, *High-Strength concrete at High Temperature – An overview*, Building Fire Research Laboratory Online Library, National Institute of Standards and Technology, Gaitherburg, 2002.

[15] Brite Euram III BRPR-CT95-0065 HITECO, *Understanding and industrial application of High Performance Concrete in High Temperature Environment – Final report*, 1999.

[16] R. Felicetti, P. Gambarova, M.P. Natali Sora, G. Rosati, *Caratterizzazione mecánica di calcestruzzi ad alta ed altissima resistenza esposti ad alta temperatura*, Brite Euram III report, 1999.

[17] UNE-EN 1991-1-2, Eurocódigo 1: Acciones en estructuras. Parte 1-2: Acciones generales. Acciones en estructuras expuestas al fuego, Mayo 2004.

THIS PAGE IS INTENTIONALLY
LEFT BLANK